DEVELOPING COMMERCIALLY SCALABLE IRON AND TITANIUM METAL-ORGANIC FRAMEWORKS FOR GAS STORAGE AND WATER PURIFICATION

A Dissertation

by

ANGELO ANTHONY KIRCHON

Submitted to the Office of Graduate and Professional Studies of
Texas A&M University
in partial fulfillment of the requirements for the degree of

DOCTOR OF PHILOSOPHY

Chair of Committee,	Hong-Cai (Joe) Zhou
Committee Members,	Sarbajit Banerjee
	Michael Nippe
	Hae-Kwon Jeong
Head of Department,	Simon North

December 2020

Major Subject: Chemistry

ABSTRACT

Since their discovery in the late 1990s, Metal-Organic Frameworks (MOFs) have turned into one of the fastest growing classes of materials studied in the chemical literature. MOFs have shown promise in applications such as gas storage, chemical separations, chemical sensing, catalysis, and even drug delivery. Their wide range of potential applications can be attributed to their ultra-high surface area, high crystallinity and tunable physical and chemical properties. However, the potential applications of MOFs have been slow to develop into viable and sustainable products at the commercial or industrial level.

Chapter I of this dissertation discusses the background of Metal-Organic Frameworks (MOFs), the current limitations of MOFs that prevent wide spread commercial production such as stability, processing cost, and synthesis cost as well as how the research performed aimed to address these challenges.

In Chapter II details a method that was developed in order to synthesize a Hierarchally Porous (HP) variant of a commercially available MOF named PCN-250(Fe_3O). The method developed utilizes the addition of fatty acids during MOF synthesis in order to induce and engineer hierarchal porosity within PCN-250(Fe_3O). The resulting Hierarchally Porous MOFs (HP-MOF) exhibited completely different mesoporosity in size, volume, and position. Furthermore, the PCN-250(C9-1.4M) material obtained adsorbs/removes 100% of Methylene Blue, a common organic dye, from aqueous solution, as compared to the microporous variant of PCN-250(Fe_3O), which only removes 31%

Chapter III builds on the use of PCN-250(Fe_3O) as a material for removing organic dyes from water, but utilizes PCN-250(Fe_3O) as a catalyst, not just an adsorbent. PCN-250 was reported to be a successful and recyclable Fenton and photo-Fenton catalyst that degrades 100% of Methylene Blue. Overall, 4 different variants of PCN-250 were synthesized and named PCN-250(Fe_3O), PCN-250(Fe_2Ni), PCN-250(Fe_2Co) and PCN-250(Fe_2Mn). The catalytic degradation efficiency for both Fenton and photo-Fenton reactions was improved by the isomorphic substitution of Mn and Co for Fe, but inhibited by the incorporation of Ni.

Chapter IV details the development of a photo-catalytic system for the degradation of Per/Poly-Fluorinated Alkyl Substances (PFASs) using a commercially scalable Ti-Based MOF. With the developed photo-catalytic system, the concentration of Perfluorooctanoic acid (PFOA) can be reduced by 49% and with a 21.1% fluoride mineralization efficiency in 24 hours. Overall, this work has shown the ability to successfully design Metal-Organic Frameworks based photo-catalytic platforms for chemically reducing (degrading) Per- and polyfluoroalkyl substances (PFAS) in water and is to the best of our knowledge the first successful example of using MOFs for PFAS degradation.

Chapter V, details the development of a novel MOF processing method that maximizes the surface area while minimizing cost. The method is a suspension-based processing 3 step method that maximizes the porosity of MOFs by more effectively solubilizing unreacted starting materials and more importantly, removing area of low

crystallinity from the surface of MOF particles. In the last chapter, Chapter VI, a summary of the current work is given along with my thoughts and outlooks on future of MOFs.

DEDICATION

To my family and friends, especially my Mom and Dad

Thank you for all your love and support.

ACKNOWLEDGEMENTS

First, I would like to thank my research advisor and committee chair, Professor Hong-Cai (Joe) Zhou. Thank you for trusting me with the responsibility you did. I learned not only how to be a successful scientist from you but you gave me opportunities to become a successful leader and always pushing me to be the best I could be. I also wish to express my appreciation to my committee members, Prof. Sarbajit Banerjee, Prof. Michael Nippe and Prof. Hae-Kwon Jeong for guiding and supporting me throughout my Ph.D. study.

I would like to thank all my colleagues who offer generous supports and helps that lead to the success of this dissertation. I feel so grateful to work with all Zhou group members, especially Dr. Stephen Fordham, Dr. Zachary Perry, Dr. Gregory S. Day, Dr Juiluo Li, Dr. Yu Fang, Dr. Liang Feng, Dr. Peng Zhang, Dr. Sayan Banerjee, Hannah Drake, Wenmiao Chen, and Jeremy Willman. In particular, I'd like to thank Dr. Zachary Perry for being my first student mentor in graduate school and really teaching me about the field of MOFs and porous materials. I'd like to thank Hannah Drake and Dr. Liang Feng as my class mates within our group. I think all of our hard work paid off and together we were able to succeed all while making the group a better place. Thank you for being such great lab mates.

I would also like to share my acknowledgment to my wonderful collaborators especially Framergy, Inc. I am so lucky to work with such an amazing team over at framergy. Thank you Jason Ornstein, Ray Ozdemir, Anne Boehme and Carlos Ybanez, My work would have not be possible without your support.

I would also like to acknowledge my mentors all throughout my science career including my undergraduate advisor Dr. Daren Timmons, my advisor at Lawrence Livermore National Lab, Dr. Michael Bagge-Hansen, and my high school chemistry teacher, Ms. Nancy McHugh. All three of you played a major role in my success as a scientist and I am extremely thankful for you.

Finally, I want to thank my family and friends, especially my Mother (Frances), Father (Joseph), Brother (Joseph) and Fiancé (Taylor) for their support, understanding, and love. It is their support not only during my Ph.D. but throughout my whole life that made the journey to a Ph.D. possible. Thank you for believing in me and always encouraging me to be the best person I could be.

CONTRIBUTORS AND FUNDING SOURCES

Contributors

This work was supported by a dissertation committee consisting of Professor Hong-Cai Zhou, Professor Sarbajit Banerjee and Professor Michael Nippe of the Department of Chemistry and Professor Hae-Kwon Jeong of the Department of Chemical Engineering. The Ideas in Chapter II and V were developed with help from Dr. Gregory S. Day from the Zhou Research Group. SEM images from all chapter were obtained by Dr. Juilio Li, LC-MS data was collected by Smriti Shakar and Dr. Yohannes Rezenom, ICP-MS data was obtained by Yutao Huang and Wenmaio Chen and HPVA data was obtained by Sayan Banerjee. All other work conducted for the dissertation was completed by the student independently.

Funding Sources

This work was made possible in part by Center for Gas Separations, an Energy Frontier Research Center (EFRC) funded by U.S. Department of Energy (DOE), Office of Science, Office of Basic Energy Sciences under award Number DE-SC0001015, by a Robert A. Welch Chair in Chemistry under award Number A-0030, National Science Foundation, Small Business Innovation Research (NSF-SBIR) Grant Number: 1632486, Environmental Protection Agency, Small Business Innovation Research (EPA-SBIR) Phase I – Contract Number 68HERD19C0012, and by the Qatar National Research Fund under Award Number NPRP9-377-1-080 S.

Its contents are solely the responsibility of the authors and do not necessarily represent the official views of the funding offices.

LIST OF ABBREVIATIONS

°C	Degrees Celsius
Å	Angstrom
AOP	Advanced Oxidation Process
ARP	Advanced Reduction Process
BDC	Benzene-1,4-Dicarboxylic Acid
BE	Binding Energy
BET	Brunauer, Emmett and Teller
BJH	Barrett, Joyner and Halenda
CCUS	Carbon Capture, Utilization and Storage
CV	Crystal Violet
DFT	Density Functional Theory
DOE	Department of Energy
DLS	Dynamic Light Scattering
DMF	*N,N*-Dimethylformamide
EDS	Energy-Dispersive X-ray Spectroscopy
EtOH	Ethanol
EPA	Environmental Protection Agency
FA	Formic Acid
FT-IR	Fourier Transform-Infrared Spectroscopy
HKUST	Hong King University of Science and Technology
HP	Hierarchically Porous

ICP-MS	Inductively Coupled Plasma-Mass Spectrometry
IUPAC	International Union of Pure and Applied Chemistry
LC-MS	Liquid Chromatography - Mass Spectrometry
MB	Methylene Blue
MeOH	Methanol
MIL	Materials from Institut Lavoisier
MOF	Metal-Organic Framework
NIST	National Institute of Standards
NM	Nanometer
NMR	Nuclear Magnetic Resonance
PCN	Porous Coordination Network
PCP	Porous Coordination Polymer
PFAS	Per- and Polyfluoroalkylated substances
PFOA	Perfluorooctanoic acid
PFOS	Perfluorooctanoic sulfate
PXRD	Powder X-Ray Diffraction
RB	Rhodamine B
SCXRD	Single Crystal X-Ray Diffraction
$scCO_2$	Super Critical Carbon Dioxide
SEM	Scanning Electron Microscopy
TEOA	Triethananolamine
TFA	Trifluoroacetic Acid

TGA	Thermogravimetric Analysis
TOC	Toxic Organic Compounds
UiO	University of Oslo
UV-vis	Ultraviolet and Visible
XPS	X-ray Photoelectron Spectroscopy
ZIF	Zeolitic Imidazolate Framework

TABLE OF CONTENTS

LIST OF FIGURES

LIST OF TABLES

CHAPTER I

INTRODUCTION*

In the mid-1990's a new class of porous materials was discovered, resulting in a long-lasting impact on the field of chemistry, biology, physics, medicine, and material science.[1] These materials are known as Metal-Organic Frameworks (MOFs) or Porous Coordination Networks (PCNs).[2] Due to their wide range of structures and functionalities, MOFs have been researched for broad range of potential applications which include gas storage and separation[3], catalysis[4,5], drug delivery[6], chemical sensing[7], energy storage[8] and more.

MOFs are organic-inorganic hybrid materials that are constructed by bonding secondary building units or SBU's to one another, thru a series of metal-ligand coordination bonds. MOFs extend beyond the formation of just one metal to ligand coordination bond through other metal units (M-L-M), generating one-, two-, or three-dimensional frameworks. This initial framework extends to make a ordered, polymer type structure, complete with voids or channels resulting in a porous, crystalline material. The porosity of a MOF is defined as the ability to maintain a porous structure without guest molecules in the pores. This means that when all guest molecules (solvent/gas) are removed, typically under heating and vacuum, the material does not collapse, resulting in

---

* This chapter is partially reproduced with permission from: Kirchon, A.; Feng, L.; Drake, H. F.; Joseph, E. A.; Zhou, H.-C. From Fundamentals to Applications: A Toolbox for Robust and Multifunctional MOF Materials. *Chem. Soc. Rev.*, **2018**, 47, 8611-8638. Copyright 2018 by The Royal Society of Chemistry.

permanent porosity.[2,9] This discovery, which was reported in 1999 by Dr. Omar Yaghi, who now works at UC-Berkeley, changed the science world forever.[1]

Over the last 21 years, synthetic MOF chemists have built a synthetic toolbox comprising of techniques that allow both the chemical (polarity, hydrophobicity, charge, acidity, chemical and thermal stability) and physical (pore size, pore shape, framework flexibility, crystal size and shape) properties of MOFs to be tuned to perfection.[10,11] It is this capability that has allowed MOFs to become not only a place to engineer designer chemical and biological processes[11–14], but MOFs are also an exceptional host platform for stabilizing unstable species. For example, MOFs have been used to stabilize enzymes which resulted in enhanced catalytic activity[15,16] and even stabilize reactive intermediates of challenging reactions.[17–19] Overall, the ability to stabilize various species can help change how small molecules in both the energy (H_2, CH_4, MeOH, etc…) and pharmaceutical sectors (drug molecules) are both studied and synthesized.

In terms of developing other novel processes, MOFs have quickly caught the interest of the industrial energy and chemical sectors. The ability to tune their chemical and physical properties has allowed MOFs to be engineered for some real world-changing applications. For example, in 2020, a MOF-based system developed by Exxon-Mobile, Berkeley Lab, and UC-Berkeley was reported to adsorb up 90% of the carbon dioxide (CO_2) in a gas stream that simulates the humid flue gas emitted by modern power plants.[20] This reports marks a major advance for Carbon Capture, Utilization and Storage (CCUS) systems, which are necessary for fighting climate change at the power generation level.

Also reported in 2020, a MOF system discovered by Northwestern University boasts a methane (CH_4) uptake value of 0.66 gram per gram of MOF, which exceeds the US Department of Energy's (DOE) gravimetric target value (0.5 gram per gram of MOF) and exhibits one of the highest capacities for deliverable hydrogen (H_2), both on a weight and volume basis.[21] This material paves the way for replacing gasoline and diesel fuel with clean-burning hydrogen, which can power zero-emission fuel-cell vehicles, or with methane, which generates relatively low levels of combustion products compared to gasoline or diesel.

Other recent advances in MOFs has allowed a University of Texas designed MOF to be developed into a broad-range chemical sensor. This technology launched by Lantha Sensors, is able to detect parts-per-million concentrations of up to 23 various chemicals containments in water.[22] Additionally, a MOF system developed by Framergy, the Materials Institute Lavoisier and Texas A&M University, has shown the ability to degrade per- and polyfluoroalkylated substances (PFASs). PFAS, which are also known as "forever chemicals", are extremely toxic organic compounds found in some water systems that pose a major health risk to the general public. [23]

Although these invention breakthrough have been developing at a much faster rate in the last several years, it has not always been that way in the MOF field. Historically, one of the major limitations of many MOF systems is a lack of aqueous stability. Over the last 20 years, MOF chemists have proven that one of the principles that governs a MOFs chemical and thermal stability is called Person's hard soft acid based (HSAB) principle. The HSAB principle states that chemical species can be segregated into two categories,

Hard and Soft. It further explains that molecular species such as metal salts that are stable in aqueous conditions or insoluble in water, are constructed when soft acids bind with a soft bases or a hard acids bind with hard bases. When this theory is applied to MOFs, it results in stable MOFs being classified into two categories: high-valency metal–carboxylate frameworks and low-valency metal–azolate frameworks. As a result, Iron (Fe^{+3}), Titanium (Ti^{+4}) and Zirconium (Zr^{+4}) based metal organic frameworks, when constructed with carboxylate based ligands, show great aqueous stability in both acidic and basic conditions.[1,24–26] This stability and development of a synthetic toolbox which allows for precise design of the frameworks chemical functionality, have made all MOF very attractive to both the industrial energy and chemical sectors.

Overall, MOFs are an extremely versatile synthetic platform for advancing both science and technology. However, there still many challenges that need to be addressed both at the macroscopic and molecular level in order for MOFs to reach their potential. Moreover, the field of MOFs grew so fast during the early 2000's, that there are many gaps within both the fundamental and applied research. For example, when MOFs were synthesized and originally reported, the applications of MOFs were primarily focused on gas storage and separation.[2,27] Many potential research areas and applications were overlooked due to this narrow outlook. Therefore, this Doctoral Thesis and the research within aims to investigate and fill in some of the research gaps in in developing stable Iron (Fe^{+3}) and Titanium (Ti^{+4}) carboxylate based MOFs, for aqueous based applications such water remediation and as well as clean energy applications such as methane (CH_4) storage.

CHAPTER II

HIERACHALLY POROUS PCN-250: MODULATION VS. TEMPLATING [*]

2.1 Introduction

Compared with traditional porous solids, such as zeolites, activated carbon, and mesoporous silica, MOFs allow for the precise design of framework porosity as well as tailoring of the pore environments at the molecular or atomic level. Unfortunately, the pore sizes of most reported MOFs to date are limited to the micropore range (pore diameter smaller than 2 nm), which are suitable only for the Absorption, separation, and catalysis of small guest molecules, such as gases, small organic molecules, and small coordination complexes. The limited pore sizes may decrease mass transportation rates, restrict the diffusion of substrates to catalytic active sites, and can even hinder the development of composite materials with larger components such as nanoparticles, enzymes, and proteins.[9,28,29]

In order to combat the issue of molecular diffusion in MOFs, the synthesis and development of Hierarchically Porous MOFs (HP-MOFs) have gained significant momentum in recent years. HP-MOFs are defined as MOFs that contain engineered mesopores/macropores in addition to the intrinsic micropores associated with that specific framework. Compared to mesoporous MOFs, HP-MOFs can dramatically improve mass

---

[*] This chapter is partially reproduced with permission from: **Kirchon, A.;** Li, J.; Xia, F.; Day, G. S.; Becker, B.; Chen, W.; Sue, H.-J.; Fang, Y.; Zhou, H.-C. Modulation versus Templating: Fine-Tuning of Hierarchally Porous PCN-250 Using Fatty Acids To Engineer Guest Absorption., *Angew. Chem. Int. Ed.* **2019,** 58 (36), 12425-12430**.**. Copyright 2019 by Wiley‐VCH,. KGaA, Weinheim.

transportation without losing their intrinsic molecular Absorption and separation capabilities. However, the direct synthesis of HP-MOFs is challenging and time-consuming. The preparation of HP-MOF usually involves one of the two methods: modulation or templated synthesis. Modulation refers to the use of molecules that coordinate to the metal clusters in a similar geometry as the ligand but have lower binding affinities than that of the desired ligand, in order to regulate the coordination equilibrium of a growing MOF crystal. It has been well documented that the use of modulating agents, not only can lead to the synthesis of defect-free MOFs, but they can also be used to systematically control defect generation, leading to HP-MOF formation. For example, the pKa of the modulator, coordination modes of the modulator, and even the size/length of the modulator can affect HP-MOF generation. [30–33]

Alternatively, it has been found that during the templated synthesis of HP-MOFs, the templating agents tend to form aggregates. These aggregates are traditionally composed of surfactants or other amphiphilic molecules, which form micelles within a reaction solution leading to the generation of HP-MOFs. Evidence suggests that the mesopore diameter and location is strongly dependent on the hydrophobic volume of these self-assembled aggregates.[34–36] However, it has been long reported that micelles cannot form unless the concentration of the amphiphilic molecules is above the critical micelle concentration (cmc), and this concentration depends on several variables, including chemical identity, molecular size, solution pH, and even the reaction temperature. For example, micelles formation is not favorable if the molecule has less than 7 atoms and is

more favorable with molecules containing 7-16 atoms.[37] Furthermore, due to its solvation strength, the cmc of a surfactant in DMF has been reported to be 10-30 times higher than that of aqueous systems. For this reason, there have been no reports of templating MOFs using DMF as the solvent. [36,38–45]

Therefore, in order to study the effects of modulating versus templating during the generation of HP-MOFs, a system was developed that utilizes aliphatic mono-carboxylic acids with different lengths that can act as either modulators or templating agents during the generation of HP-MOFs (Figure 1). By varying the concentrations and the lengths of mono-carboxylic acid molecules utilized during the solvothermal synthesis, it is proposed

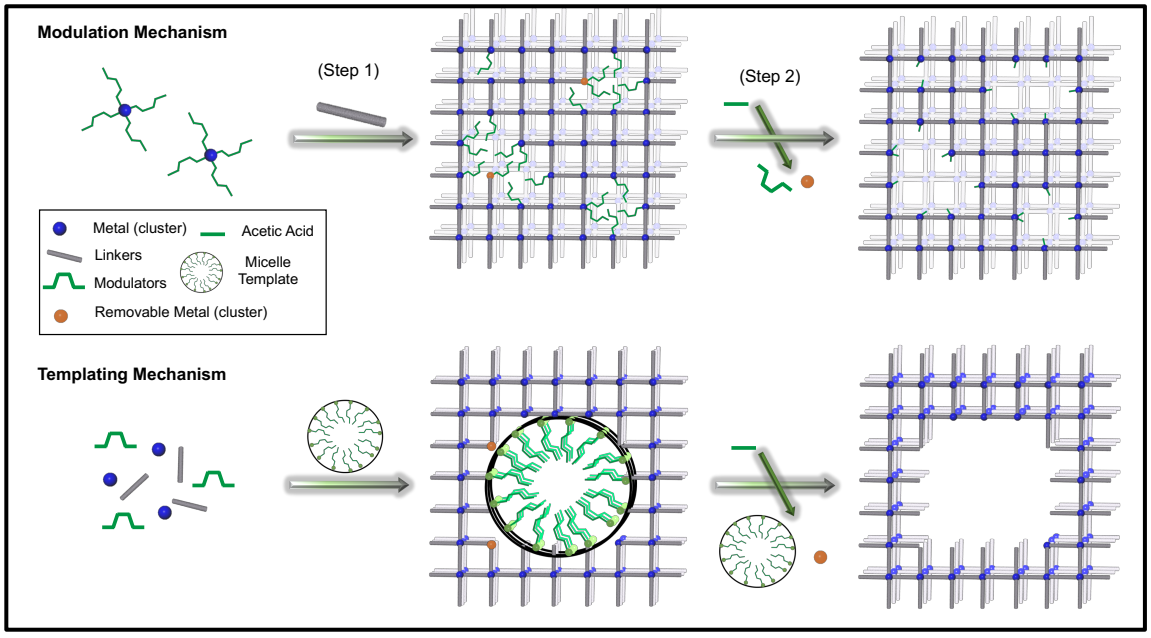

Figure 1. Schematic Illustration of Modulation Mechanism vs. Templating Mechanism for the formation of HP-MOFs using Fatty Acids. Ref #79

that the mechanism of mesopore formation (modulating or templating) can be effectively tuned, and different variants of HP-MOFs can be obtained. For the modulation-based mechanism, the mono-carboxylic acid molecules act as typical modulators generating mesopores through increased steric effects. In the templating-based mechanism, the hydrophobic alkyl chains of the mono-carboxylic acid molecules self-assemble into micellular type structures, which act as templates that subsequently generate mesopores within the obtained MOF.

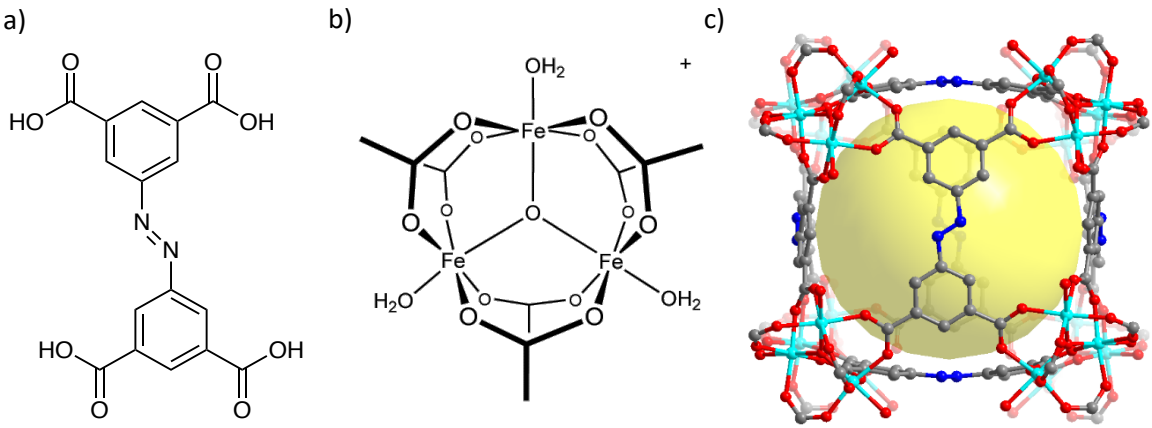

Figure 2. a) ABTC=3, 3', 5, 5'-azobenzenetetracarboxylate b) Fe3-μ3-oxo clusters c) PCN-250 building unit (Yellow Sphere represents the accessible pore space for PCN-250). Ref #79

PCN-250(Fe_3O), also known as MIL-127(Fe_3O) (Figure 2, is a well-studied MOF that is constructed from Fe_3-oxo clusters and tetratopic azobenzene-based linkers (ABTC = 3,3',5,5'-azo-benzene-tetra-carboxylate). PCN-250(Fe_3O), has been shown to be stable in aqueous solutions from pH=1 to pH=12.[46–48] It has been studied for gas storage applications such as CH_4 and H_2[47] as well as gas separations including Ethylene (C_2H_4) and Ethane (C_2H_6)[49]. Unfortunately, due to its small pore size, potential applications that take advantage of the excellent stability of PCN-250(Fe_3O) have not yet been investigated. Therefore, we have selected PCN-250(Fe_3O), as a prime candidate for studying how modulation versus templating phenomena affect the mesopore size, shape, and location, and how this affects the subsequent aqueous application of the obtained HP-MOF material.

2.2 Experimental Methods

Synthesis of Na4ABTC: Na4ABTC was synthesized according to a previously reported method. In a typical procedure, 5-nitroisophtalic acid (19 g) and sodium hydroxide (50 g) were suspended in 250 mL of Milli-Q water and reacted at 60ºC with continuous stirring for 1 hour. Next, glucose (100 g) was dissolved in 100 mL of warm water and the resulting solution was added dropwise to the yellow slurry that became dark brown due to reduction of the nitro groups. The mixture was allowed to cool down for 30 minutes followed by exposure to an air stream for 16 hours with continuous stirring at room temperature. Next, the crude was cooled in an ice bath prior to isolation of the solid by filtration with vacuum. 69.5 % yield (12.52 g) 1H NMR (400 MHz, H2O-d2, δ) 8.62 (d, 4H) 7.68 (t, 2H)

Synthesis of PCN250(C3-1.4M): Solution 1, which consisted of the .720 g of Fe(NO2)3(H2O)6, 8 mL of Dimethylformamide (DMF), and 1.4M propanoic acid (1.49 mL) was heated to 100 ºC for 1 Hour. Next, Solution 2 was prepared which consisted .240 g Na4ABTC dissolved in 8 mL DMF and heat to 150ºC for 1 hour. Next, the solutions were added together in an enclosed reaction vessel (40 mL vial) and heated to 150 ºC for 12 hours. After 12 hours, the reaction was allowed to cool to room temperature and the sample was collected vial centrifugation. The products were then washed 3x with DMF with the final wash being followed by immersing the product in DMF for 12 hours. Following the 12 hours, the As Synthesized (AsSyn) MOF product was obtained. In order to remove the acid modulators/templates form the structure, 250 mg of the sample was added to a 20 mL vial. Next 8 mL of a solution of 25% glacial acetic acid and 75% DMF

was prepared was added to the vial. This solution was allowed to sit at 25 ºC, for desired time (e.g. 1hr. 12hr, 24hr, etc…). After the desired time the product was collected via centrifugation then washed 3x with DMF with the final wash being followed by immersing the product in DMF for 12 hours. This was repeated with a methanol (MeOH) wash 3x with the final wash being a solvent exchange at RT for 48 hours. Lastly, the product was dried at 75ºC for 6 hours.

Synthesis of PCN250(C6-0.7M): Solution 1, which consisted of the .720 g of Fe(NO2)3(H2O)6, 8 mL of Dimethylformamide (DMF), and 0.7M hexanoic acid (1.95 mL) was heated to 100 ºC for 1 Hour. Next, Solution 2 was prepared which consisted .240 g Na4ABTC dissolved in 8 mL DMF and heat to 150ºC for 1 hour. Next, the solutions were added together in an enclosed reaction vessel (40 mL vial) and heated to 150 ºC for 12 hours. After 12 hours, the reaction was allowed to cool to room temperature and the sample was collected vial centrifugation. The products were then washed 3x with DMF with the final wash being followed by immersing the product in DMF for 12 hours. Following the 12 hours, the As Synthesized (AsSyn) MOF product was obtained. In order to remove the acid modulators/templates form the structure, 250 mg of the sample was added to a 20 mL vial. Next 8 mL of a solution of 25% glacial acetic acid and 75% DMF was prepared was added to the vial. This solution was allowed to sit at 25 ºC, for desired time (e.g. 1hr. 12hr, 24hr, etc…). After the desired time the product was collected via centrifugation then washed 3x with DMF with the final wash being followed by immersing the product in DMF for 12 hours. This was repeated with a methanol (MeOH) wash 3x

with the final wash being a solvent exchange at RT for 48 hours. Lastly, the product was dried at 75ºC for 6 hours.

Synthesis of PCN250(C6-1.4M): Solution 1, which consisted of the .720 g of Fe(NO2)3(H2O)6, 8 mL of Dimethylformamide (DMF), and 1.4M hexanoic acid (3.90 mL) was heated to 100 ºC for 1 Hour. Next, Solution 2 was prepared which consisted .240 g Na4ABTC dissolved in 8 mL DMF and heat to 150ºC for 1 hour. Next, the solutions were added together in an enclosed reaction vessel (40 mL vial) and heated to 150 ºC for 12 hours. After 12 hours, the reaction was allowed to cool to room temperature and the sample was collected vial centrifugation. The products were then washed 3x with DMF with the final wash being followed by immersing the product in DMF for 12 hours. Following the 12 hours, the As Synthesized (AsSyn) MOF product was obtained. In order to remove the acid modulators/templates form the structure, 250 mg of the sample was added to a 20 mL vial. Next 8 mL of a solution of 25% glacial acetic acid and 75% DMF was prepared was added to the vial. This solution was allowed to sit at 25 ºC, for desired time (e.g. 1hr. 12hr, 24hr, etc…). After the desired time the product was collected via centrifugation then washed 3x with DMF with the final wash being followed by immersing the product in DMF for 12 hours. This was repeated with a methanol (MeOH) wash 3x with the final wash being a solvent exchange at RT for 48 hours. Lastly, the product was dried at 75ºC for 6 hours.

Synthesis of PCN250(C6-2.1M): Solution 1, which consisted of the .720 g of Fe(NO2)3(H2O)6, 8 mL of Dimethylformamide (DMF), and 2.1 M hexanoic acid (5.85 mL) was heated to 100 ºC for 1 Hour. Next, Solution 2 was prepared which consisted .240

g Na4ABTC dissolved in 8 mL DMF and heat to 150ºC for 1 hour. Next, the solutions were added together in an enclosed reaction vessel (40 mL vial) and heated to 150ºC for 12 hours. After 12 hours, the reaction was allowed to cool to room temperature and the sample was collected vial centrifugation. The products were then washed 3x with DMF with the final wash being followed by immersing the product in DMF for 12 hours. Following the 12 hours, the As Synthesized (AsSyn) MOF product was obtained. In order to remove the acid modulators/templates form the structure, 250 mg of the sample was added to a 20 mL vial. Next 8 mL of a solution of 25% glacial acetic acid and 75% DMF was prepared was added to the vial. This solution was allowed to sit at 25 ºC, for desired time (e.g. 1hr. 12hr, 24hr, etc…). After the desired time the product was collected via centrifugation then washed 3x with DMF with the final wash being followed by immersing the product in DMF for 12 hours. This was repeated with a methanol (MeOH) wash 3x with the final wash being a solvent exchange at RT for 48 hours. Lastly, the product was dried at 75ºC for 6 hours.

Synthesis of PCN250(C9-0.7M): Solution 1, which consisted of the .720 g of $Fe(NO_2)_3(H_2O)_6$, 8 mL of Dimethylformamide (DMF), and 0.7M nonanoic acid (2.63 mL) was heated to 100 ºC for 1 Hour. Next, Solution 2 was prepared which consisted .240 g Na4ABTC dissolved in 8 mL DMF and heat to 150ºC for 1 hour. Next, the solutions were added together in an enclosed reaction vessel (40 mL vial) and heated to 150 ºC for 12 hours. After 12 hours, the reaction was allowed to cool to room temperature and the sample was collected vial centrifugation. The products were then washed 3x with DMF with the final wash being followed by immersing the product in DMF for 12 hours.

Following the 12 hours, the As Synthesized (AsSyn) MOF product was obtained. In order to remove the acid modulators/templates form the structure, 250 mg of the sample was added to a 20 mL vial. Next 8 mL of a solution of 25% glacial acetic acid and 75% DMF was prepared was added to the vial. This solution was allowed to sit at 25 ºC, for desired time (e.g. 1hr. 12hr, 24hr, etc…). After the desired time the product was collected via centrifugation then washed 3x with DMF with the final wash being followed by immersing the product in DMF for 12 hours. This was repeated with a methanol (MeOH) wash 3x with the final wash being a solvent exchange at RT for 48 hours. Lastly, the product was dried at 75ºC for 6 hours.

Synthesis of PCN250(C9-1.4M): Solution 1, which consisted of the .720 g of Fe(NO2)3(H2O)6, 8 mL of Dimethylformamide (DMF), and 1.4M nonanoic acid (5.26 mL) was heated to 100 ºC for 1 Hour. Next, Solution 2 was prepared which consisted .240 g Na4ABTC dissolved in 8 mL DMF and heat to 150ºC for 1 hour. Next, the solutions were added together in an enclosed reaction vessel (40 mL vial) and heated to 150 ºC for 12 hours. After 12 hours, the reaction was allowed to cool to room temperature and the sample was collected vial centrifugation. The products were then washed 3x with DMF with the final wash being followed by immersing the product in DMF for 12 hours. Following the 12 hours, the As Synthesized (AsSyn) MOF product was obtained. In order to remove the acid modulators/templates form the structure, 250 mg of the sample was added to a 20 mL vial. Next 8 mL of a solution of 25% glacial acetic acid and 75% DMF was prepared was added to the vial. This solution was allowed to sit at 25 ºC, for desired time (e.g. 1hr. 12hr, 24hr, etc…). After the desired time the product was collected via

centrifugation then washed 3x with DMF with the final wash being followed by immersing the product in DMF for 12 hours. This was repeated with a methanol (MeOH) wash 3x with the final wash being a solvent exchange at RT for 48 hours. Lastly, the product was dried at 75ºC for 6 hours.

Synthesis of PCN250(C9-2.1M): Solution 1, which consisted of the .720 g of Fe(NO2)3(H2O)6, 8 mL of Dimethylformamide (DMF), and 2.1 M nonanoic acid (7.89 mL) was heated to 100ºC for 1 Hour. Next, Solution 2 was prepared which consisted .240 g Na4ABTC dissolved in 8 mL DMF and heat to 150ºC for 1 hour. Next, the solutions were added together in an enclosed reaction vessel (40 mL vial) and heated to 150 ºC for 12 hours. After 12 hours, the reaction was allowed to cool to room temperature and the sample was collected vial centrifugation. The products were then washed 3x with DMF with the final wash being followed by immersing the product in DMF for 12 hours. Following the 12 hours, the As Synthesized (AsSyn) MOF product was obtained. In order to remove the acid modulators/templates form the structure, 250 mg of the sample was added to a 20 mL vial. Next 8 mL of a solution of 25% glacial acetic acid and 75% DMF was prepared was added to the vial. This solution was allowed to sit at 25 ºC, for desired time (e.g. 1hr. 12hr, 24hr, etc…). After the desired time the product was collected via centrifugation then washed 3x with DMF with the final wash being followed by immersing the product in DMF for 12 hours. This was repeated with a methanol (MeOH) wash 3x with the final wash being a solvent exchange at RT for 48 hours. Lastly, the product was dried at 75ºC for 6 hours.

Synthesis of PCN250(C14-1.4M): Solution 1, which consisted of the .720 g of Fe(NO2)3(H2O)6, 8 mL of Dimethylformamide (DMF), and 1.4 M mystic acid (7.65 g) was heated to 100 ºC for 1 Hour. Next, Solution 2 was prepared which consisted .240 g Na4ABTC dissolved in 8 mL DMF and heat to 150ºC for 1 hour. Next, the solutions were added together in an enclosed reaction vessel (40 mL vial) and heated to 150ºC for 12 hours. After 12 hours, the reaction was allowed to cool to room temperature and the sample was collected vial centrifugation. The products were then washed 3x with DMF with the final wash being followed by immersing the product in DMF for 12 hours. Following the 12 hours, the As Synthesized (AsSyn) MOF product was obtained. In order to remove the acid modulators/templates form the structure, 250 mg of the sample was added to a 20 mL vial. Next 8 mL of a solution of 25% glacial acetic acid and 75% DMF was prepared was added to the vial. This solution was allowed to sit at 25 ºC, for desired time (e.g. 1hr. 12hr, 24hr, etc…). After the desired time the product was collected via centrifugation then washed 3x with DMF with the final wash being followed by immersing the product in DMF for 12 hours. This was repeated with a methanol (MeOH) wash 3x with the final wash being a solvent exchange at RT for 48 hours. Lastly, the product was dried at 75ºfor 6 hours.

Dye Absorption experiments: Cycle 1 was performed using 80 mg of the selected adsorbent (No further drying or activating was performed prior to starting experiments). The adsorbent was put into a 80 mL Celstir apparatus (Purchased from DWK Life Sciences) along with 80 mL of 10 mg/L dye solution (methylene blue (MB), crystal Violet (CV), rhodamine B (RB)). The apparatus was stirred using a magnetic stir plate at

approximately 200 rpm and various time points were taken during this time. For a specific time point, 1 mL of solution was removed using a 1 mL syringe and filtered through a 2 um syringe filter. This solution was diluted with 1 mL of H_20 and then a UV-Vis spectrum was obtained in order to determine the concentration of MB in solution. Following the selected time, the adsorbent was collected via centrifugation and soaked in 20 mL of DMF for 2 hours (2x) in order to desorb the dye. Next the adsorbent was solvent exchanged with Methanol (20 mL) for 12 hours and then subsequent dried in an oven at 75 ºC for 6 hours. Cycle 2 and 3 were then performed in the same manner as Cycle 1 using 60 mg and 60 mg/L of adsorbent and MB solution for Cycle 2 and 40 mg and 40 mg/L for Cycle 3.

Materials

All the reagents and solvents were commercially available and used as received or synthesized according to the literature reported procedures. 80 mL Celstir apparatus was purchased from DWK Life Sciences. Syringe Filters were purchased from VWR (Syringe Filters with Polypropylene Housing).

Instrumentation

Powder X-ray diffraction (PXRD): was carried out with a Bruker D8-Focus Bragg-Brentano X-ray Powder Diffractometer equipped with a Cu sealed tube (λ = 1.54178 Å) at 40 kV and 40 mA.

Scanning Electron Microscopy (SEM) measurements were carried out on JEOL JSM-7500F. JEOL JSM-7500F is an ultra-high-resolution field emission scanning

electron microscope (FE-SEM) equipped with a high brightness conical FE gun and a low aberration conical objective lens.

Thermal Gravimetric Analysis (TGA) was performed using a Mettler-Toledo TGA/DSC STARe-1 system which was equipped with a GC100 gas controller.

N2 sorption measurements were conducted using a Micromeritics ASAP 2020 and 2420 system.

UV-Vis spectroscopy measurements were performed using a 2mL Quartz Cuvette and a UV-2450 Spectrophotometer from Shimadzu

Dynamic Light Scattering (DLS) was performed using Malvern Zetasizer Nano-ZS and a 2mL Quartz Cuvette.

2.3 Results and Discussion

A novel synthetic approach was set up in order to introduce hierarchical pores into traditionally microporous PCN-250(Fe_3O). In the first step, a fatty acid molecule is added to the mixture of MOF components during the solvothermal process. Monocarboxylic acids with different lengths were screened to optimize the porosity of the final product (HP-MOF). As shown in Figure 3, when a 3-carbon long modulator (Propanoic Acid-C3) was used, only a microporous sample named PCN-250(C3-1.4M)-AsSyn was obtained. Through determination of surface area and pore volume of the obtained material, it was determined that PCN-250(C3-1.4M)-AsSyn adopts the exact same structure (as determined from PXRD) and porosity as the previously published PCN-250(Fe_3O)[47]. Although, C3 carboxylic acid hardly changes the structure of microporous PCN-250, the use of modulators with the length of 6 (Hexanoic Acid – C6), and 9-carbons long (Nonanoic Acid – C9) yield HP-MOFs that display high porosity and good crystallinity.

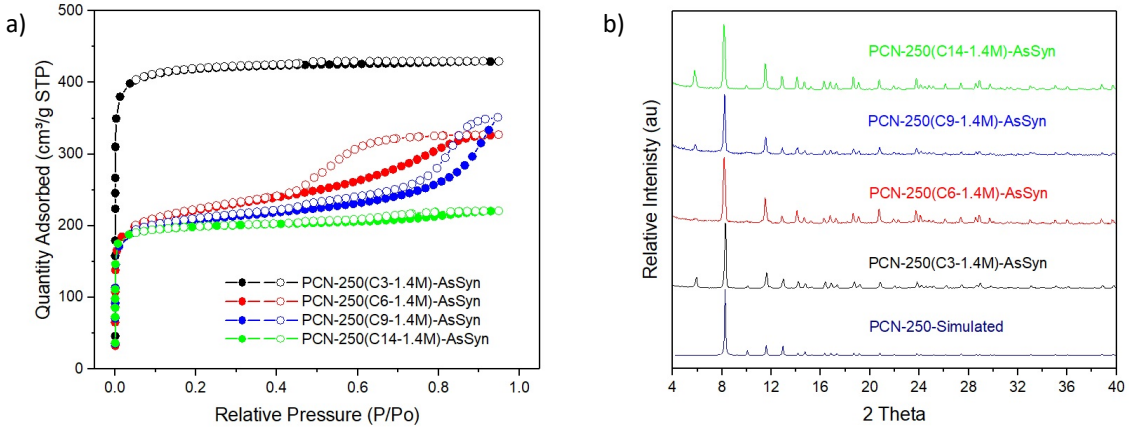

Figure 3. a)N_2 Absorption isotherm and b)Powder X-Ray Diffraction of all 4 PCN-250(CX-1.4M)-AsSyn. Ref #79

(Figure 3). In contrast, when the length of the modulator increased to 14 carbons long (Myristic Acid- C14), the obtained product displays highly decreased pore volume and surface area, when compared to its C3, C6 and C9 counterparts. Therefore, by tuning the length of the modulator (fatty acid), introducing different types of hierarchal porosity into the microporous PCN-250(Fe_3O) when using the C6 and C9 acids was successful.

Following this determination, an acetic acid-based, post-synthetic chemical etching technique was performed in order to maximize overall porosity of the hierarchally porous PCN-250(C6-1.4M)-AsSyn and PCN-250(C9-1.4M)-AsSyn samples. In this process, the acetic acid serves three purposes: 1) It acts as a replacement ligand for any monocoordinated long chain molecules/templates; 2) It helps promote the removal of any unreacted starting materials from within the pores; 3) It acts as an etching agent in order to remove areas of low crystallinity on the surface of crystals as well as remove partially connected clusters from within the structure.

Based on this method, the mesopore volume was optimized for the time of etching as shown in Figure 3. When holding the acid concentration and temperature constant, the mesopore volume changes with varying etching times. For example, as shown in Table 1, the mesopore volume for PCN-250(C6-1.4M) continuously increases from .264 cm^3/g for the As-Syn sample, to .362 cm^3/g after 30 min of etching and is maximized after 1 hour of etching at .446 cm^3/g. With further etching time, (Figure 4 and Table 1) the overall gas uptake and mesopore volume start to decrease.

	As-Syn	30 Min	1 Hour	6 Hour
PCN-250(C6-1.4M)	.264 cm^3/g	.362 cm^3/g	.446 cm^3/g	.231 cm^3/g
PCN-250(C9-1.4M)	.281 cm^3/g	.353 cm^3/g	.423 cm^3/g	.230 cm^3/g

Table 1. Pore Volume of Various Timed Etching Samples of PCN-250 etched samples. Ref #79

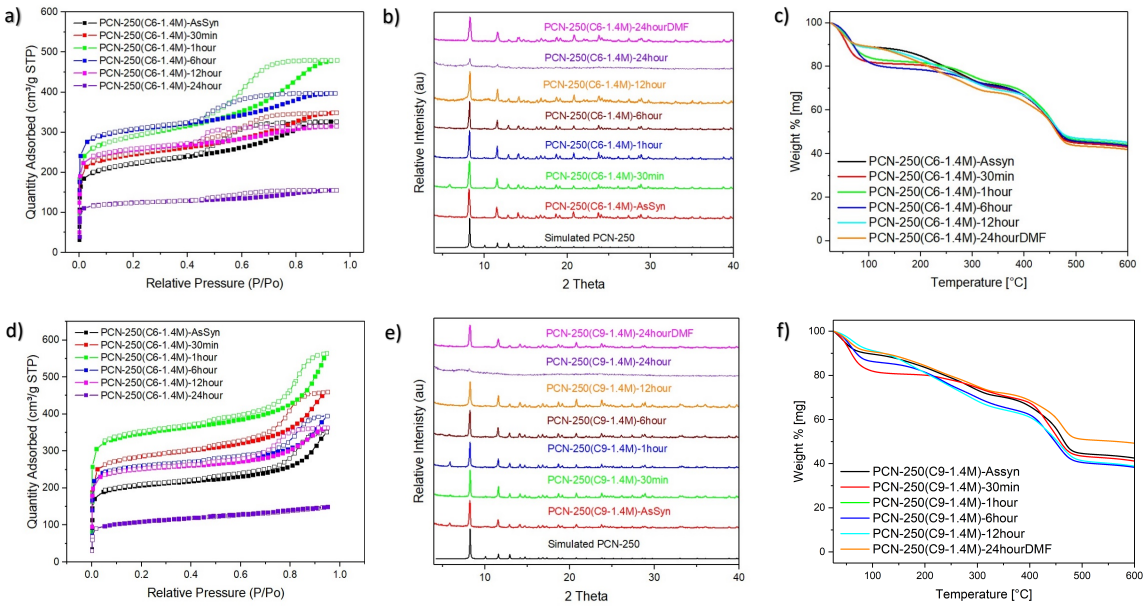

Figure 4. a)N_2 Absorption isotherm and b)Powder X-Ray Diffraction c)Thermal Gravimetric Analysis of all PCN-250(C6-1.4M) etches samples d) N_2 Absorption isotherm and e)Powder X-Ray Diffraction f)Thermal Gravimetric Analysis of all PCN-250(C9-1.4M) etches samples. Ref #79

In order to study the etching process at the atomic level, inductively coupled plasma-mass spectrometry (ICP-MS) was used in order to test the concentration of iron (Fe) present in the etching solutions. As the data shows below in Table 2, as the etching time increases, so does the concentration of iron in the etching solution. In order to verify that the iron in solution was due to etching and not due to pore cleansing of unreacted starting material, soaking the MOF sample in a DMF solution for 24 hours was performed as a control. The extremely low concentration of iron in solution, 0.43 μg/L for the C6 modulated sample and 0.42 μg/L for the C9 sample, as well as the increase in iron concentration with prolonged etching time, suggest the etching process is successful as well as tunable.

SAMPLE	IRON CONCENTRATION
PCN-250(C6-1.4M)-30MIN	53.95 μg/L
PCN-250(C6-1.4M)-1HOUR	131.25 μg/L
PCN-250(C6-1.4M)-6HOUR	158.77 μg/L
PCN-250(C6-1.4M)-12HOUR	244.57 μg/L
PCN-250(C6-1.4M)-24HOUR	1957.71 μg/L
PCN-250(C6-1.4M)-24HOUR-DMF	0.43 μg/L
PCN-250(C9-1.4M)-30MIN	78.79 μg/L
PCN-250(C9-1.4M)-1HOUR	98.62 μg/L
PCN-250(C9-1.4M)-6HOUR	112.62 μg/L
PCN-250(C9-1.4M)-12HOUR	180.64 μg/L
PCN-250(C9-1.4M)-24HOUR	1657.23 μg/L
PCN-250(C9-1.4M)-24HOUR-DMF	0.42 μg/L

Table 2. Inductively Coupled Plasma-Mass Spectrometry (ICP-MS) data for Fe concentrations in different timed etching solutions. Ref #79

The use of hexanoic acid (C6) and nonanoic acid (C9) both significantly changed the porosity of the obtained PCN-250(Fe_3O) samples by generating HP-MOFs. The optimized PCN-250(C6-1.4M) displays a clear Type IV "S-Shaped" isotherm, with a pore diameter between 4-8 nm (Figure 5d). Conversely, the optimized PCN-250(C9-1.4M) shows a Type IV isotherm, with both a 4 nm and a much larger pore diameter between 6-18 nm (Figure 5e)

In order to investigate how the concentration of fatty acids would affect the mesopore structure within the obtained MOFs, both C6 and C9 were used in three different concentrations (0.7M, 1.4M, and 2.1M). When the fatty acid of choice is used in 0.7 M [PCN-250(C6-0.7M) and PCN-250(C9-0.7M)] or 1.4M [PCN-250(C6-1.4M) and PCN-250(C9-1.4M)] concentrations, all four of the generated samples display a clear Type IV or "S-Shaped" isotherm (Figures 5a and 5c), which indicates an HP-MOF structure. However, when the acid concentration was increased to 2.1M, both PCN-250(C6-2.1M) and PCN-250(C9-2.1M) displayed a Type I isotherm (Figure 5e), indicating only microporous structures were obtained.

When taking a deeper look at the N_2 isotherms of the four different obtained HP-MOFs, differences in their desorption curves (hysteresis loops) can be seen. PCN-250(C6-0.7M), PCN-250(C9-0.7M) and PCN-250(C6-1.4M) all display a desorption hysteresis in the N_2 isotherm that is consistent with an H2-type desorption loop. H2 hysteresis desorption loops are known to signal the presence of pores with narrow mouths (Ink Bottle Pores) or internal mesopores with little to no direct connectivity to the particle surface.[50] However, PCN-250(C9-1.4M) displays another type of hysteresis, named H1. H1-type hysteresis desorption loops are reported to signal cyclical pore geometries as well as mesopores that are connected to the surface of the particle which yields the guest molecules experiencing little to no pore blocking effects.[50–53]

Furthermore, using the Barrett-Joyner-Halenda (BJH) pore size model applied to the desorption cycles, the four HP-MOFs display different pore sizes as well. PCN-250(C6-0.7M), PCN-250(C9-0.7M), and PCN-250(C6-1.4M) all display mesopore sizes of approximately 4-6 nm in diameter, while PCN-250(C9-1.4M) displays much larger mesopores of approximately 8-16 nm in diameter (Figures 5b and 5d). In addition, SEM was performed on the various samples in order to gain information on mesopore location within the MOF crystals. As shown in Figure 6f, visual mesopores or gaps can be seen on

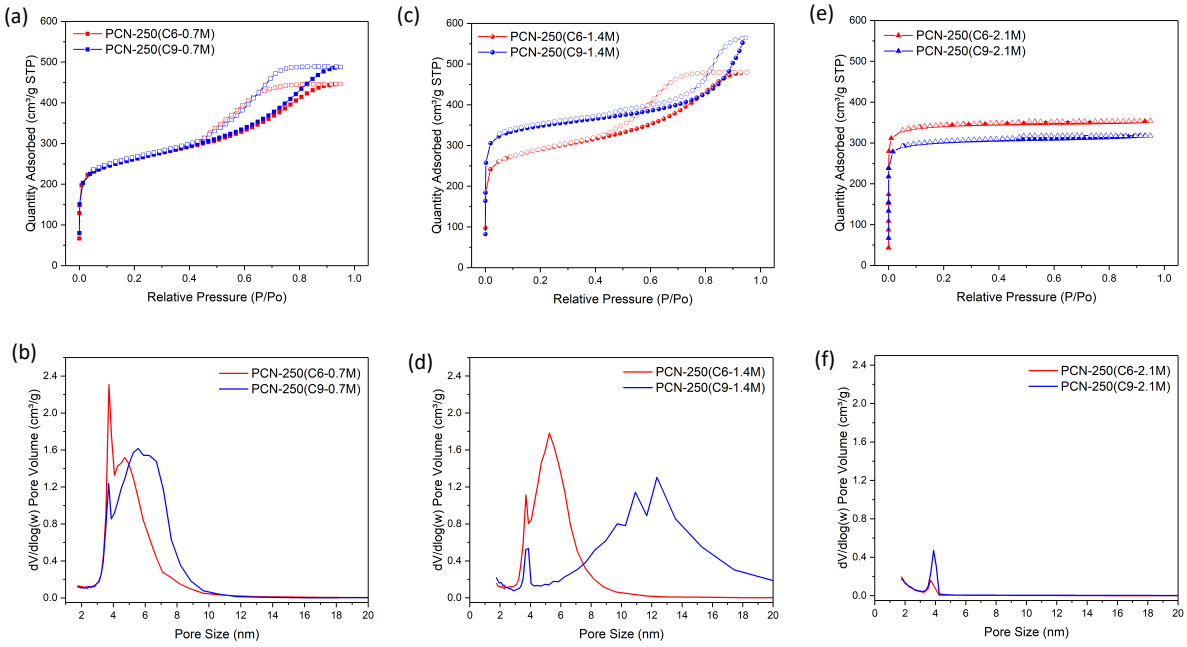

Figure 5. N_2 isotherms of various PCN-250 Samples, filled data markers (Absorption), open data markers (desorption): a) PCN-250(CX-0.7M) b) PCN-250(CX-1.4M) c) PCN-250(CX-2.1M) and Pore Size distributions using BJH Desorption Model d) PCN-250(CX-0.7M) e) PCN-250(CX-1.4M) f) PCN-250(CX-2.1M)..Ref #79

the surface of the particles of PCN-250(C9-1.4M). In contrast, PCN-250(C6-1.4M) particles (Figure 6e) display an extremely smooth surface with no visual evidence of mesopores. Furthermore, with the evidence from isotherm types, hysteresis types, pore sizes, and SEM micrographs, it has been shown that there are two distinct mesopore structures that can be obtained by varying the length and concentration of mono-carboxylic acid molecules utilized during the solvothermal synthesis.

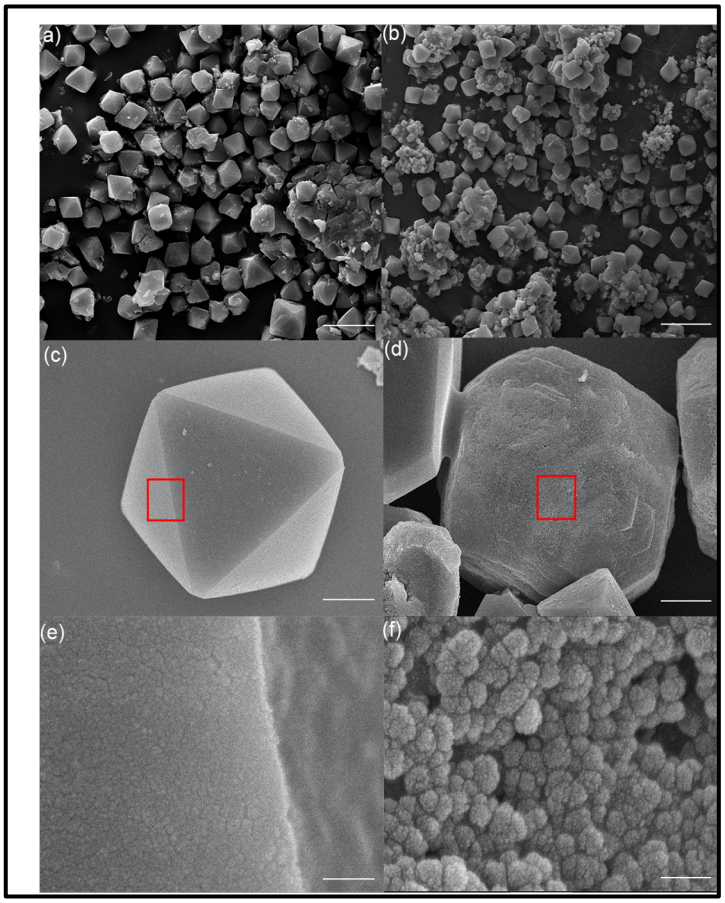

Figure 6. SEM Micrographs of (a,c,e) PCN-250-(C6-1.4M) and (b,d,f) PCN-250-(C9-1.4M) SEM Micrographs of single crystal of (c) PCN-250-(C6-1.4M) and (d) PCN-250-(C9-1.4M). Enlarged photo of red reticular zone in (c) and (d). Scale bar for (a) and (b): 50 μm. Scale bar for (c) and (d): 5 μm. Scale bar for (e) and (f): 100 nm. Ref #79

As explained in Section 2.1, it was hypothesized that there could be two different mechanisms of mesopore formation within HP-MOFs using mono-carboxylic acid molecules. The first, as shown in Figure 1, is a modulation-based mechanism, which is responsible for the structure of PCN-250(C6-0.7M), PCN-250(C9-0.7M), and PCN-250(C6-1.4M). Mechanism 2, which is thought to be responsible for the structure of PCN-250(C9-1.4M) (Figure 1) is a templating-based mechanism.

In order to examine if a templating mechanism predominates in the formation of PCN-250(C9-1.4M), it was proposed that micelles or other self-assembled aggregates could be characterized in the synthetic solutions of each MOF. In order to obtain this evidence, Dynamic Light Scattering (DLS) experiments were at 90ºC. (Experiments were performed at 90ºC due to the limitations of the DLS instrument). In order for the data to be calculated, the viscosity and refractive index of the base solvent is needed at the measurements temperature and 90ºC was the highest temperature found in the literature.[54] As shown in Table 3 no particles were observed in any of the 0.7M, 1.4M and 2.1M C3 synthetic solutions. Furthermore, in the C14 synthetic solutions, no micelle type particles were observed in 0.7M solution but were observed in the 1.4 and 2.1M solution of approximately 60 and 160 nm respectively.

Sample Name	T (°C)	Number Mean (nm)
(C3-0.7M)-1	90	0
(C3-0.7M)-2	90	0
(C3-1.4M)-1	90	0
(C3-1.4M)-2	90	0
(C3-2.1M)-1	90	0
(C3-2.1M)-2	90	0
C6-0.7M)-1	90	0
(C6-0.7M)-2	90	0
(C6-1.4M)-1	90	0
(C6-1.4M)-2	90	0
(C6-2.1M)-1	90	0
(C6-2.1M)-2	90	0
(C9-0.7M)-1	90	0
(C9-0.7M)-2	90	0
C9-1.4M)-1	90	9.89
(C9-1.4M)-2	90	11.76
(C9-2.1M)-1	90	45.27
(C9-2.1M)-2	90	44.06
(C14-0.7M)-1	90	0
(C14-0.7M)-2	90	0
(C14-1.4M)-1	90	64.09
(C14-1.4M)-2	90	55.38
(C14-2.1M)-1	90	188.4
(C14-2.1M)-2	90	132.3
DMF-Pure-1	90	0
DMF-Pure-2	90	0

Table 3. Dynamic Light Scattering (DLS) Data Table of the MOF synthetic solutions excluding the $Fe(NO)_3$-(H_2O) Ref #79

More importantly, no micelle sized particles were detected in any of the PCN-250(C6-X.XM) synthetic solutions whereas relatively small, nanometer-sized particles were detected in the PCN-250(C9-1.4M) and PCN-250(C9-2.1M). These particles are thought to be micelles generated by the self-assembly of nonanoic acid in the presence of a polar solvent such as DMF. It is believed that this data falls in line with the findings of previously reported literature that micelles can, in fact, be formed in DMF if the surfactant has the correct molecular length and concentrations, furthermore, previous reports show that the length and concentration of the surfactant (fatty acid) help govern the critical micelles concentration (cmc) and the formation of micelles in DMF, which are significantly higher than in aqueous solutions.[36,55] Lastly, for PCN-250(C9-1.4M), the micelles generated were of approximately 11 nm, which is in good agreement with the calculated pore size distribution for PCN-250(C9-1.4M).

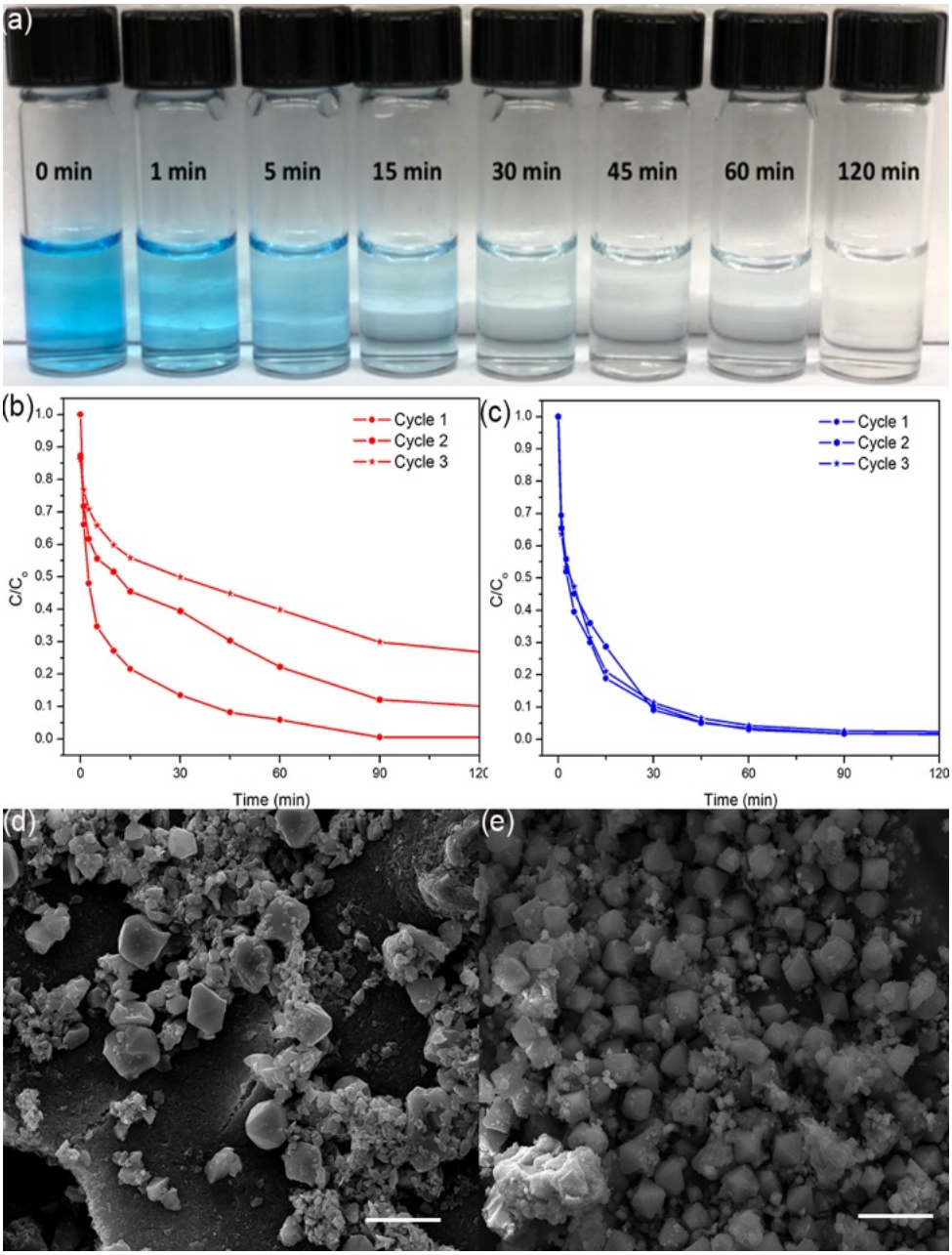

Figure 7. a) Image of Methylene Blue solution after UV-Vis measurements were taken (Diluted by 50%) for PCN-250(C9-1.4M). b) Concentration vs time plot for PCN-250(C6-1.4M) and c) PCN-250(C9-1.4M) d) SEM images post dye desorption for PCN-250(C6-1.4M) and c) PCN-250(C9-1.4M). Scale bar for (d)(e): 50 μm. Ref #79

In order to show the how the different hierarchal structures could have an impact on the applications of these MOFs, the ability PCN-250(C9-1.4M) and PCN-250(C6-1.4M) to remove organic dyes from aqueous solutions was tested. Methylene Blue (MB) was employed as a model dye, and UV-Vis spectroscopy was implemented to monitor the Absorption process of MB from an aqueous solution under vigorous stirring at ambient temperature and pressure. The initial concentration of the MB solution was 10 mg/L, and during the Absorption process, various time points were taken in order to gain an insight into the kinetics of the Absorption process. Figure 7b and 7c both show PCN-250(C6-1.4M) and PCN-250(C9-1.4M) displaying good Absorption kinetics, removing 65% and 48% of the MB, respectively, after only 5 minutes. Furthermore, after 2 hours of Absorption time, 99% removal of MB from the aqueous solution was achieved by both samples.

In order to investigate the effect the introduction of mesoporous into PCN-250(Fe_3O) would have on the dye Absorption performance, the same test was performed using a microporous PCN-250(Fe_3O). As seen from Figure 8, PCN-250(C6-1.4M) and PCN-250(C9-1.4M) significantly outperform the microporous PCN-250(Fe_3O). PCN-250(Fe_3O) can remove approximately 21% of the MB dye within the first 5 minutes, but then significantly slows down. After 1 hour and 6 hour, there was 33% and 45% MB removed, respectively. Furthermore, the Absorption capacities of PCN-250(Fe_3O), PCN-250(C6-1.4M) and PCN-250(C9-1.4M) were determined to be 97 mg/g, 112 mg/g and 136 mg/g for MB respectively. The low Absorption capacity and kinetics of the microporous

sample can be attributed to surface pore blocking, whereas the mesoporous samples do not have such limitation.

Additionally, to show the broad range of cationic dyes that PCN-250(C9-1.4M) can extract from an aqueous solution, Crystal Violet (CV) and Rhodamine B (RB) were

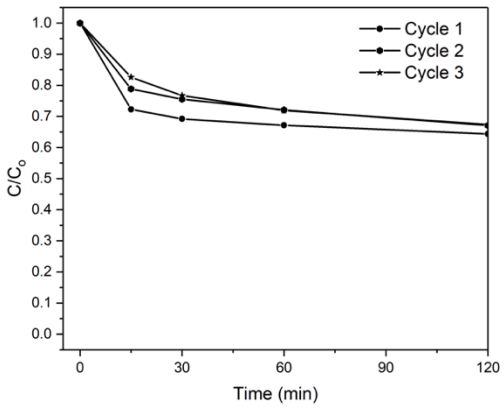

Figure 8. Microporous PCN-250(Fe_3O) Methylene Blue Dye Absorption

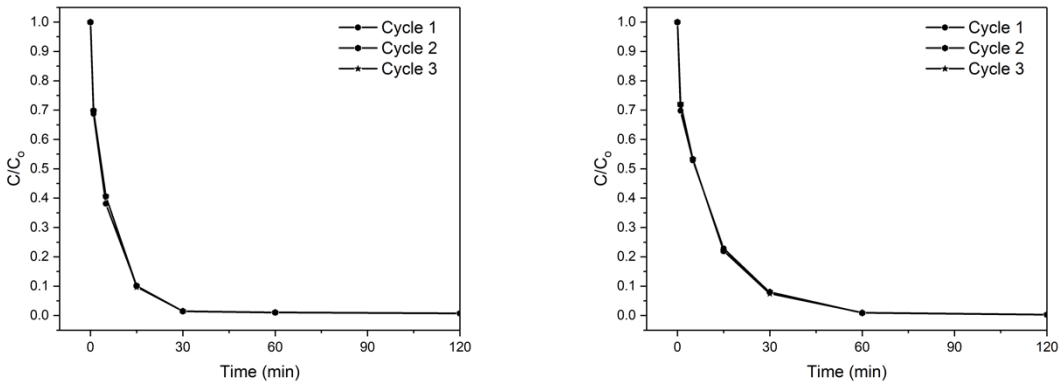

Figure 9. a) PCN-250(C9-1.4M) Crystal Violet (CV) Dye Absorption; b) PCN-250(C9-1.4M) Rhodamine B (RB) Dye Absorption. Ref #79

also tested. As seen in Figure 9, both dyes were effectively 100% sequestered in under 2 hours.

Next, the effect of the mesopore location(type) on the dye desorption process and the recyclability of the adsorbents was investigated. After the Absorption of the MB dye, the MOF samples were isolated via centrifugation and washed with 25 mL of DMF. Following the DMF wash, the samples were dried in air at 75ºC for 6 hours, then SEM micrographs were obtained and compared to the pre-Absorption micrographs. Pre-Absorption, PCN-250(C6-1.4M) and PCN-250(C9-1.4M) both had a fairly uniform particle size and morphology (Figures 6a and 6b). Following the Absorption and desorption of the dye, PCN-250(C9-1.4M) maintains its crystal integrity while PCN-250(C6-1.4M) does not (Figures 7d and 7e). It is hypothesized that the PCN-250(C6-1.4M) crystals were broken apart into various smaller sizes and shapes, due to the exothermic dye desorption process. The internal mesopores do not allow for facile dye desorption, while the presence of surface mesopores in PCN-250(C9-1.4M) does permit facile dye desorption, leading to the preservation of crystal integrity and morphology.

Due to the loss of PCN-250(C6-1.4M) crystal integrity, the dye Absorption performance also suffered. As shown in Figure 7b, PCN-250(C6-1.4M) Absorption kinetics slowed with subsequent Absorption experiments, signifying that not only does the presence of mesopores affect dye Absorption process when compared to a microporous sample, but mesopore location and access to the crystal surface also affects the recyclability of a MOF adsorbent.

2.4 Conclusion

Introducing mesoporosity into existing microporous materials is an growing area of research. Although many preparations of HP-MOFs have been developed over the last decade, the literature indicates that these techniques still have limited scope and tunability. Therefore, a system was designed in order to study the differences in modulation based methods and templating based methods.

In this system, different lengths and concentrations of fatty acids, (C3, C6, C9 and C14), which can act as either modulators or templates, were introduced into the PCN-250 synthesis. The obtained MOFs exhibit completely different porosity, with both PCN-250(C6-1.4M) and PCN-250(C9-1.4M) samples exhibiting hierarchal porosity. Through the use of Dynamic Light Scattering (DLS), it was determined that when nonanoic acid is used in 1.4M concentration or higher, the nonanoic acid molecules can forms micelles. This micelle formation dictates the generating of HP-MOF through a templating mechanism, in which PCN-250(C9-1.4M) displays both large surface and internal mesopores (6-18 nm). On the other hand, when hexanoic acid is used, due to its short length (lower than 7 carbons), it cannot form micelles, in turn yielding a HP-MOF through a modulation based mechanisms that displays smaller, only internal mesopores (4-8 nm). Although the two HP-MOFs exhibit comparable gas uptake, their dye removal behaviors are totally different due to the differences in mesopore locations. PCN-250(C9-1.4M), which has both surface and internal mesopores, displays great recyclability by removing 99% of MB over three cycles. However, PCN-250(C6-1.4M), which has only the internal

mesopores displays, poor recyclability, removing as low as 37% of MB after the third cycle.

Overall, this work offers to the best of our knowledge, the first report of micelle based templating of MOFs in Dimethylformamide (DMF) as well as an introduction to a movement of developing hierarchally porous structures of previous known MOFs for new and untested applications.

CHAPTER III

EFFECT OF ISOMORPHIC METAL SUBSTITUTION ON THE FENTON AND PHOTO-FENTONEFFICENCY OF PCN-250*

3.1 Introduction

Water treatment and purification has become a major area of interest in the chemical and environmental science communities over the last decade. This is due to the increased consumption and disposal of organic molecules such as dyes, steroids, refrigerants, antibiotics and other toxic organic chemicals. Advanced oxidation processes (AOPs) are considered a promising method for the remediation of such wastewaters.[56] One of the most efficient AOPs is the use of Fenton and photo-Fenton reactions. As shown in Figure 10, Fenton and photo-Fenton reactions typically use iron (Fe) based catalysts that react with hydrogen peroxide (H_2O_2) in order to generate hydroxide radicals (·OH), resulting in the oxidation of various pollutants into non-toxic byproducts.[57–60] Small molecule, iron based homogenous catalysts such as coordination complexes or Fe salts were originally investigated and reported as effective catalysts for these processes in the mid-late 1900's, however they displayed severe drawbacks such as a high pH-dependence, specifically with homogenous catalysts typically yielding ferric hydroxide sludge at pH values above 4.0.[61–65] Therefore, heterogeneous Fenton processes using solid catalysts,

---

* This chapter is partially reproduced with permission from: Kirchon, A.; Zhang, P.; Li, J.; Joseph, E. A.; Chen, W.; Zhou, H.-C. Effect of Isomorphic Metal Substitution on the Fenton and Photo-Fenton Degradation of Methylene Blue Using Fe-Based Metal–Organic Frameworks. *ACS Appl. Mater. Interfaces*, **2020**, 12 (8), 9292–9299. Copyright 2020 by The American Chemical Society

such as iron oxide nanoparticles, were investigated as a potential alternative. However, these nanoparticle based technologies have displayed several drawbacks such as high metal leaching, nanoparticle aggregation and high recovery costs.[61,62]

$$\textbf{Equation 1}: Fe^{2+} + H_2O_2 \rightarrow Fe^{3+} + \dot{O}H + OH^-$$

$$\textbf{Equation 2}: Fe^{3+} + H_2O_2 \rightarrow Fe^{2+} + O\dot{O}H + H^+$$

$$\textbf{Equation 3}: \dot{O}H + Organic\ Molecule \rightarrow Oxidized\ Prodocts$$

Figure 10. Fenton Chemistry Scheme

Metal-organic frameworks (MOFs) offer new opportunities for the development of Fenton type catalysts due to their chemical tunability, well-defined structures, large pore volumes and high surface areas. Compared with traditional porous solids, such as zeolites, activated carbons and mesoporous silicas, MOFs allow for the precise design of their framework structures and the tailoring of their pore environments at the molecular level.[9] Additionally, MOFs allow for the generation of composite materials such as MOF-carbon or MOF-nanoparticle composites, which have recently been reported as successful and promising candidates for eliminating the drawbacks reported for homogenous catalysts.[66–69]

One of the key aspects of MOFs is the that metal identity, metal oxidation state and even metal ratios in a mixed-metal MOF system can all be effectively tuned with precision.[47,70,71] Mixed-metal MOF systems, which are defined as MOFs that contain at

least 2 different metal ions as nodes in the same MOF phase,[72] have demonstrated promising results regarding the improved performance of MOFs in applications that range from catalysis[73] to gas storage[3] and even electron and ion transport.[74] For example, in 2018, Hmadeh and coworkers reported the synthesis of mixed-metal ZIF-8 and ZIF-67, noting that doping ZIF-8 with Co^{+2} enhances the photo-degradation of methylene blue dye under visible light irradiation.[70] More importantly, iron based-MOFs have recently shown promise in Fenton and photo-Fenton reactions. However it is predicted that there is still significant room for improvement in both reactivity and recyclability of these catalysts.[75–77] Moreover, it has been shown that substitution of iron with other transition metals in both MOFs and nanoparticles can lead to enhancement in the degradation of other organic pollutants such as phenols.[75,78]

As in the last chapter, PCN-250(Fe_3O) was researched for water based applications such as dye Absorption, it is also a promising candidate for aqueous based catalytic processes. One of the main features that distinguish PCN-250(Fe_3O) as a promising candidate as a Fenton and photo-Fenton catalyst is that it is a Fe based material with the ability to incorporate secondary metals within the cluster with a well-defined Fe:M ratio while maintaining high stability and porosity. This metal substitution can potentially allow the reaction rates to be effectively tuned [47–49,79] In order to evaluate the effects different metals can have in the Fenton and photo-Fenton reaction rates, as well as the overall viability of PCN-250 as a heterogenous catalyst, a series of mixed-metal MOFs named PCN-250(Fe_2M) (M= Ni, Co, Mn, Fe) were synthesized. Furthermore, their viability as Fenton and photo-Fenton catalysts for the degradation of methylene blue was tested.

3.2 Experimental Methods

Synthesis of H_4ABTC: H_4ABTC was synthesized according to a previously reported method.[80] In a typical procedure, 5-nitroisophtalic acid (19 g) and sodium hydroxide (50 g) were suspended in 250 mL of ultrapure water purified using a Milli-Q Water -Ultrapure Water System and reacted at 60ºC with continuous stirring for 1 hour. Next, glucose (100 g) was dissolved in 100 mL of warm ultrapure water and the resulting solution was added dropwise to the yellow slurry that became dark brown as the nitro groups were reduced. The mixture was allowed to cool down for 30 minutes, followed by exposure to a bubbling air stream for 16 hours with continuous stirring at room temperature. Next, the crude mixture was cooled in an ice bath prior to isolation of the solid by filtration with vacuum. Finally, the solid was dissolved in 250 mL of water and acidified with HCl 37% to produce an orange precipitate. H_4ABTC was isolated by filtration, thoroughly washed with water and dried in an oven (92% yield).

Preparation of preformed clusters $Fe_2M(m3\text{-}O)(CH_3COO)_6$ (M = Co, Ni, Mn, Fe): A solution of sodium acetate trihydrate (42 g, 0.31 mol) in water (70 ml) was added to a filtered, stirred solution of iron(III) nitrate nonahydrate (8 g, 0.02 mol) and the metal(II) nitrate (0.1 mol) in water 70 ml, and the brown precipitate was filtered off, washed with water and ethanol and dried in air.

Synthesis of PCN-250(Fe_2M) (M = Co, Ni, Mn, Fe): H_4ABTC (1 g), Fe_2M (Mn, Fe, Co, Ni) (1 g) and acetic acid (100 ml) in 200 ml of DMF were ultrasonically dissolved in a 500 ml Pyrex bottle. The mixture was heated in an oven at 140 °C for 12 h. After cooling down to room temperature, dark brown crystals were collected by filtration. Next

the crystals were washed according to the procedure in the reference below.[48] Finally the product was dried in a 75 °C oven for 24 hours.

Dye Absorption Experiments: 20 mg of the selected MOF adsorbent was used. (No further drying or activating was performed prior to starting experiments). The adsorbent was put into an 80 mL Celstir apparatus (Purchased from DWK Life Sciences) along with 40 mL of 15 mg/L dye solution (methylene blue (MB). The apparatus was stirred using a magnetic stir plate at approximately 200 rpm and samples were taken at various time points. For each specific time point, 1 mL of solution was removed using a 1 mL syringe and filtered through a .22 um syringe filter. This solution was diluted with 1 mL of H_2O and then a UV-Vis spectrum was obtained in order to determine the concentration of MB in solution.

Catalytic Degradation Experiments: Catalytic Degradation Experiments were performed in a constant temperature 25 °C (using a water bath) in an 80 mL Celstir apparatus (Purchased from DWK Life Sciences) which was stirred using a magnetic stir plate at approximately 200 rpm with samples removed at regular intervals. In a typical experiment, 20 mg of the MOF catalyst was used along with 40 mL of 15 mg/L dye solution methylene blue (MB) and 21 microliters of H_2O_2- 35wt%. For each sample, 1 mL of solution was removed using a 1 mL syringe and filtered through a 0.22 um syringe filter and immediately quenched with excess pure n-butanol. This solution was diluted with 1 mL of H_2O and then a UV-Vis spectrum was obtained in order to determine the concentration of MB in solution. All experiments were performed in the dark environment and with the addition of a full wavelength halogen lamp was used as the light source

for the Photo-Fenton reactions. During the reactions, the H_2O_2- 35wt% was added and light source was turned on at the zero time point, with the MOF being added to the solution starting at the -60 min timepoint.

Materials

All the reagents and solvents were commercially available. Sodium Hydroxide, 5-Nitroisophtalic acid, glucose, hydrochloric acid, sodium acetate trihydrate, iron(III) nitrate nonahydrate, manganese (II) nitrate, cobalt (II) nitrate, nickel (II) nitrate, dimethylformamide, acetic acid, ethanol and methanol were purchased from VWR, Fisher Scientific, or Sigma Aldrich and used without any further modification or purification.

Instrumentation

Powder X-ray diffraction (PXRD) was carried out with a Bruker D8-Focus Bragg-Brentano X-ray Powder Diffractometer equipped with a Cu sealed tube (λ = 1.54178 Å) at 40 kV and 40 mA.

Thermal Gravimetric Analysis (TGA) was performed using a Mettler-Toledo TGA/DSC STARe-1 system which was equipped with a GC100 gas controller.

N_2 sorption measurements were conducted using a Micromeritics ASAP 2020

Thermogravimetric Analysis (TGA) was performed with about 10 mg of the sample was heated on a Mettler-Toledo TGA/ DSC thermogravimetric analyzer from room temperature to 800 °C at a rate of 5 °C·min^{-1} under Argon flow of 20 mL· min^{-1} .

UV-Vis spectroscopy measurements were performed using a 2mL Quartz Cuvette and a UV-2450 Spectrophotometer from Shimadzu.

Inductively Coupled Plasma Mass Spectrometry (ICP-MS) - Calibration standards were prepared from certified reference standards from RICCA Chemical Company. Samples were further analyzed with a PerkinElmer NexION 300D ICP mass spectrometer. Resulting calibration curves have minimum $R^2 = 0.9999$. Additionally, to maintain accuracy, quality control samples from certified reference standards and internal standards were utilized. The individual results of the triplicate samples were averaged to determine the metal concentration.

X-ray photoelectron spectroscopy (XPS) was performed using an Omicron XPS/UPS system with Argus detector uses Omicron's DAR 400 Mg X-ray source.

Scanning Electron Microscopy (SEM) measurements were carried out on JEOL JSM-7500F. JEOL JSM-7500F is an ultra-high-resolution field emission scanning electron microscope (FE-SEM) equipped with a high brightness conical FE gun and a low aberration conical objective lens.

3.3 Results and Discussion

Following the synthesis as described in the methods section, Powder X-ray Diffraction (PXRD) measurements were performed of each PCN-250 samples to verify the PCN-250 structure. As shown in Figure 11a, all four samples display the characteristic peaks of previously published PCN-250 and matched well with the simulated pattern confirming the presence of the isostructural single-phase of PCN-250 for all four materials.[47,48]

Next, N_2 gas Absorption experiments were performed to determine the porosity and surface area of all 4 samples. As shown in Figure 11b, all four samples present a Type I isotherm of IUPAC (International Union of Pure and Applied Chemistry) classification without a discernible hysteresis loop, indicating the existence of uniform micropores in the structure.[81] The samples also displayed great porosity and high surface areas that match well with the previously published versions of PCN-250. The surface areas of PCN-250(Fe_3), PCN-250(Fe_2Ni), PCN-250(Fe_2Co) and PCN-250(Fe_2Mn) are 1460 m^2/g, 1492 m^2/g, 1428 m^2/g and 1472 m^2/g, respectively. Thermal gravimetric analysis (TGA) was also performed on the samples to determine their thermal stability. All four samples display good thermal stability up to about 420 °C, as shown in Figure 11c. Using the data from the N_2 sorption tests, TGA and PXRD analysis, it was further confirmed that all 4 samples display the same single phase of PCN-250 with all displaying high porosity and thermal stability.

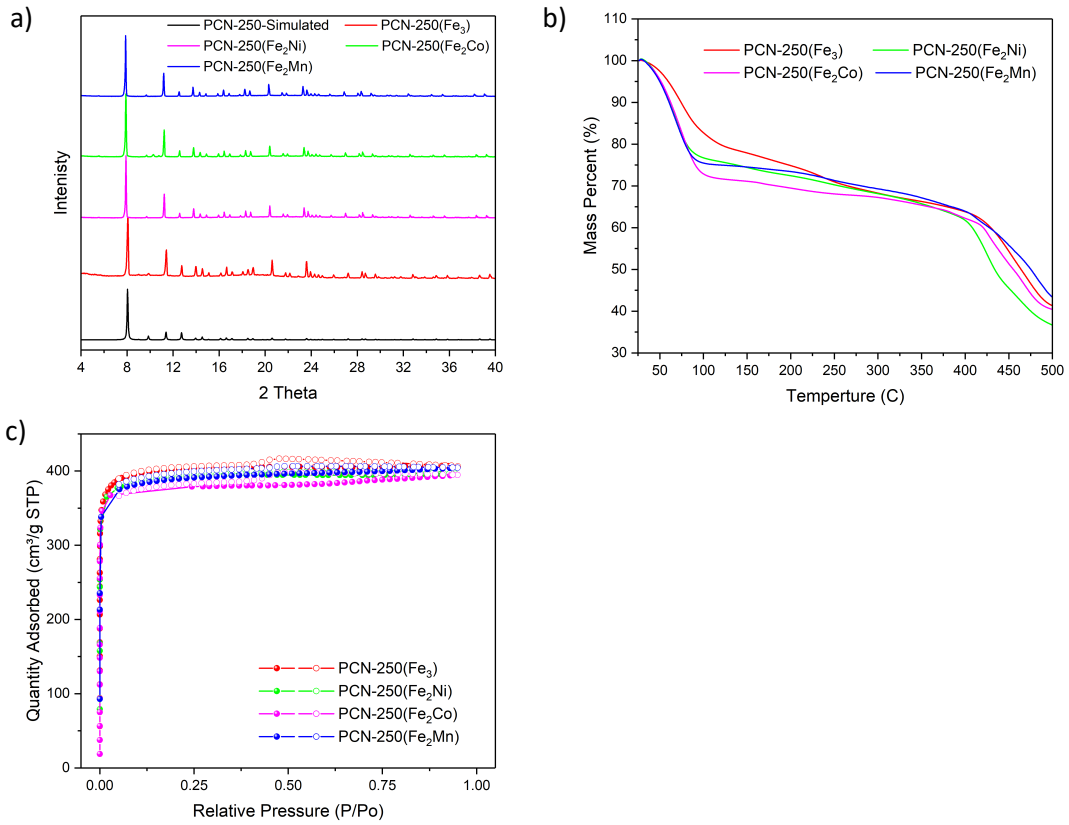

Figure 11. a) PXRD of all PCN-250 samples, b) thermal grammatic analysis, c) N_2 Absorption isotherms Ref #130

Next, Inductively Coupled Plasma-Mass Spectroscopy (ICP-MS), Scanning Electron Microscopy-Energy Dispersive X-Ray Spectroscopy (SEM-EDS), and X-ray Photoelectron Spectroscopy (XPS) were all used in order to confirm the isomorphic substitution of Mn, Co and Ni for Fe within the three mixed-metal samples. ICP-MS was performed on each sample in order to determine the metal ion ratios. As displayed in Table 4, PCN-250(Fe_3) was confirmed to be 100% iron, while the mixed-metal samples of PCN-

250(Fe_2Ni), PCN-250(Fe_2Co) and PCN-250(Fe_2Mn) displayed Iron:Metal (Fe:M) ratios of 2:1. Next, SEM-EDS was performed on each sample for two reasons. The first was to verify that all MOF samples displayed the same crystal morphology as well as similar crystal sizes. This can be seen by looking at Figure 12a, 12c, 12f, and 12i, where all four samples display a cubic octahedron shape as well as crystal sizes between approximately 2-8 microns. EDS mapping, was performed in order to verify the isomorphic and evenly distributed substitution of Mn, Co and Ni into the PCN-250 structures and was confirmed by analyzing the micrographs displayed in Figure 12e, 12h and 12k. Furthermore, the ratio of Fe:M calculated by ICP-MS was verified by the EDS mapping of metal species, with Mn, Co and Ni percentages being calculated as 33%, 37% and 33% respectively. EDS mapping of Fe within each sample, as displayed in Figures 12b, 12d, 12g, and 12j, illustrates an even distribution of Fe:M throughout the crystal samples.

Sample	Iron (Fe) Percentage	Metal (M) Percentage
PCN-250(Fe)	100 %	-
PCN-250(Fe_2Mn)	67 %	33 %
PCN-250(Fe_2Co)	67 %	33 %
PCN-250(Fe_2NI)	66 %	34 %

Table 4. Inductively Coupled Plasma- Mass Spectroscopy (ICP-MS) for mixed-metal variants of PCN-250. Ref #130

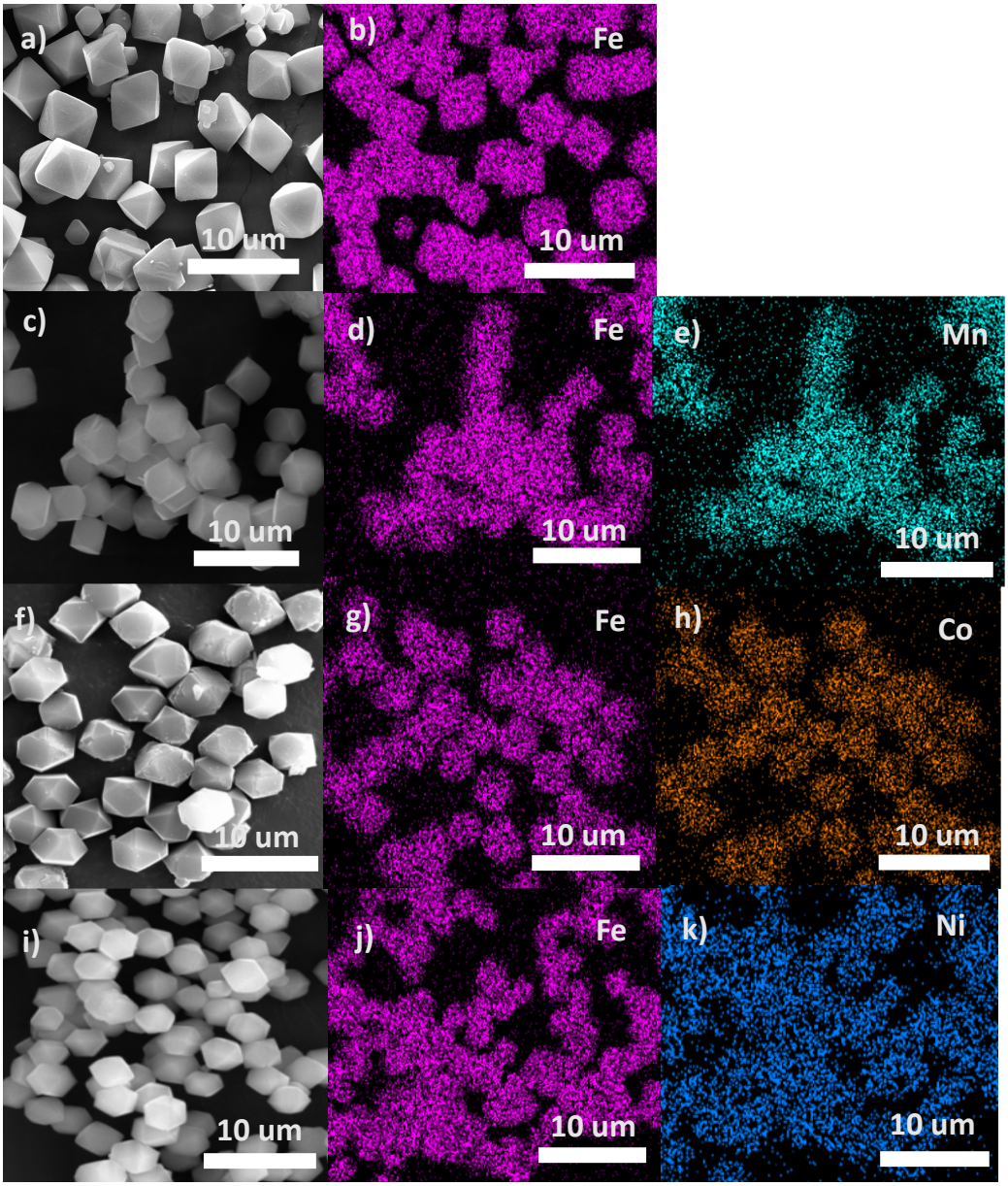

Figure 12. a) SEM micrograph of PCN-250(Fe_3), b) EDS mapping of Fe in PCN-250(Fe_3), c) SEM micrograph of PCN-250(Fe_2Mn), d) EDS mapping of Mn in PCN-250(Fe_2Mn), e) EDS mapping of Fe in PCN-250(Fe_2Mn), f) SEM micrograph of PCN-250(Fe_2Co), g) EDS mapping of Co in PCN-250(Fe_2Co), h) EDS mapping of Fe in PCN-250(Fe_2Co), i) SEM micrograph of PCN-250(Fe_2Ni), j) EDS mapping of Ni in PCN-250(Fe_2Ni), k) EDS mapping of Fe in PCN-250(Fe_2Ni). Ref #130

Finally, X-ray Photoelectron Spectroscopy (XPS) was used to further verify the isomorphic substitution of Mn, Co and Ni for Fe by identifying the chemical state and the binding energy of Fe and the secondary metals Mn/Co/Ni within the samples. The survey data for all XPS results is reported in Figure 13a. Specifically, for PCN-250(Fe_2Mn), the

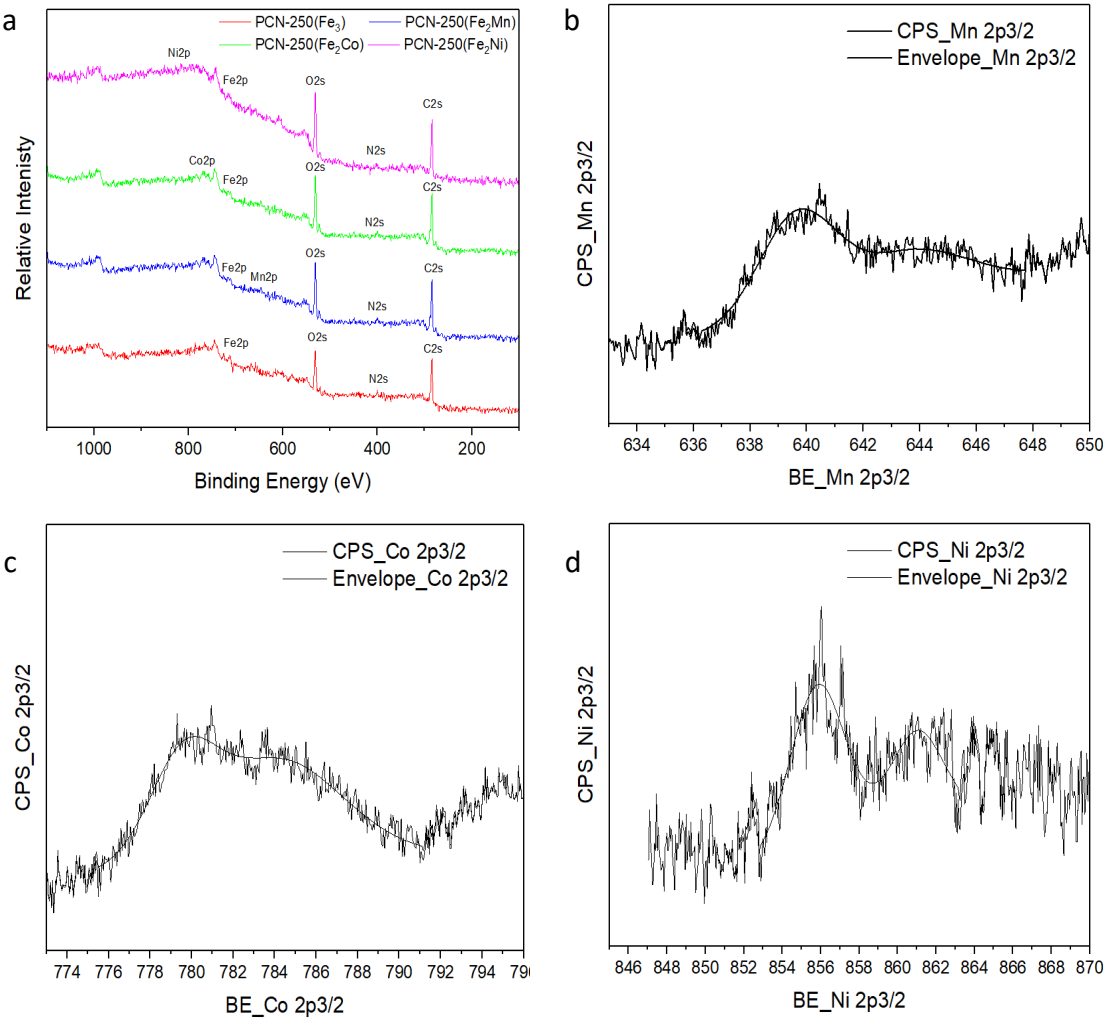

Figure 13. a) XPS survey data for all four samples; b) XPS Mn2p_3/2 data for PCN-250(Fe_2Mn); c) XPS Co2p_3/2 data for PCN-250(Fe_2Co); d) XPS Ni2p_3/2 data for PCN-250(Fe_2Ni). Ref #130

BE for the Mn 2p 3/2 orbital was determined to be 639.9 eV as display in Figure 13b. When compared to the published values found within the NIST database[82], the values obtained for PCN-250(Fe_2Mn) fall within the reported range for similar species such as Fe_2MnO_4 nanoparticles (these compounds best model the metal environment within the MOF – M_3O_4 where M = Metal Species) of 639.8 eV - 640.0 eV[83,84]. Moreover, the BE for Mn 2p 3/2 orbital of PCN-250(Fe_2Mn) has shifted from the accepted values for Mn_3O_4 of 641.5 eV - 641.6 eV[83–85]. Additionally, for PCN-250(Fe_2Co) and PCN-250(Fe_2Ni), the obtained values of 779.9 eV and 855.6 eV agree with previously reported values of Fe_2CoO_4[86] and Fe_2NiO_4[86] as reported in Figure 13c and 13d. Overall, the ICP-MS, SEM-EDS and XPS results all confirm the successful isomorphic substitution of Mn, Co and Ni for Fe within PCN-250.

In order to evaluate each samples activity for the removal and degradation of TOCs from aqueous solutions, as well as correlate the TOC removal efficiency with the bimetallic properties of each MOF, the PCN-250 samples were evaluated based on three criteria: dye Absorption, dye degradation using Fenton reaction conditions and dye degradation using photo-Fenton reaction conditions. Methylene Blue (MB) was selected as a model TOC to be used in this study because its concentration could be easily and accurately determined using UV-Vis spectroscopy. First, each sample was tested for only its dye Absorption performance (no H_2O_2 or light) and as shown in Figure 4a, all samples displayed similar dye Absorption properties. PCN-250(Fe_3) displayed a dye Absorption profile in which approximately 23% of MB was removed from the 15 mg/L (ppm) solution after approximately 120 minutes. After 120 minutes, the sample does not absorb a

significant amount of dye until the experiment was terminated at 720 minutes. This Absorption profile can be attributed to the strong Absorption of the dye within the micropores of the MOF crystals as previously reported by *Kirchon et al*[79]. Furthermore, this is also the case for all three mixed-metal samples of PCN-250 with PCN-250(Fe_2Ni), PCN-250(Fe_2Co) and PCN-250(Fe_2Mn) removing 23%, 28% and 31% of the dye respectively, indicating these MOFs have comparable dye Absorptions due to their comparable physical properties such as surface area and crystal size.

Next, the samples were tested as catalysts for Fenton and photo-Fenton reactions, specifically the degradation of MB. Iron, as laid out in numerous publications over the years, acts as a catalyst that is used to oxidize wastewater contaminants in the presence of hydrogen peroxide (H_2O_2). This process occurs when iron(II) is oxidized by hydrogen peroxide to iron(III), forming a hydroxyl radical and a hydroxide ion. Then, iron(III) is reduced back to iron(II) by another molecule of hydrogen peroxide, forming a hydroperoxyl radical and a proton. The net effect is a disproportionation of hydrogen peroxide to create two different oxygen-radical species, with water as a byproduct.[75,77,78] Furthermore, the free radicals generated by this process then engage in secondary reactions such as the non-selective oxidation of organic pollutants. In the case of photo-Fenton reactions, a light source such as a halogen lamp is used to assist in the radical generation process. As shown in Figure 4b and Figure 4c, PCN-250(Fe_3) displays decent performance for the degradation of MB under Fenton conditions removing 88% of MB after 720 minutes and when exposed to photo-Fenton reaction conditions, PCN-250(Fe_3) displayed significantly better performance, achieving 100% dye degradation after 630

minutes. In order to investigate the influence of secondary metal incorporation, all three mixed-metal variants of PCN-250 were tested under the same conditions. The results show that the catalytic degradation efficiency for both Fenton and photo-Fenton reactions can be significantly improved by the incorporation of Mn and Co, while it can be inhibited by the incorporation of Ni. Specifically, for PCN-250(Fe_2Mn), which displayed the highest catalytic degradation rates, 100% degradation of MB was achieved in 720 minutes using Fenton reaction conditions and full degradation was achieved within 300 minutes under photo-Fenton conditions. Next, in order to verify that the catalytic degradation of MB was due to the presence of the MOF in conjunction with H_2O_2 or light source and not the H_2O_2 or light source alone, two control experiments were performed in the absence of the MOF sample. The first was the same degradation experiment performed with only the H_2O_2 and the second was performed using H_2O_2 and the halogen light source. It should be noted that the MOF sample was omitted from both experiments. As shown in Figure 4d, both experiments yielded little to no dye degradation. This confirmed that the MOF, which acts the catalyst, is responsible for the catalytic process of radical generation and dye degradation.

In order to explain the behavior of these bimetallic MOF samples, the reaction mechanism proposed in various publications must be considered. [73,75,78,87,88] It is explained that the isomorphic substitution of Fe with Mn and Co ions allows for the partial electron

sharing among the Mn and Co species and the Fe through the oxo bridge resulting in a faster regeneration of Fe(II) from Fe(III), which is a limiting factor during the degradation process. On the other hand, in the case of PCN-250(Fe_2Ni), the Ni(II) species are stable during the process and cannot effectively engage in the electron sharing.[78,87]

In order to prove this claim, X-ray Photoelectron Spectroscopy (XPS) was performed on all four samples. As displayed in Figure 16, the binding energy (BE) of the

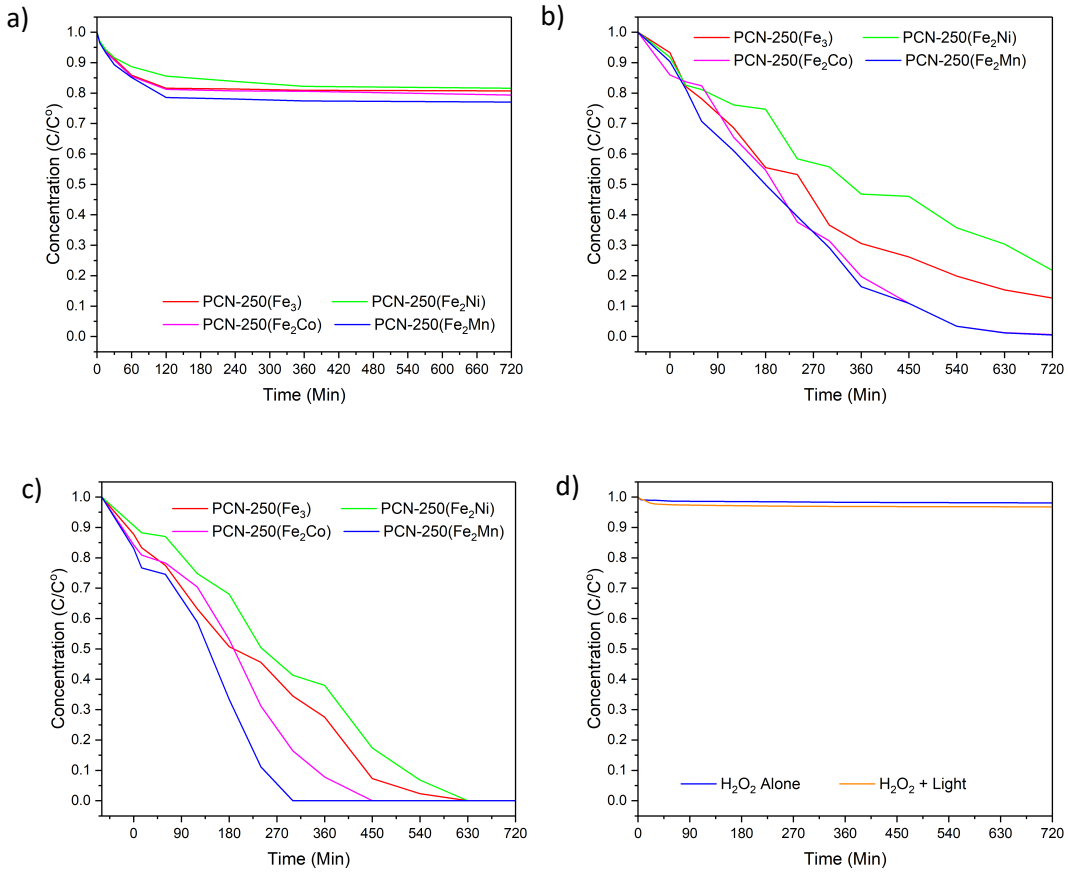

Figure 14. Methylene Blue a) Absorption, b) Fenton Reaction, c) Photo-Fenton Reaction d) Control experiments run with PCN-250(Fe2Mn)using only H_2O_2 or light source. Ref #130

Fe $2p_{3/2}$ for the all Fe sample named PCN-250(Fe_3) was determined to be 711.2 eV. As for the mixed-metal samples, the binding energy for Fe $2p_{3/2}$ was measured as 710.9 eV, 711.1 eV and 712.0 eV for PCN-250(Fe_2Mn), PCN-250(Fe_2Co) and PCN-250(Fe_2Ni), respectively. The shift of BE indicated the strong interaction between the Fe and the substituted metal species, validating the isomorphic substitution of Mn, Co, and Ni into PCN-250. Also, the shift of BE follows the same order of electronegativity that Mn < Co < Ni. The less electronegative Mn (1.55) species keep Fe electro-rich, thus moving the peak to lower BE. On the contrast, the more electronegative Ni (1.91) species leads to electro-deficient Fe and higher BE. The lower BE for the PCN-250 samples allows for an easier and quicker transition between oxidation states during the Fenton catalytic process. Therefore, it is expected from this XPS data that PCN-250(Fe_2Mn) should be the best catalyst, which agrees with the experimental data.

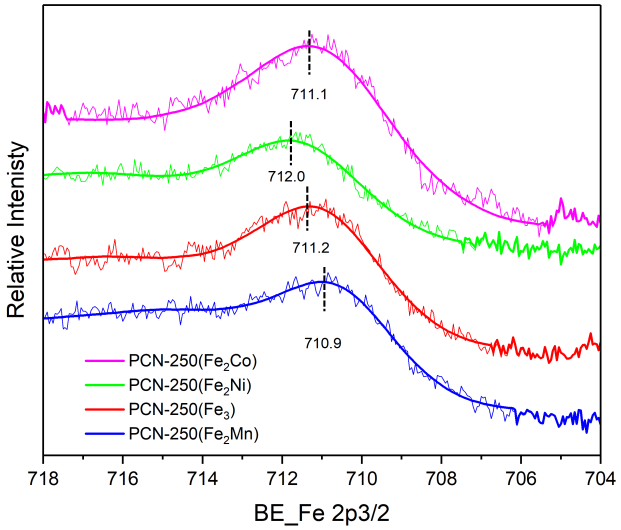

Figure 15. X-ray Photoelectron Spectroscopy (XPS) data for Fe $2p_{3/2}$ for all four PCN-250 samples. Ref #130

Furthermore, post-reaction PXRD and SEM analysis were performed on each sample in order to verify that the MOF structure remained intact during the photo-Fenton degradation process. As shown in Figure 16 and Figure 17, the PXRD patterns and SEM micrographs all match with the pre-catalytic analysis. Finally, ICP-MS tests were performed on the reaction supernatant of the photo-Fenton degradation reactions in order to determine if metal leaching from the MOF occurs during the reaction process. As reported in Table 5, an extremely low concentration of each metal was detected ([M] < 1 mg/L) (except for Ni from the PCN-250(Fe_2Ni) sample). Due to the proportion of MOF used (20 mg) during the reaction, it was determined that no significant metal leaching occurs as compared to previous reports of metal leaching within MOF-Fenton systems.[65] Overall, the data obtained confirmed that PCN-250 is stable under the Fenton and photo-Fenton reaction conditions.

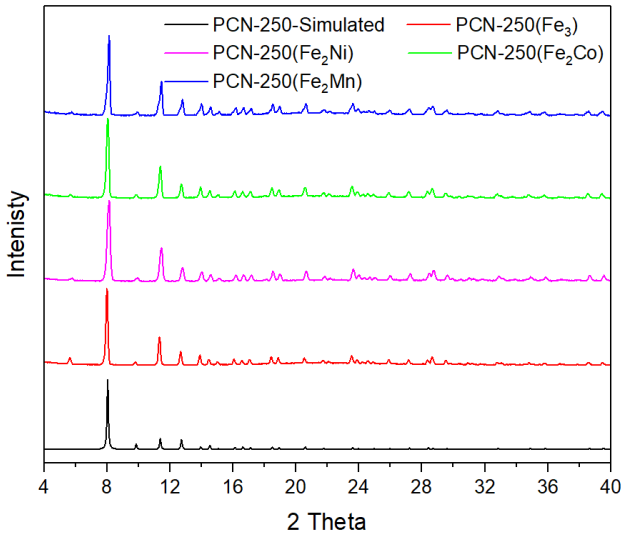

Figure 16. PXRD of PCN-250 samples post reaction. Ref #130

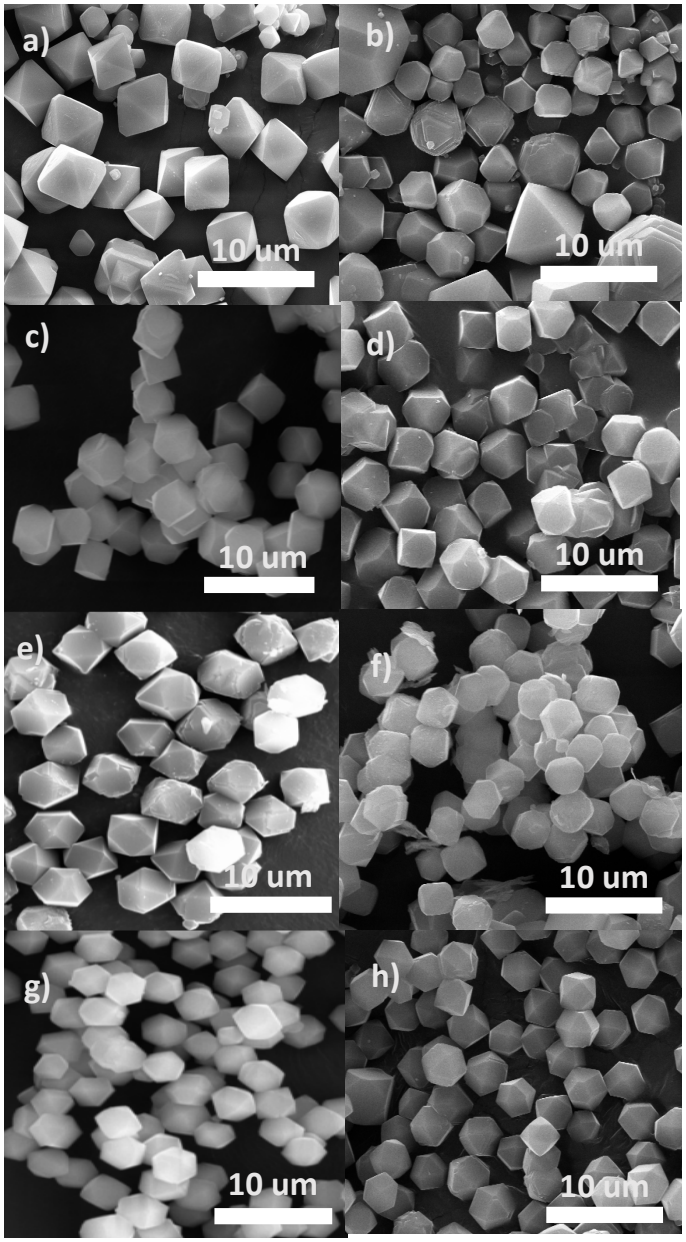

Figure 17. SEM micrographs of Pre- and Post- photo-Fenton reaction a) PCN-250(Fe_3) Pre-reaction; b) PCN-250(Fe_2Mn) Pre-reaction; c) PCN-250(Fe_2Co) Pre-reaction; d) PCN-250(Fe_2Ni) Pre-reaction; e) PCN-250(Fe_3) Post-reaction; f) PCN-250(Fe_2Mn) Post-reaction; g) PCN-250(Fe_2Co) Post-reaction; h) PCN-250(Fe_2Ni) Post-reaction. Ref #130

Sample	Analyte	Conc.	Units
PCN-250(Fe_3)	Fe	0.020	mg/L
PCN-250(Fe_2Mn)	Fe	0.004	mg/L
	Mn	0.001	mg/L
PCN-250(Fe_2Co)	Fe	0.743	mg/L
	Co	12.051	mg/L
PCN-250(Fe_2Ni)	Fe	0.004	mg/L
	Ni	0.002	mg/L

Table 5. ICP-MS data post-reaction supernatant for photo-Fenton reaction for all 4 samples. Ref #130

With the PCN-250(Fe_2Mn) sample displaying the best performance in the photo-Fenton reactions, its reusability and cyclability was tested by performing three cycles with the same MOF catalyst. After each cycle the MOF was filtered and washed with 50 mL of DMF to fully remove the dye. Subsequently the MOF was solvent exchanged with water to remove the DMF from the structure and dried in an oven at 70°C for 12 hours in order to prepare the sample for its next cycle. As shown in Figure 6, PCN-250(Fe_2Mn) displays little to no loss of activity after 3 cycles, still degrading 100% of the MB in an aqueous solution in approximately 300 min.

Several other Fe-based MOFs have been reported as Fenton and photo-Fenton type catalysts including MIL-53[40,41], MIL-100[25,42,43], MIL-88B[24] and Fe-bpydc[44]. These reports were compared to PCN-250(Fe_3) and PCN-250(Fe_2Mn) as both Fenton and photo-Fenton catalysts as shown Table 6. MIL-100(Fe) was reported as a photo-Fenton type catalyst by Zhao et al in 2015 and it was reported that MIL-100(Fe) could catalyze the degradation of

46.0% of Methylene Blue after 240 min at 25°C using 1.0 g/L MOF loading, 500 mg/L solution of MB and 40 mM H_2O_2[43]. Moreover, using the Fenton process at 30°C, Martinez et al reported MIL-100(Fe) could catalyze the degradation of 93.6% of Methylene Blue after 60 min using 0.6 g/L MOF loading, 500 mg/L solution of MB and 7.4 mM H_2O_2[42]. Moreover, Guo et al reported MIL-53(Fe) and several of its derivatives as Fenton type catalysts for the degradation of phenol. In 2015, they reported a mixed valent Fe(II) and Fe(III) variant of MIL-53 which could degrade 90.0% after 180 min at 35°C[39] and then in 2017 they reported a mixed-metal Fe/Mn variant named Fe/Mn-MOF-71 which could degrade 99.9% after 180 min also at 35°C [23]. Overall, the performance of both PCN-250(Fe3) and PCN-250(Fe2Mn) are competitive when compared to the previously reported catalysts, but without a standard reaction temperature, catalysts loading, TOC type and even TOC concentration, full and direct comparison of these MOFs is quite challenging.

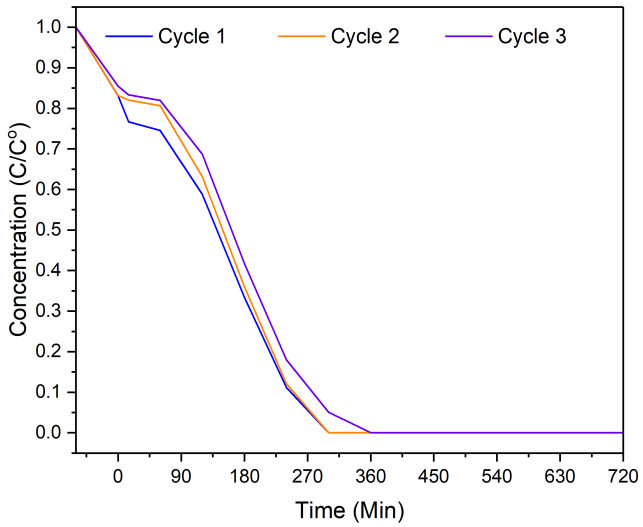

Figure 18. Cycling catalytic degradation data for PCN-250(Fe_2Mn). Ref #130

MOF	[CAT] (g/L)	TOC type	[TOC] (mg/L)	Removal Efficiency	Reaction Type	Temp (°C)	Ref
PCN-250(Fe_3)	0.5	MB	15	88% after 720 min	Fenton	25	This work
PCN-250(Fe_2Mn)	0.5	MB	15	100% after 720 min	Fenton	25	This work
Fe/Mn-MOF-71	0.4	Phenol	1000	99.9% 180 min	Fenton	35	75
Fe(BDC)(DMF)(F)	0.06	Phenol	1000	90.0% 180 min	Fenton	35	76
Fe-bpydc	0.01	Phenol	23.5	90% after 120 min	Fenton	25	44
MIL-100	0.5	SMT	20	100% after 180 min	Fenton	25	25
MIL-100	0.6	MB	500	93.6% after 60min	Fenton	30	42
MIL-88B	0.1	Phenol	50	99% after 30 min	Fenton	20	24
MIL-100	1.0	MB	500	46.0% after 240 min	photo-Fenton	25	43
MIL-53(Fe)	0.1	CA & CBZ	40	98.2% / 90.0% after 270 min	photo-Fenton	25	40
MIL-53(Fe)	0.1	RhB	10	98% after 50 min	photo-Fenton	25	41
PCN-250(Fe_3)	0.5	MB	15	100% after 630 min	photo-Fenton	25	This work
PCN-250(Fe_2Mn)	0.5	MB	15	100% after 290 min	photo-Fenton	25	This work

Table 6. Comparison of Fe-based MOF used for Fenton and photo-Fenton reactions for the degradation of different TOCs; MB = Methylene blue, SMT = sulfamethazine, CA = clofibric acid, CBZ = carbamazepine, RhB = rhodamine B. Ref #130

3.4 Conclusion

In conclusion, 4 different variants of PCN-250 were synthesized and named PCN-250(Fe_3), PCN-250(Fe_2Ni), PCN-250(Fe_2Co) and PCN-250(Fe_2Mn). The results show that the catalytic degradation efficiency for both Fenton and photo-Fenton reactions can be improved by the incorporation of Mn and Co, while it can be inhibited by the incorporation of Ni. Furthermore, the Mn substituted samples display good recyclability over 3 cycles demonstrating that the highly-porous and robust PCN-250 has potential to be used for Fenton and photo-Fenton reactions in water purification applications as well as other aqueous based catalytic processes. Overall, this work successfully demonstrates the ability to not only perform isomorphic substitution of various metals within MOFs, but also demonstrates the effect of the substitution on resulting catalytic performance.

CHAPTER IV

CATALTIC DEGREDATION OF PER- AND POLYFLUROALKYL SUBSTANCES USING TI-BASED METAL-ORGANIC FRAMEWORKS

4.1 Introduction

As mentioned in the previous two chapters, the presence of toxic organic compounds (TOCs) in the world's water systems is becoming a very difficult problem to solve. Emerging contaminants such as per- and polyfluoroalkyl substances (PFAS) are rapidly accumulating in soils, sediments and water bodies, threatening the health of wild lives and humans. For example, perfluorooctanoic acid (PFOA) and perfluorooctanesulfonic acid (PFOS) are now ubiquitous in the environment. Research has shown that PFOA and PFOS exert multiple toxic effects on humans including immunotoxicity, hepatotoxicity, developmental toxicity and carcinogenicity.[6] Moreover, PFOS was listed in the international Stockholm Convention on persistent organic pollutants as an Annex B substance, and PFOA has been named as a new candidate under the same framework. [89–92]

Remediation of soil and groundwater contaminated by these PFAS type chemicals is extremely challenging for two main reasons. The first is that the pure volume of the contaminated soil and groundwater and the relatively low concentrations of these contaminants. For example, the US Environmental Protection Agency (EPA) suggests that the concentration of PFAS such as PFOA and PFOS in water systems should be below 0.07 parts-per-billion (ppb). Therefore conventional water purification methods such as

using activated carbon filtrations are not efficient enough to remove such low levels of containments. [90,93,94]

The second reason is that fluorinated chemicals such as PFOA or PFOS are extremely stable compounds. The high electronegativity of fluorine (4.0 for F vs. 2.5 for carbon) yields a significant dipole moment to the bond where the electron density is concentrated around the fluorine, leaving the carbon relatively electron deficient ($C^{\delta+}$ - $F^{\delta-}$). This bond, which is labeled as "the strongest in organic chemistry", has a bond dissociation energy (BDE) of up to 544 kJ/mol. This strength of the carbon fluorine bond is the reason for such extreme thermal and chemical stabilities. Although this is great for their applications in water-repellent fabrics, nonstick products (e.g., Teflon), polishes, waxes, paints, cleaning products, and fire-fighting foams, it is extremely disadvantageous for remediation efforts. [94,95]

It was first reported in the early 1950's and validated in the 1970's that PFAS were resistant to biological based degradation methods such as using micro-organisms (yeast) to decompose the chemicals, whereas the non-fluorinated variant of PFAS were degraded Unfortunately, the overall toxicity of PFAS was not well-known or understood until the late 1970's when 3M, the major manufacturer of these chemicals, released several reports of PFAS toxicity in rats, mice, monkeys and aquatic invertebrates. But it wasn't until the 1990's and early 2000's that the research into PFAS remediation accelerated. [96–99]

Two distinct research disciplines have emerged for PFAS remediation: adsorptive removal and molecular degradation. Over the last 20 years, many different types of materials have been tested and engineered for the adsorptive removal of PFAS such as

carbon nanotubes, porous silicas, polymer resins, zeolites and even more recently, Metal-Organic Frameworks.[100–106] Although these materials have been proven successful at PFAS removal, the major drawback at the industrial water processing scale is the cost for material regeneration when their Absorption capacity has been exhausted. For example, the successful chemical regeneration of materials such as zeolites, polymer resins and organic modified silicas can only be achieved using a combination of sodium salts or ammonium salts (NaOH, NaCl, NH_4Cl, NH_4OH) and organic solvents (such as CH_3OH, C_2H_5OH and C_3H_6O). [107–111]

Due to this high cost of regeneration, the major focus of PFAS remediation research has shifted to developing systems that can not only remove but degrade PFAS. Advanced Oxidation Processes (AOP), which consist of using reagents such as ozone (O_3), O_3/UV, O_3/H_2O_2, and even H_2O_2/Fe^{2+} (Fenton's reagent) as described in Chapter III, were some of the earliest systems studied for PFAS degradation. Although, the hydroxyl radical (·OH), which is the typical active species in AOPs, has a standard redox potential of 2.80 V, it is ineffective at breaking C-F bonds. C-F bonds are known as the strongest in organic chemistry with a redox potential (F to F^-) of 2.87 V. As a result, AOPs such as Fenton and photo-Fenton reactions are not suitable candidates for PFAS degradation. [56,112,113]

On the other hand, Advanced Reduction Processes (ARPs) have been shown to be effective at the degradation and even mineralization (full degradation to small nontoxic molecules and ions such as CO_2, H^+, F^- of PFAS. The terms ARP was first used in the late 1990's to describe the degradation of high oxidized organic species such as vinyl chloride, perchlorate, bromates, nitrates, chromium(VI) ions and even chloro-phenols. Special

attention has been recently directed to ARPs due to their capability to effectively degrade PFAS in water.[91,114–117] When using heterogenous supports (e.g. TiO_2, Ga_2O_3, In_2O_3), ARPs consist of using an activation method such as photolysis, radiolysis, and sonolysis that generates e^-, h^+ pair as shown below in Figure 19. Once generated, the e^- and h^+ pair will separate into a free e^- and a free h^+. The free hydrated electron (e^-) has high reduction capacity (-2.9 V) which can react and degrade PFAS directly. In addition, h^+ reacts with H_2O in the solution and produces hydroxyl radicals which can also degrade PFAS degradation products that have already been reduced, potentially achieving full PFAS mineralization. [91,118–120]

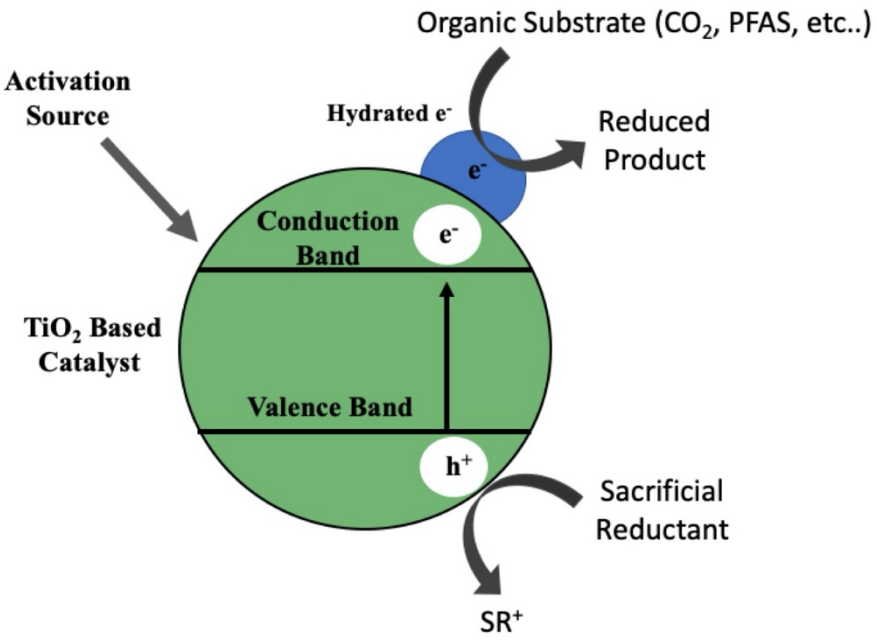

Figure 19. Schematic illustration of PFAS degradation using TiO_2 photocatalyst

As previous mentioned, TiO_2 based photo-catalysts have been shown to be effective for PFAS degradation. For example, in 2015, Chen and coworkers reported that TiO_2-MWCNT composite material that could degrade 90% of PFAS in 480 min. [121]Furthermore, in 2016 Li and Coworkers reported a series of TiO_2 modified nobel metal nanoparticles (Pt, Pd, Ag) which can degrade up to 99% of PFAs within 300 minutes. Although these materials are successful at the degradation of PFAS, they suffer from the typical drawbacks of using nanoparticles in large scale catalytic processes such as pore recyclability, loss of activity over time due to nanoparticle aggregation and even the use of expensive and impractical metals such as Pd and Pt in order to achieve high degradation efficiencies. [122]

As shown in Chapter III, MOFs are a terrific platform for developing sustainable and efficient photo-catalysts that can overcome the drawbacks of nanoparticle based technologies. Similar to that of Fe-based MOFs, Ti-based MOFs show tremendous stability in both acidic and basic aqueous conditions due to their strong binding energy with carboxylate based linkers The first Ti-MOFs showing attractive photochemical responses were MIL-125 and its amino-analogue, MIL-125-NH_2. They have been reported to be successful photo-catalysts for a broad range of reactions such as CO_2 reduction, H_2 generation from water splitting, Photocatalytic polymerizations and even TOC degradation reactions. [114,123,124] Based on these reports, the work within this chapter aims to investigate a Ti-based MOF named MIL-177-HT for the application in the degradation of PFAS, specifically PFOA. [23]

4.2 Experimental Methods

Synthesis of H_4mdip: 33 grams (0.20 mol) of isophthalic acid and 3.1 grams of paraformaldehyde (0.10 mol) were dissolved in 100 ml of fuming sulfuric acid (20-24%). The resulting solution was refluxed at 115 °C overnight. After cooled down, it was carefully poured on chilled water and forming precipitate was filtered. Then, the solid was hydrolyzed either with hydrochloric acid in methanol or with sodium hydroxide in methanol and acidified with hydrochloric acid in methanol. Then the product is filtered and dried, and then recrystallized from ethyl acetate (yield: 16.0 grams, 0.047 mol,47%). HNMR(300MHz,DMSO D6)δ4.28(s,2H),δ8.08(s,4H),δ8.31 (s,2H), δ 13.26 (s, 4H).

Synthesis of MIL-177-LT: To a 25 mL round bottom flask, H_4mdip (200 mg, 0.58 mmol) and formic acid (10 mL) were added and stirred at room temperature until the solid dispersed uniformly. Then $Ti(iPrO)_4$ (400 μL, 1.32 mmol) was added dropwise, to avoid formation of large pieces of white precipitate. Afterward, the reaction mixture was heated under reflux for 24 h. After cooling to room temperature, the white solid product was filtered under reduced pressure and washed with ethanol. Large-scale synthesis (such as 10 or 100 g scales) can easily be achieved with this method.

Synthesis of MIL-177-HT: The solid MIL-177-LT compound (200 mg) was ground into a fine powder, transferred to a Petri dish and dispersed uniformly, forming a thin layer. The MIL-177-LT powder was then heated to 280 °C for 12 h, forming the MIL-177-HT structure as a dark yellow powder.

PFOA Absorption : Either 1.0 g/L, 2.5 g/L or 5.0 g/L (80 mg, 200 mg, or 400 mg) of MIL-177-HT was used. (No further drying or activating was performed prior to

starting experiments). The adsorbent was put into an 80 mL Celstir apparatus (Purchased from DWK Life Sciences) along with 80 mL of 100 ppb PFOA solution, 1.0%, 2.5% or 5.0% TEOA (0.8 mL, 2.0 mL or 4.0 mL) and covered in Aluminum foil in order to prevent light activation of the catalyst. The apparatus was stirred using a magnetic stir plate at approximately 200 rpm and samples were taken at various time points. For each specific time point, 1 mL of solution was removed using a 1 mL syringe and centrifuged at 10000 rpm in order to remove MOF from solution. This solution was directly used in LC-MS analysis in order to determine PFOA concentration.

PFOA Degradation: Either 1.0 g/L, 2.5 g/L or 5.0 g/L (150 mg, 375 mg, or 750 mg) of MIL-177-HT was used. (No further drying or activating was performed prior to starting experiments). The adsorbent was put into an 400 mL photo-reactor apparatus (Purchased from Ace Glass) along with 150 mL of 100 ppb PFOA solution, 1.0%, 2.5% or 5.0% TEOA (1.5 mL, 3.75 mL or 7.5 mL). The apparatus was stirred using a magnetic stir plate at approximately 200 rpm with 450 watts Hg-Vapor Light source (185 nm – 600 nm) and samples were taken at various time points. For each specific time point, 1 mL of solution was removed using a 1 mL syringe and centrifuged at 10000 rpm in order to remove MOF from solution. This solution was directly used in LC-MS analysis in order to determine PFOA concentration.

Liquid Chromatography - Mass Spectroscopy (LC-MS) Quantitative Analysis of PFOA in Both Absorption and Degradation Reactions: The target compounds (PFOA) in samples were detected and quantified on a triple quadrupole mass spectrometer (Altis, Thermo Scientific, Waltham, MA) coupled to a binary pump HPLC

(Vanquish, Thermo Scientific). MS parameters were optimized for the target compound under direct infusion at 5 µL min^{-1} to identify the SRM transitions (precursor/product fragment ion pair) with the highest intensity (Table 7). Samples were maintained at 4 °C on an autosampler before injection. The injection volume was 10 µL. Chromatographic separation was achieved on a Hypersil Gold 5 µm 50 x 3 mm column (Thermo Scientific) maintained at 30 °C using an 8-minute solvent gradient method. Solvent A was water (0.1% formic acid). Solvent B was acetonitrile (0.1% formic acid). The flow rate was 0.5 mL min^{-1}. Sample acquisition and analysis was performed with TraceFinder 3.3 (Thermo Scientific).

Compound	Polarity	Precursor (m/z)	Product (m/z)	Collision Energy (V)	RF Lens (V)
PFOA	Negative	413.000	368.988	10.23	42

Table 7. Quantitative SRM Transitions for compounds

Fluoride Ion Measurements: Fluoride Ion measurements were taken using a Thermo Fisher Orion Star A214 pH/ISE meter using a Thermo Scientific Orion Fluoride Selective Electrode. Standard curves were built using a 1ppm, 2ppm and 10 ppm stock solutions. Each sample and standard solution was used in a 1:1 ratio of sample and TISIB II with CDTA total ionic strength adjustment buffer. Prior to measurements of samples, MOF was removed from solution using centrifugation at 6000 rpm. All measurements were taken 5 times in order to obtain reported value and error.

Materials

Paraformaldehyde, isophthalic acid, formic acid, Sodium Hydroxide hydrochloric acid, fuming sulfuric acid titanium isopropoxide, perfluorooctanoic acid, dimethylformamide, ethanol and methanol were purchased from VWR, Fisher Scientific, or Sigma Aldrich and used without any further modification or purification.

Instrumentation

Powder X-ray diffraction (PXRD) was carried out with a Bruker D8-Focus Bragg-Brentano X-ray Powder Diffractometer equipped with a Cu sealed tube (λ = 1.54178 Å) at 40 kV and 40 mA.

Thermal Gravimetric Analysis (TGA) was performed using a Mettler-Toledo TGA/DSC STARe-1 system which was equipped with a GC100 gas controller. Thermogravimetric Analysis (TGA) was performed with about 10 mg of the sample was heated on a Mettler-Toledo TGA/ DSC thermogravimetric analyzer from room temperature to 800 °C at a rate of 5 °C·min^{-1} under Argon flow of 20 mL· min^{-1} .

N_2 sorption measurements were conducted using a Micromeritics ASAP 2020 using 99.99% purity N_2 gas

Scanning Electron Microscopy (SEM) measurements were carried out on JEOL JSM-7500F. JEOL JSM-7500F is an ultra-high-resolution field emission scanning electron microscope (FE-SEM) equipped with a high brightness conical FE gun and a low aberration conical objective lens.

4.3 Results and Discussion

As previous reported by Fu and coworkers in 2012, a Ti-based MOF named MIL-125-NH_2, was used in pair with triethanolamine (TEOA) as a sacrificial reductant in order to achieve the photocatalytic reduction of CO_2 to the formate anion under visible light irradiation. Based on this report, as shown in Figure 20, TEOA was selected as the sacrificial reductant to be used in our MIL-177-HT based PFAS degradation system.[114,125,126]

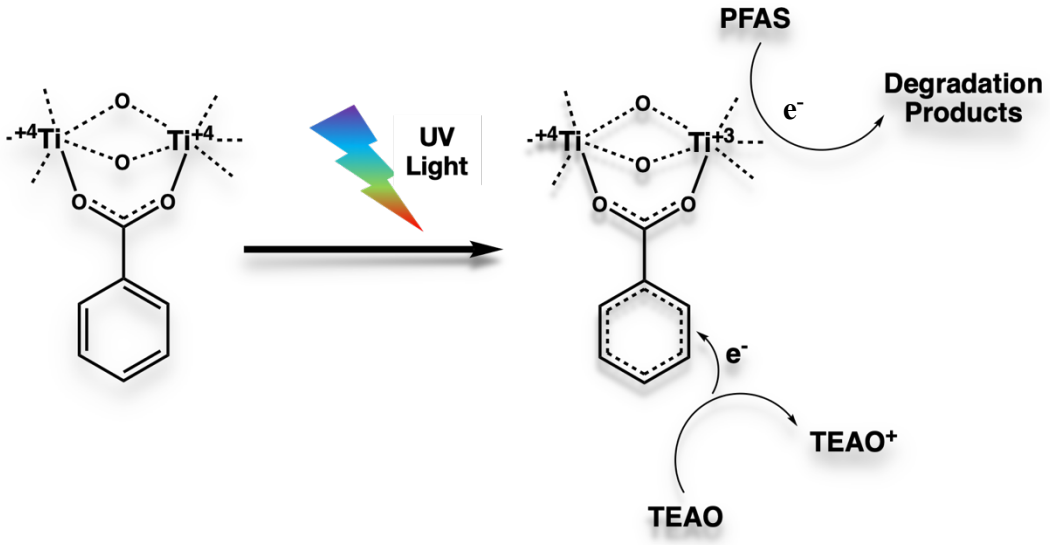

Figure 20. Schematic illustration of PFAS degradation using Ti based MOF as a photocatalyst and TEOA as a sacrificial reductant

MIL-177-HT, which was first reported in 2018 by Dr. Christian Serre and coworkers, is constructed by a tetratopic carboxylate based linker named H_4mdip, which connects one-dimensional (1D) infinite Ti–O subunits $(Ti_6O_9)_n$ nanowires, resulting in porous 3D MOF with hexagonal or honeycomb like channels (Figure 21). MIL-177-HT

was selected as the perfect MOF candidate for two main reasons. The first is its exceptional chemical and thermal stability. MIL-177-HT is reported to be stable in conditions such as 1M HNO_3, 1M HCl and 1M H_2SO_4. It also possesses a thermal stability of approximately 400 ºC. The second reason is that MIL-177-HT displays an experimental band gap of 3.67 eV, which allows for photo-responsive behavior close to that of TiO_2, yielding a potential for high photo-catalytic activity. [23]

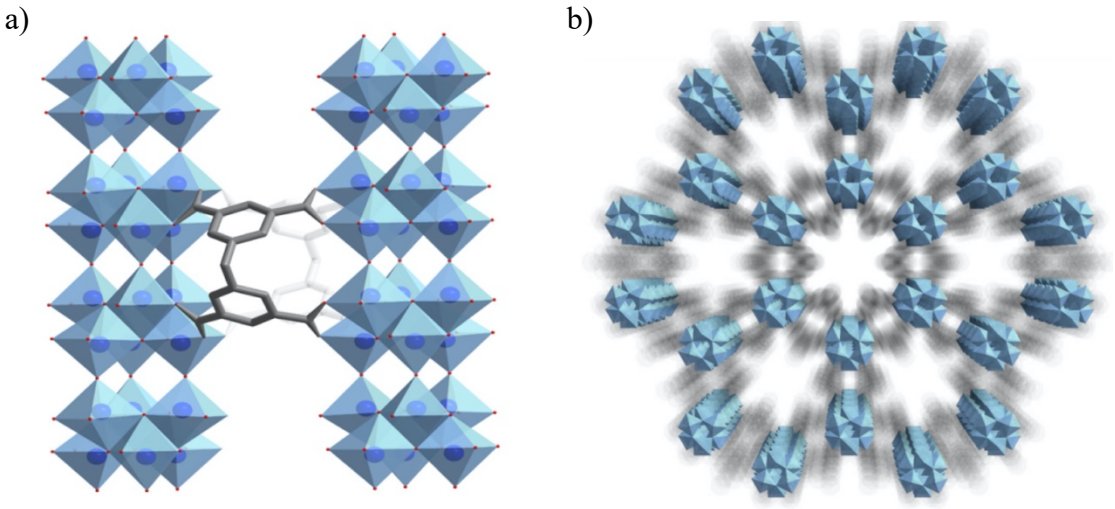

Figure 21. Schematic Illustration of MIL-177-HT ; a) Adjacent infinite ultrathin $(Ti_6O_9)n$ nanowires with a thickness of ca. 1 nm connected by mdip linkers (in gray). b) Channels between the $(Ti_6O_9)n$ nanowires array running along the c-axis with a diameter of ca. 0.9 nm

Following the MOF synthesis as described in Section 4.2, N_2 Absorption measurements and Powder X-Ray Diffraction measurements (PXRD) were taken in order to verify the structure as well as porosity of the obtained MOF. As shown in Figure 22,

the obtained MOF displays good crystallinity, with the PXRD pattern matching the previously published data, confirming the structure of MIL-177-HT. Moreover, MIL-177-HT displays permanent porosity as measured by N_2 Absorption measurements, with a BET surface area of 595 m^2/g.

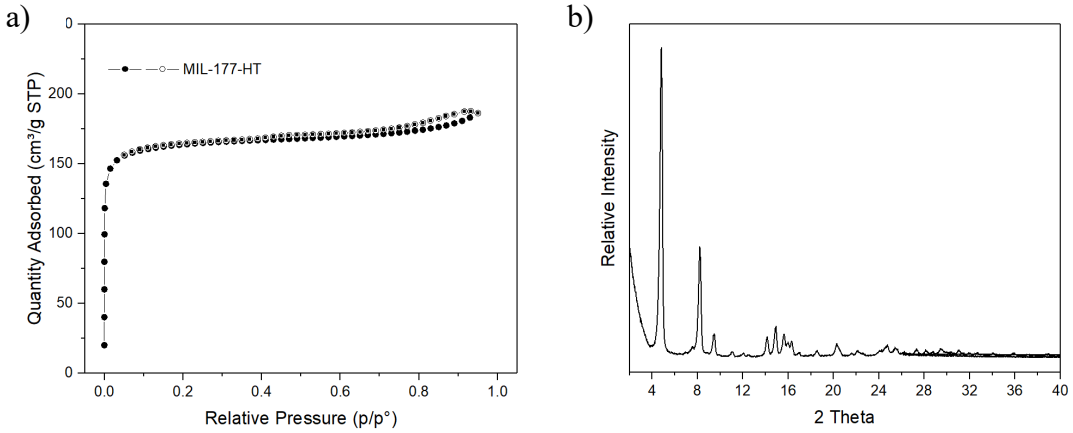

Figure 22. Structure Characterization of MIL-177-HT ; a) N_2 Absorption. b) Powder X-Ray Diffraction

MIL-177-HT was obtained in high yield and it was tested for its performance in PFOA degradation and Absorption. The testing was performed using a starting PFOA concentration of 100 ppb in ultra-purified water (obtained from Milli-Q water purification system). 100 ppb was selected as the desired starting concentration in order to model real PFOA contaminations within water systems. 1.0 g/L was selected as the starting catalyst (MOF) concentration along with 1.0% TEOA. Time points were taken at 0 min, 1 hour, 3 hours, 6 hours, 12 hours and 24 hours in order to monitor the PFOA removal process. Using this method, two different experiments were run in order to compare how the system

performs when there is no light source (Absorption) and when the light source is used (degradation). Furthermore, all experiments were performed in triplicate in order to obtain accurate data for PFOA concentrations within solution as working at such low concentrations could yield high experimental error in PFOA quantification.

As shown in Figure 23a, when using 1.0 g/L catalyst concentration and 1.0% TEOA in solution, the PFOA concentration is reduced from 100 ppb to 93 ppb for the Absorption (light off) experiment, while the PFOA concentration was reduced from 100 ppb to 87 ppb for the degradation (light on) experiment. While, the PFOA was not reduced significantly, the concentration, a reduction in PFOA concentration was observed in the degradation experiment over the Absorption experiment, which signaled success in PFOA degradation occurred due to the photo-catalytic reduction of PFOA.

In order to further study and optimize the system, three different TEOA concentrations were tested (1.0%, 2.5% and 5.0% along with two different catalyst loadings (1.0 g/L and 2.5 g/L). As displayed in Figure 23a, when the TEOA concentration was increased to 2.5% and 5.0%, a reduction in PFOA concentration from 100 ppb to 83 ppb and from 100 ppb to 75 ppb was achieved for the degradation (light on) experiments respectively. Moreover, as the TEOA concentration increased to 2.5% and 5.0%, an increase in PFOA Absorption (light off) PFOA was achieved. When 2.5% TEOA was used, the PFOA concentration was reduced to 91 ppb and 89 ppb for the 5.0% TEOA loading. This data yields evidence that as the TEOA concentration is increased, both the Absorption of PFOA increase within the MOF. Additionally, an increase in TEOA concentration, significantly increases the PFOA removal when the light source is on

(degradation), potentially due to a larger concentration of sacrificial reductant close to the catalyst active sites.

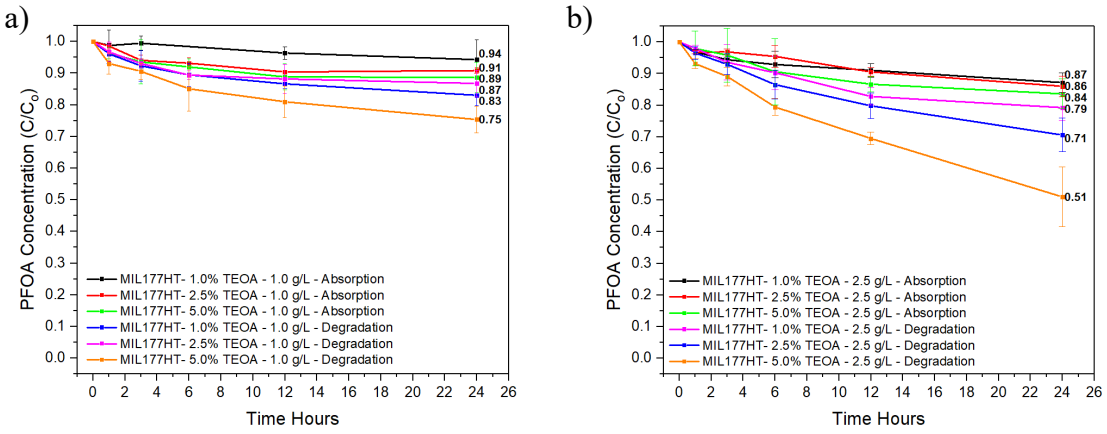

Figure 23. Concentration curves for PFOA in solution during both Absorption and degradation experiments a) 1.0 g/L MIL-177-HT loading, b) 2.5 g/L MIL-177-HT loading

Next, as mentioned above, in order to study how the increase of catalyst loading affected the PFOA removal, 2.5 g/L catalyst loading was tested. As shown in Figure 23b, a significant increase in PFOA removal was seen. Under the 2.5 g/L loading conditions, the adsorptive removal followed the same pattern as the 1.0 g/L loadings. The PFOA concentration was reduced to 87 ppb, 86 ppb and 84 ppb for the 1.0% TEOA, 2.5% TEOA and 5.0% TEOA concentrations respectively. Likewise, a significant reduction in PFOA was observed when using 2.5 g/L during the degradation experiments. For example, the PFOA concentration was reduced to 79 ppb, 71 ppb and 51 ppb for the 1.0% TEOA, 2.5% TEOA and 5.0% TEOA concentrations respectively.

Following the completion of the experiments, PXRD and N_2 Absorption experiments were performed on the recovered MIL-177-HT samples for both the Absorption and degradation experiments when using 5.0% TEOA loading. These two experiments were selected because TEOA is not only a sacrificial reductant but also a organic base that is capable of coordinating to the Ti metal centers, totally breaking down the MOF. As displayed in Figure 24, both samples retain their crystallinity with the PXRD pattern matching the As-Synthesized or Pre-reaction MOF samples. There is a small drop in surface area for both samples, displaying a BET surface area of 430 m^2/g and 415 m^2/g for the post Absorption and post degradation samples respectively. Furthermore, Inductively Coupled Plasma-Mass Spectroscopy (ICP-MS) was used in order to monitor the concentration of Ti in solution following each reaction. As shown in Table 8, the concentration of Ti ions in the reaction supernatant is extremely low, which suggests that the reduction in surface area in the MOF samples post reaction is not due to MOF

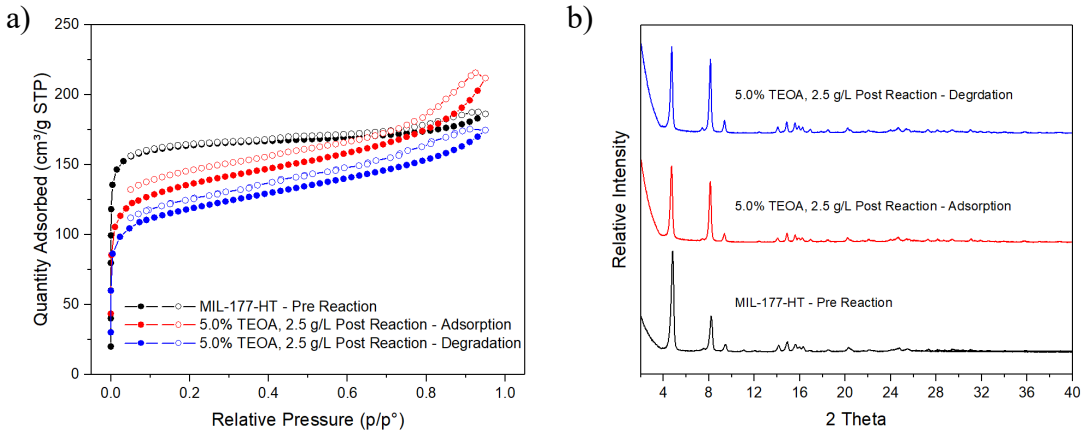

Figure 24. Structural Characterization of MIL-177-HT following 5.0 % TEOA, 2.5 g/L MIL-177-HT loading experiments a) N_2 Absorption; b) Powder X-Ray Diffraction

breakdown but potential incomplete washing of the MOF for successful removal of degradation products or solvent molecules, or breakdown during the activation prior to N_2 Absorption measurements, for resulting in a reduced surface area.

Experiment	Ti Concentration (mg/L)
2.5 g/L CAT, 5.0 % TEOA - Absorption	0.000907
2.5 g/L CAT, 5.0 % TEOA - Degradation	0.000588

Table 8. Concentration of Titanium Metal Ions in Reaction Supernatant Solution using Inductively Coupled Plasma-Mass Spectroscopy (ICP-MS)

In order to validate that the pathway of PFOA degradation is in fact a reduction based pathway, as well as further validate, beyond the disappearance of PFOA, that degradation is actually occurring within this system, fluoride ion detection measurements were performed. As described on Section 4.1, oxidation based pathways such as Fenton based AOP's cannot break C-F bonds, yet reduction based pathways that generate hydrated electrons (which are hypothesized to be reducing species in the system), can in fact break C-F bonds. Therefore, if F^- ions are detected in solution, C-F bonds are broken, yielding evidence of a reduction based degradation. These measurements were performed on the reaction solution for a degradation experiment using 2.5 g/L MOF loading, 5% TEOA and 1 ppm (1000 ppb) PFOA solution. A 10-fold increase in PFOA concentration was used as compared to all previous experiments, in order to allow both, the degradation

products and potential fluoride ions, to be within detectable ranges for the fluoride meter (Range of .01 ppm – 100 ppm F^- Ion Detection).

As shown in Table 9, the F^- Ion concentration detected in the 1 ppm stock PFOA solution was $0.084 \pm .002$ ppm. Moreover, for the 2.5 g/L CAT, 5.0 % TEOA – Absorption (light off) reaction, the F^- Ion concentration shows a very small increase of approximately 0.021 ppm to $0.105 \pm .006$ ppm. Conversely, for the 2.5 g/L CAT, 5.0 % TEOA – Degradation (light on) reaction, the F^- Ion concentration significantly increased to approximately 3.168 ± 0.166 ppm. Overall, this increase suggests a 21.1 % defluorination after 24 hours (based on 1 ppm PFOA and 15 fluoride molecules per PFOA could generate 15 ppm F^- for full defluorination). This defluorination rate is both plausible and acceptable based upon the total loss of PFOA of 49% for the previous 2.5 g/L CAT, 5.0 % TEOA degradation reaction using 100 ppb PFOA stock solution (Figure 23). Overall, the lack on F^- Ions in both the stock solution and Absorption (light off) experiment, paired with the significant increase for the degradation (light on) experiment, yield further evidence of degradation of PFOA through a reduction based mechanism that can in fact break C-F bonds.

Solution	Fluoride Concentration (ppm)
1 ppm PFOA Stock Solution	0.084 ± 0.002
2.5 g/L CAT, 5.0 % TEOA 1 ppm PFOA - Degradation (light on)	3.168 ± 0.166
2.5 g/L CAT, 5.0 % TEOA 1 ppm PFOA - Absorption (light off)	0.105 ± 0.006

Table 9. Fluoride ion concentration measurements for PFOA stock and reaction solutions

Next, non-targeted LC-MS experiments were performed on both the 1 ppm stock PFOA solution as well as the 2.5 g/L MOF loading, 5% TEOA degradation reaction supernatant. The purpose of these experiments were to potentially elucidate what degradation products are being generated during the catalytic cycle. Figure 25a displays the LC chromatograph for the 1 ppm stock solution. There is only 1 observed peak which has an observed mass of 413 m/z as shown in Figure 25b. This observed peak is correlated to the mass of PFOA and is consistent with previous published examples of PFOA MS analysis.

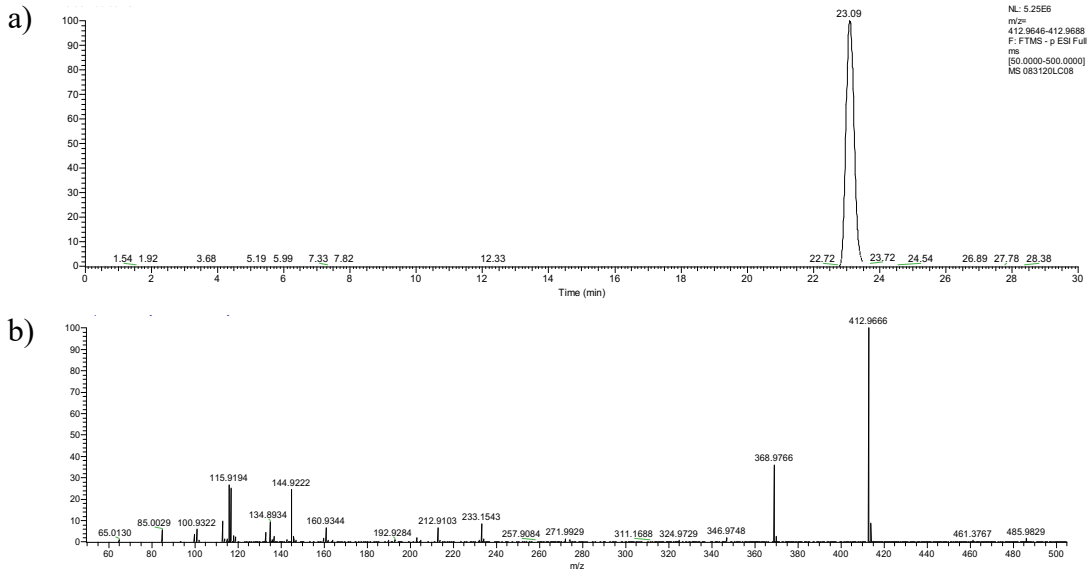

Figure 25. Liquid Chromatography-Mass Spectroscopy (LC-MS) data for 1 ppm stock PFOA solution a) LC b) MS

In contrast, Figure 26a displays the non-scaled LC chromatograph of the degradation reaction (light on). In order to clearly show all obtained peaks, Figure 26b displays the LC chromatograph with all peaks scaled to 100 relative intensity. Four distant peaks were observed at 1.3, 14, 23, and 25 mins. Following LC-MS and MS/MS analysis (All MS/MS spectra are reported in Appendix B) of Peak 1, it was determined that two different short chain PFAS molecules eluted from the column at 1.3 min (peak 1) (Figure 26c). These masses were determined to be 118 m/z and 162 m/z, which are correlated to the degradation products with chemical formulas of C_2F_4O and $C_3F_4O_3H_2$ respectively. It is noteworthy that Peak 1 is significantly more intense than any other peak, with the non-

scaled intensity of Peak 1 being 1 order of magnitude greater than Peak 2 and 2 orders of magnitude greater than Peaks 3 and 4. This suggests that the mass fragments of Peak 1 are the major intermediate degradation products of the reaction. Figure 25d displays the mass of 343 m/z which elutes from the column at 14 min (Peak 2) which correlates to a molecular formula of $C_7F_{11}O_3H_2$. Figure 26e displays the mass of 413 m/z which elutes from the column at 23 min (Peak 3). The mass fragments and elution time of Peak 3 matches the analysis of PFOA ($C_8F_{15}O_2H$) in the stock solution. Peak 4, which elutes from the LC column at 25 min, is correlated to a mass to charge ratio of 398 m/z and was identified as $C_8F_{15}O_1H$ (Figure 26f). Overall, the presence of both shorter chain PFAS molecules paired with the detection of F^- ions in solution, both the LC-MS and F^- Ion measurements yield evidence of not only PFOA degradation, but that degradation progressed through a reduction based mechanism as displayed in Figure 19.

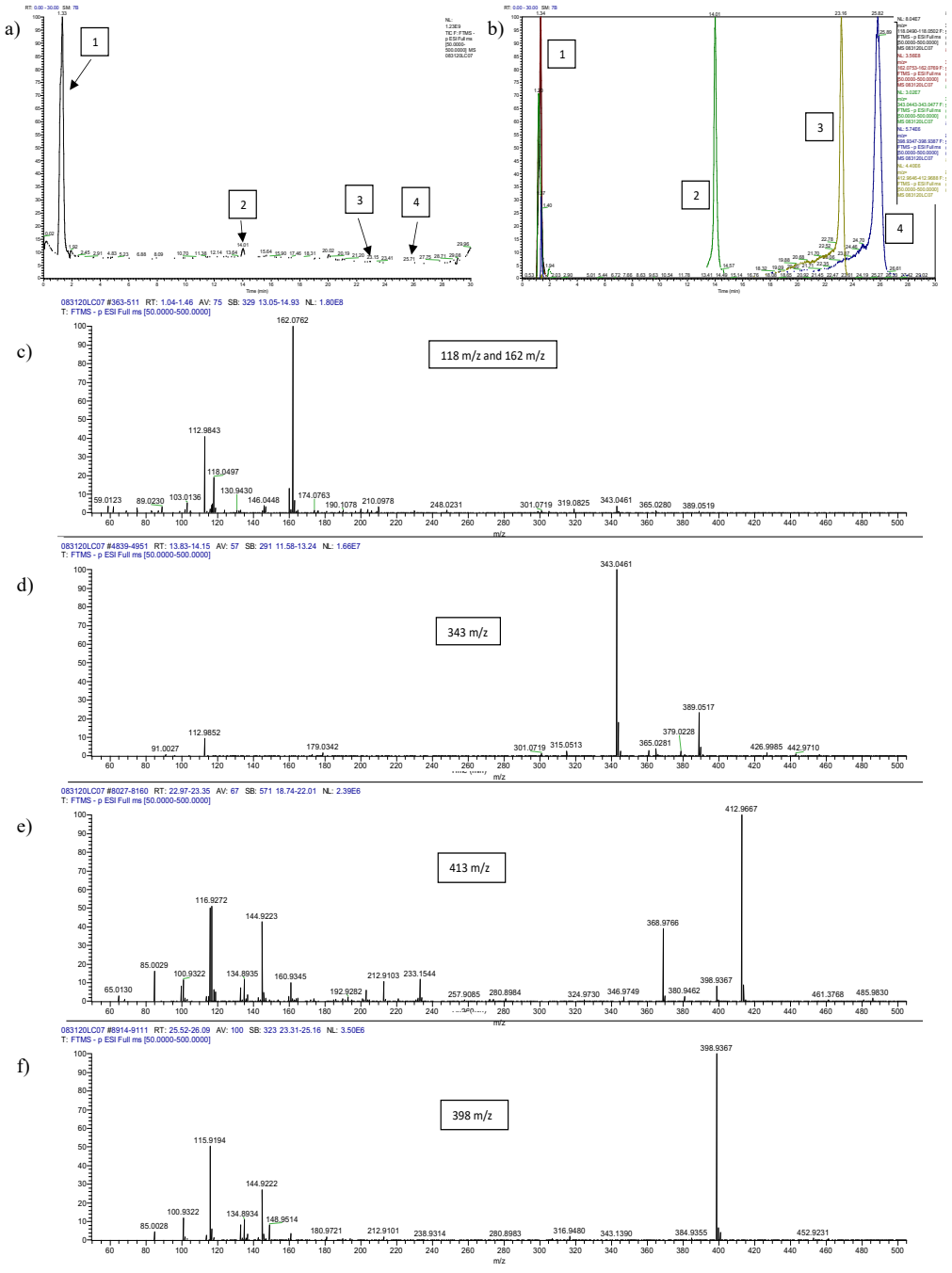

Figure 26. Liquid Chromatography-Mass Spectroscopy (LC-MS) data for 2.5 g/L MOF loading, 5% TEOA degradation reaction supernatant a) LC b) LC scaled to 100 relative intensity c) MS data Peak 1 d) MS data Peak 2 e) MS data Peak 3 f) MS data Peak 4

Finally, in order to show that the degradation of PFOA is due to the presence of the MOF as a photo-catalyst, two different control degradation (light on) experiments were performed. The first was using 5% TEOA, without any MOF and the second was using 2.5 g/L MOF loading with no TEOA present. As shown in Figure 27, the PFOA concentration does not decrease from 100 ppb outside of the measurement error when using no MOF and decreases to 91 ppb when using only the MOF. Therefore, it can be concluded that the PFOA degradation does not occur without the MOF based photo-catalyst as well as the TEOA present.

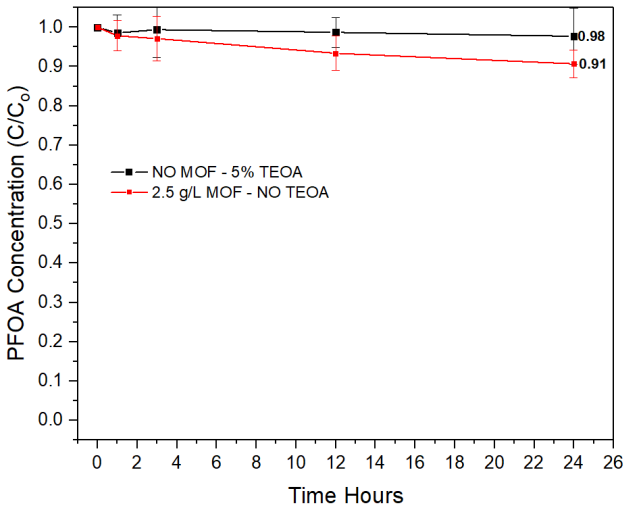

Figure 27. Control degradation (light on) experiment using 5% TEOA, without any MOF, 100 ppb PFOA

4.4 Conclusion

Over the last 50 years, Per- and polyfluoroalkyl substances (PFAS) such as Perfluorooctanoic acid (PFOA) have become ubiquitous in the environment. This is a major cause for concern as they are known as bioaccumulating substances and they have been linked to health issues such as cancer formation and birth defects.[93–95]P These synthetic surfactant type molecules contain C-F bonds, which make them resistant to typical water remediation techniques such as Advanced Oxidation Processes (AOPs).[113] Therefore, developing Advanced Reduction Processes (ARPs) have gained significant attention over the past decade. ARPs, such as the one developed in this chapter, use highly active chemical species with high redox potentials, such as hydrated electrons ($e^-_{(aq)}$) or H· radicals, in order to break the oxidation resistant C-F bonds.[91] In this system, a Titanium based MOF named MIL-177-HT was used a photo-catalyst in conjunction with Triethanolamine (TEOA) as a sacrificial reductant and a Hg-Vapor light source in order achieve the photo-catalytic degradation of PFOA. Using 2.5 g/L catalysts loading and 5% TEOA solution, 49% degradation, as monitored by LC-MS, and 21.1% fluoride mineralization of PFOA was achieved in 24 hours. Furthermore, the MOF was shown to maintain its porosity and crystallinity as monitored by PXRD and N_2 Absorption measurements. Overall, this work has shown the ability to successfully design Metal-Organic Framework based photo-catalytic platforms for chemically reducing (degrading) Per- and polyfluoroalkyl substances (PFAS) in water and is to the best of our knowledge the first successful example of using MOFs for PFAS degradation.

CHAPTER V

SUSPENION PROCESSING OF MICROPOROUS METAL-ORGANIC FRAMEWORKS*

5.1 Introduction

Although the potential applications of MOFs have been described as endless, the commercial and industrial breakthroughs utilizing MOFs have been few and far between, especially when compared to their publication rate in academia. A major reason for the disconnect between basic MOF research and their commercial development is the large monetary and time cost for material processing and activation. The activation and processing of MOFs have evolved over the years yielding 3 primary and well-developed strategies which include: conventional activation, solvent-exchange and supercritical CO2 activation.

Conventional activation is the removal of solvent and/or other guest molecules by heat and vacuum treatment. Unfortunately, conventional activation has found minimal utility for accessing the full porosity of many MOFs due to its harsh conditions often resulting in the collapse or degradation of the frameworks. Therefore, solvent-exchange was developed in order to help combat the collapse of MOFs during activation. Solvent-exchange methods replace the high boiling point solvent (e.g., dimethylformamide),

*This chapter is reproduced with permission from Kirchon, A.; Day, G. S.; Fang, Y.; Banerjee, S.; Ozdemir, O. K.; Zhou, H.-C. Suspension Processing of Microporous Metal-Organic Frameworks: A Scalable Route to High-Quality Adsorbents. iScience 2018, 5, 30–37. Copyrights 2018 Elsevier

which is required for synthesis, with a lower boiling point solvent (e.g., chloroform, MeOH), which is then removed under relatively mild heat and vacuum conditions. Typically, lower boiling point solvents have weaker interactions such as with the MOF framework. The weaker interactions result in decreased surface tension and capillary forces exerted on the framework during the solvent removal. Solvent-exchange is the most commonly used technique for MOF activation, but the time and resources required in order to perform a successful solvent exchange is typically too high for any production beyond the gram scale.

Another common technique for lab scale research is called supercritical CO_2 activation. Supercritical CO_2 ($scCO_2$) builds on premise of the solvent-exchange process, using liquid CO_2 as a solvent. For example, a solvent that is miscible with $scCO_2$ (e.g., ethanol) is exchanged within the MOFs pores for $scCO_2$ at high pressure (i.e., > 73 atm) over the course of several hours. This method further reduces the surface tension during activation compared to solvent-exchange. Although $scCO_2$ has proven successful on the lab scale, the large capital costs associated with the development of commercial or industrial scale equipment for $scCO_2$ has limited its adoption into real systems. In addition, $scCO_2$ activation has proven ineffective in producing open metal sites in MOFs. As open metal sites are often considered the key component in MOF applications such as gas storage, separation, and catalysis, methods that cannot achieve their production have not been widely adopted

Suspension based processing methods have been used for cell processing for many years. Suspension-based cell growing procedures were first used in 1956 when a

suspended magnetic stirrer was used to grow cells in round bottom flasks. Further optimization of suspension cell growth methods has allowed for a quick and easy process for achieving large quantities of high quality cell lines. Based on the success of suspension cell growth methods, as well as to combat the issues that exist with the five current MOF activation and processing methods, we have developed a method of MOF activation and processing named “Suspension Processing”. Suspension processing provides a universal, scalable, cost effective, and robust technique for the effective solvent exchange, activation and processing of MOFs.

5.2 Experimental Methods

PCN-250 Synthesis: Fe(NO3)3-9H2O (5.4 g), ABTC (1.8 g), Acetic Acid (3 L) and DMF (6 L) were added into a jacketed 10 L Pyrex high pressure reaction vessel. The vessel was then heated to 150 ºC for 12 h. The resulting reaction slurry was then removed and used without further purification. Multiple batches were synthesized in parallel to achieve kg quantities.

HKUST-1 Synthesis: HKUST-1 was synthesized following the literature procedure with minor changes to allow for larger scales. Cu(NO3)2 2.5H2O (24.0 g) was dissolved in 1 L of solvent consisting of equal parts of ethanol and deionized water. This was followed by the addition of BTC (8.0 g) into the solution. The resultant solution mixture was transferred into a 2 L Pyrex high pressure reaction vessel and placed in an oven at 110 ºC for 18 h. The resulting reaction slurry was then removed and used without further purification. Multiple batches were synthesized in parallel to achieve kg quantities.

UiO-66 Synthesis: 1 L of DMF was added to a 2 L RBF equipped with a stir bar and preheated to 140 ºC. Then ZrOCl2 (24.0 g), BDC (24.0 g) and 400 ml of Formic Acid were added to the RBF. The flask was vigorous stirred at 140 ºC for 2 hours. The resulting reaction slurry was then removed and used without further purification. Multiple batches were synthesized in parallel to achieve kg quantities.

Suspension Processing: Following the synthesis of each MOF, 0.5 L of the reaction slurries were added directly into a suspension processing apparatus with a volume of 5 L. Then 2.5 L MeOH was added to the suspension processing apparatus bringing the total volume to approximately 3 L. Next the suspension processing apparatus was put on

top of a hot/stir plate and was heated to 65 ºC while the suspended stir bar was stirred at 65 rpm for the desired amount of time (1h, 6h, 12h, etc…). Once the desired time was reached the contents of the reaction vessel were filtered without allowing the solution to cool, and the desired MOF product was obtained.

Drying and Activation: Following the isolation of the desired MOF, the material was dried in air at 70ºC for 1 day. The MOF was then activated under vacuum at the following temperatures for 10 hours (PCN-250-185ºC, UiO-66-120ºC, HKUST-1-150ºC).

TGA Method

PCN-250: Heating at 10ºC/min from 25 ºC-150 ºC, then a 10 min isothermal step, followed by a 2.5ºC/min heating ramp up to 550 ºC, all under a 50 mL/min flow of N_2

UiO-66: Heating at 5ºC/min from 25 ºC-700 ºC under a 50 mL/min flow of N_2

HKUST-1: Heating at 5ºC/min from 25 ºC-600 ºC under a 50 mL/min flow of N_2

Cost Analysis Method

Assumptions

- Cost is calculated based on VWR prices for solvents
- Price of water is considered negligible
- Labor cost based on single user processes
- DMF average price: $10.25 per liter
- MeOH average price: $2.50 per liter
- CH2Cl2 average price: $7.50 per liter

- EtOH (190 Proof) average price: $40.80 per liter
- US federal minimum wage: $7.25/hour

PCN-250

7 Days Traditional Solvent Exchange – Surface Area 1446 m2/g

As synthesized PCN-250 was washed with DMF 4 times and immersed in DMF over a 2-day period. Then it was washed with methanol 4 times and immersed in methanol over a 2-day period at 65 °C. Finally, it was washed CH2Cl2 6 times and immersed in CH2Cl2 over a 3-day period at 65 °C. Each solvent wash or immersion used 50 mL per gram of MOF. Total solvent usage: 200 mL of MeOH and DMF, and 300 mL of CH2Cl2 per gram of MOF

For one kg of MOF

- 200 L of DMF = $2050.00
- 200 L of MeOH = $500.00
- 300 L of CH2Cl2 = $2250.00
- $4800.00 Total Cost of Solvent

Process time per wash: 1 hour.

Total number of washes: 14

14 hours of Labor - $101.50 per one kg Batch

5 Days Suspension Processing– Surface Area 1564 m2/g

Approximately 8 grams of MOF present in .5 L of reaction slurry

2.5 L MeOH used per 8 grams of MOF

312.5 mL of MeOH per 1 g MOF

312.5 L per 1 kg of MOF

$781.25 of MeOH per kg of MOF

2 steps: Loading and filtering: 1 hour per step

Total labor: 2 hours - $14.50 per kg Batch

UiO-66

2 Days Traditional Solvent Exchange – Surface Area 1290 m2/g

As synthesized UiO-66 was washed with DMF 9 times and immersed in DMF over a 3-day period. Then it was washed with methanol 9 times and immersed in methanol over a 3-day period at 65 °C. Each solvent wash or immersion used 50 mL per gram of MOF. 450 mL of MeOH and 450 mL of DMF utilized for one gram of MOF.

For one kg of MOF

- 450 L of DMF = $4612.50
- 450 L of MeOH = $1125.00
- $5737.50 Total Cost of Solvent

Process time per wash: 1 hour

Total number of washes: 18

18 hours of Labor - $130.50 per kg Batch

2 Days Suspension Processing– Surface Area 1675 m2/g

Approximately 5 grams of MOF present in .5 L of reaction slurry

2.5 L MeOH used per 5 grams of MOF

100 mL of MeOH per 1 g MOF

100 L per 1 kg of MOF

$250.00 of MeOH per kg of MOF

2 steps: Loading and filtering: 1 hour per step

Total labor: 2 hours - $14.50 per kg Batch

HKUST-1

2 Days Traditional Solvent Exchange – Surface Area 1617 m2/g

As synthesized HKUST-1 was washed and immersed in distilled water 3 times and washed with 95% ethanol 3 times over a 2-day period. Each wash or immersion used 50 mL per gram of MOF. 450 mL of 95% ethanol and 450 mL of distilled water were used for one gram of MOF.

For 1 kg of MOF

- 450 L of Water = Negligible
- 450 L of 95% EtOH = $6120.00
- $6120.00 Total Cost of Solvent

Process time per wash: 1 hour

Total number of washes: 6

6 hours of Labor - $43.50 per kg Batch

2 Days Suspension Processing– Surface Area 1808 m2/g

Approximately 3.73 grams of MOF present in .5 L of reaction slurry

2.5 L MeOH used per 3.73 grams of MOF

670 mL of MeOH per 1 g MOF

670 L per 1 kg of MOF

$1675.00 - Solvent Cost per kg MOF- MeOH per kg of MOF

2 steps: Loading and filtering: 1 hour per step

Total labor: 2 hours - $14.50 per kg Batch

Materials

All the reagents and solvents were commercially available and used as received or synthesized according to the literature reported procedures. PCN-250(Fe_3O) and UiO-66 commercial samples were purchased from Stream Chemicals while the HKUST-1 (Basolite C300) commercial sample was purchased from Sigma Aldrich. Suspension processing apparatus (3 L Celstir and 80 mL) were purchased from DWK Life Sciences.

Instrumentation

Powder X-ray diffraction (PXRD): carried out with a Bruker D8-Focus Bragg-Brentano X-ray Powder Diffractometer equipped with a Cu sealed tube (λ = 1.54178 Å) at 40 kV and 40 mA.

Scanning Electron Microscopy (SEM): measurements were carried out on JEOL JSM-7500F. JEOL JSM-7500F is an ultra-high-resolution field emission scanning electron microscope (FE-SEM) equipped with a high brightness conical FE gun and a low aberration conical objective lens.

Thermal Gravimetric Analysis (TGA): performed using a Mettler-Toledo TGA/DSC STARe-1 system which was equipped with a GC100 gas controller.

N2 sorption measurements: conducted using a Micromeritics ASAP 2020 and 2420 system using ultra high purity (UHP) N_2 gas.

High-Pressure CH4 Absorption isotherms: carried out on HPVA II high pressure volumetric analyzer from micromeritics using ultra high purity (UHP) CH_4 gas.

5.3 Results and Discussion

Suspension processing utilizes an enclosed cylindrical vessel with a suspended stir rod or agitator that extends from the top of the system downward without touching the bottom as shown in Figure 28. The as-synthesized MOF, still suspended within the reaction mixture, (Figure 28 left, yellow colored area) is placed within the reaction vessel. Step 1 shows the addition of the full reaction vessel contents into the suspension processing apparatus. In Step 2, the low boiling point solvent, such as methanol (MeOH, Figure 1 center, blue colored area), is added in an amount approximately 5x the volume of the solid product. The system is then heated to the boiling point of the low boiling point solvent (in the case of MeOH, the system was heated to 65°C). The system is then stirred at a low rate, typically 65 rpm, for the desired time. After the stirring has been stopped in Step 3 the contents of the suspension apparatus are filtered while heated, yielding a highly crystalline and porous MOF product with a filtrate consisting of a mixture of the process and reaction solvents as well as dissolved reaction byproducts. The process requires minimal participation from the operator, with no solvent changes necessary during the timescale of the procedure. In addition, the apparatus utilized for lab scale suspension processing is similar in design to commercial batch reactors that typically utilize suspended mechanical stirrers, allowing for this process to act as drop-in technology for existing chemical production.

This method was first developed for PCN-250, which as previously explained, is constructed from Fe3-μ3-oxo clusters and tetratopic azobenzene-based linkers (ABTC=3,

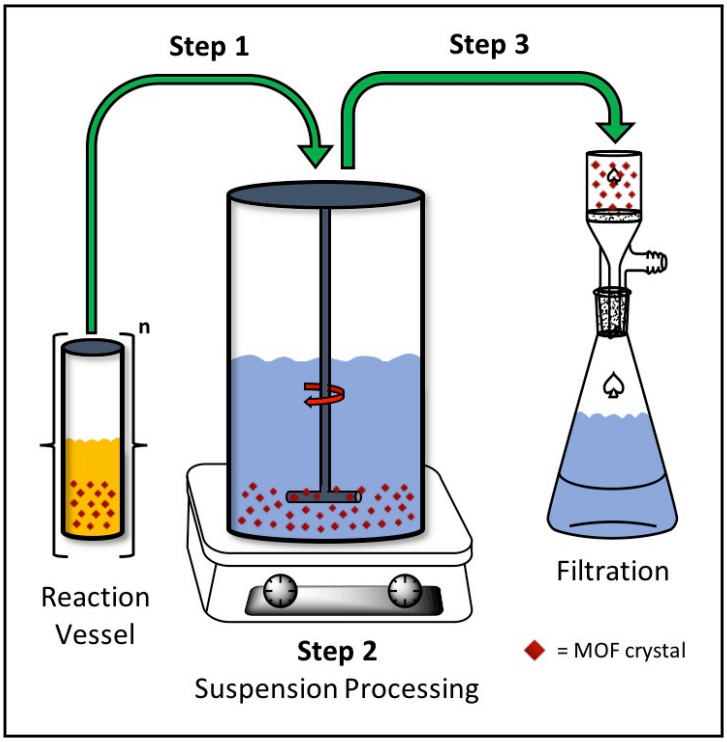

Figure 28: Suspension Processing Methodology: Step (1) addition of reaction vessel contents into suspension processing apparatus, Step (2) Suspension Processing, Step (3) Filtration. Ref #48

3', 5, 5' azobenzenetetracarboxylate). PCN-250(Fe_3O)'s high gas uptake, available open metal sites, exceptional stability, and scalability have made it a well-studied material for gas storage applications. Although PCN-250(Fe_3O)has exceptional gas storage properties, the solvent exchange process used to obtain the maximum gas uptakes, is currently reported as an 8-10-day process with approximately 9-12 steps. These steps use 3-4 different solvents and require active participation from an individual in order to wash and exchange the solvent used in each step. The use of suspension processing in place of

traditional methods, not only yields a product with increased gas uptake properties, but does so with improved time, energy, and labor-efficiency.

Analysis of the suspension processed materials was primarily conducted by Powder X-ray diffraction (PXRD) and nitrogen gas uptake experiments. A sample of as synthesized PCN-250(Fe_3O)was subjected to suspension processing in MeOH, with samples removed after the following times: 6 hours, 1 day, 2 days, 5 days, 14 days, and 20 days. Figure 2a, showcases the PXRD for the series of PCN-250(Fe_3O) samples, showing that the crystallinity of PCN-250(Fe_3O) increased during the course of the processing. In Figure 29b, the N2 gas uptake of the samples, displayed an increase in total gas uptake with increase in treatment time. Notably, the 5 day treated sample, PCN-250-5day, shows the same N2 gas uptake as reported in the literature. However, compared to the 3-4 solvents used in the reported solvent-exchange method, suspension processing never required solvent replacement or addition, only utilizing the initial process solvent added to the reaction mixture. No active participation was needed once the process was initiated. Even without exchanging the solvent, Improvements In gas uptake were still observed after 20 days of processing.

The surface area was found to dramatically increase during the first four treatments (6 hours to 5 days). After the initial surface area response, the increase in surface area slows down until it reaches a peak of 1702 m2/g after the 20th day. This surface area represents a 15% improvement over the commonly published PCN-250 surface area (1446 m2/g). As far as we are aware, this surface area is the record-high amongst published PCN-250 samples.

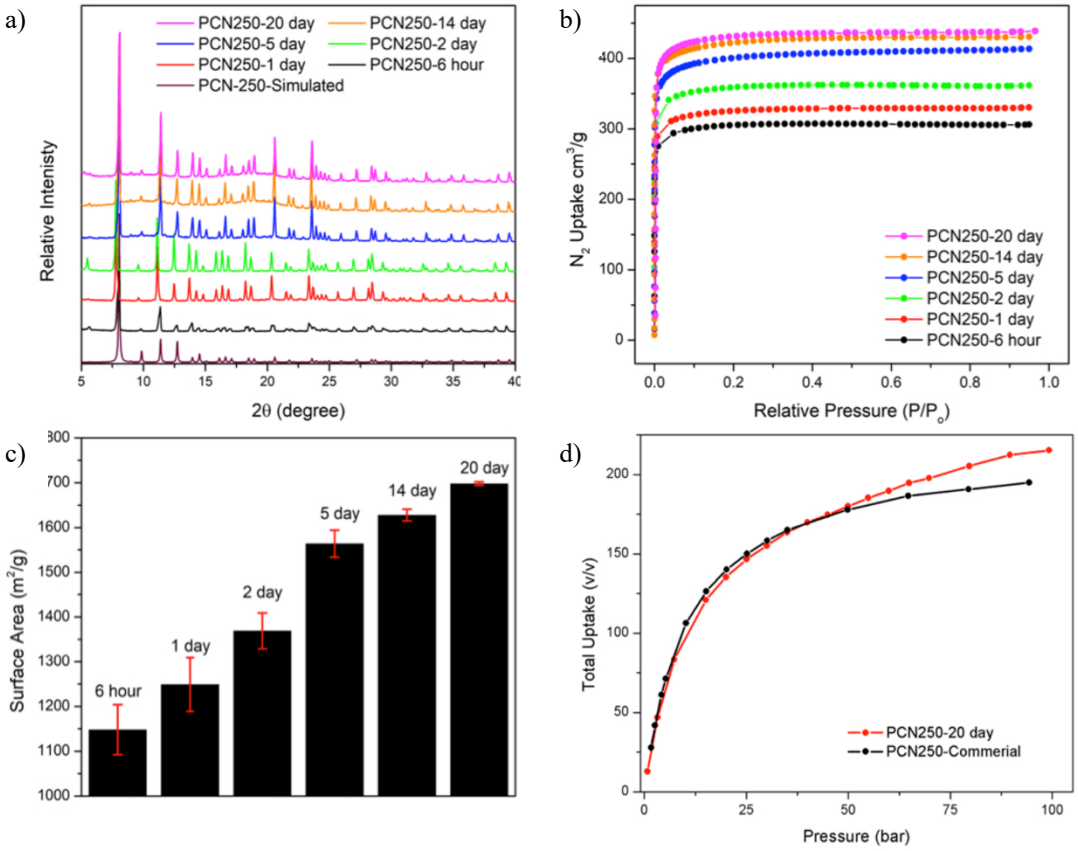

Figure 29. Suspension Processed PCN250 Characterization**:** (a) Powder X-ray Diffraction Pattern of Suspension Processed PCN-250(Fe_3O)**;** (b) N2 Absorption Isotherm at 77K Suspension Processed PCN-250(Fe_3O)**;** (c) BET Surface Area vs. Time of Processing for Suspension Processed PCN-250(Fe_3O)**;** (d) High Pressure Methane Uptake for PCN250-20 day compared to commercial PCN-250(Fe_3O). Ref #48

Lastly methane uptake measurements were performed to determine the applicability of suspension processing to a MOFs end application. Compared to a commercial PCN-250, the total methane uptake at room temperature (313K) and 95 bar increased by 11.9%, from 194 v/v to 217 v/v as shown in Figure 29d.

Due to the success of suspension processing for PCN-250, we sought to investigate the universal applicability of this method by applying suspension processing on two other well-known, commercially available, and highly studied microporous MOFs, UiO-66 and HKUST-1. The materials were synthesized as stated in the experimental methods. Their structure was validated by PXRD as shown below in Figure 30. As seen with PCN-250, both MOFs were able to obtain higher gas uptake values using suspension processing compared to traditional solvent exchange procedures. In addition, an increase in gas uptake with an increase in processing time was also observed as shown in Figure 31.

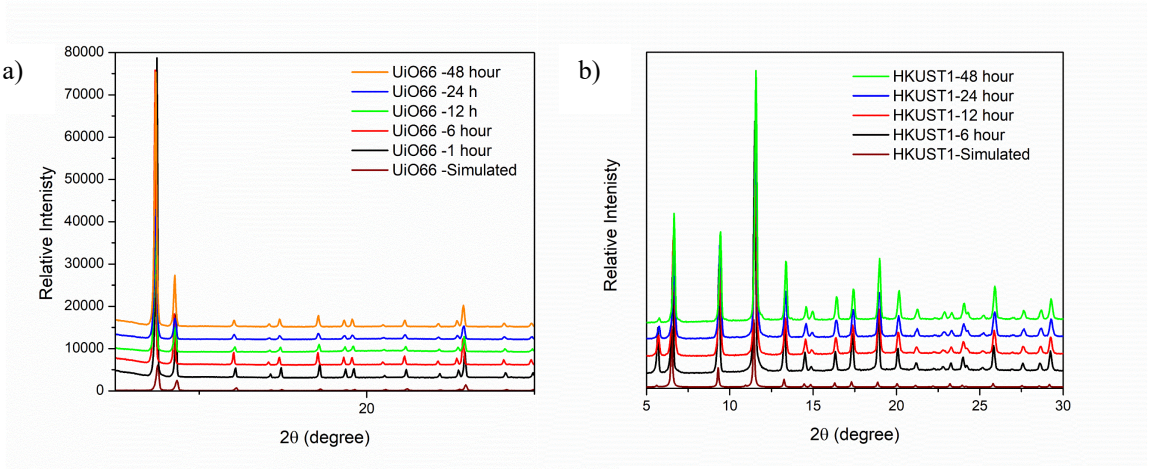

Figure 30. Powder X-ray Diffraction Pattern of Suspension Processed MOFs: (a) UiO-66 (b) HKUST-1. Ref #48

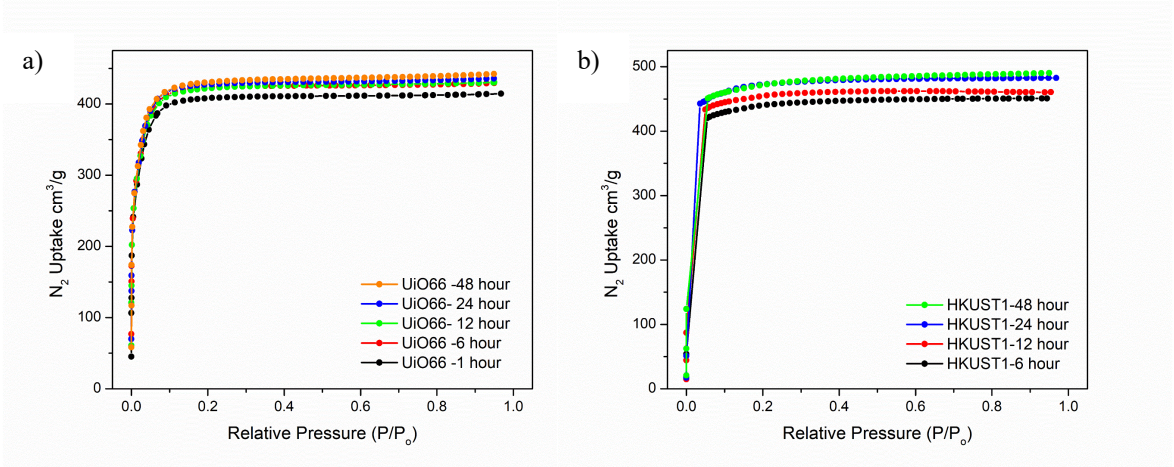

Figure 31. N_2 Isotherms of suspension processed MOFs at 77K: (a) UiO-66 (b) HKUST-1. Ref #48

For UiO-66, a BET surface area of 1675 m2/g was achieved after only 2 days of processing. This outperformed the BET surface area of the traditional solvent exchange sample of 1290 m2/g. Furthermore, suspension processing of HKUST-1 was also observed to improve the BET surface area compared to traditional solvent exchange methods (1808 m2/g vs 1615 m2/g, respectively). Samples of PCN-250, UiO-66, and HKUST-1 were purchased from commercial vendors and compared to the lab scale samples before and after suspension processing. Typically, the commercially purchased MOF adsorbents have lower BET surface areas compared to the lab prepared samples as seen in Table 10. Suspension processing of PCN-250, UiO-66 and HKUST-1, led to an increase in BET surface area and gas uptake properties over their commercial available counterparts.

	Traditional Solvent Exchange Process	Commercial Product	Suspension Processing
PCN250	1446 m^2/g	1270 m^2/g	1702 m^2/g
UiO66	1290 m^2/g	1045 m^2/g	1675 m^2/g
HKUST1	1617 m^2/g	1615 m^2/g	1808 m^2/g

Table 10. Comparison of BET Surface Area for Various MOFs. Ref #48

Mechanistic analysis of suspension processing was studied via Scanning Electronic Microscopy (SEM) and Thermal Gravimetric Analysis (TGA). Figure 32a shows that the as-synthesized PCN-250 particles were heavily aggregated. However, in Figure 32b, after suspension processing, the particles were well dispersed. This phenomenon indicates that unreacted organic ligands or surface residues have been successfully removed after the treatment. On the other hand, there're seed-like small particles on the surface of as-synthesized HKUST-1 samples. However, they were completely removed after 48 hours treatment, resulting in a smooth crystal surface for HKUST-1 (Figure 32d and 32e). This suggests the completely removal of solvent residues and defects from the MOF pores and surface. Similar phenomenon was also observed for UiO-66 samples (Figure 32g and 32h).

The discussed observations are the result of the removal of low crystallinity phases within or on the surface of the MOF by suspension processing. These results suggest that

suspension processing aids in the removal of unreacted material, minor surface defects, and low crystallinity coordination polymers via efficient dissolution and mass transport due to increased agitation and material-solvent contact. This improvement in bulk material purity, removing non-porous byproducts, allowed for an increase in gas uptake performance compared to the as-synthesized samples.

The discussed observations are the result of the removal of low crystallinity phases within or on the surface of the MOF by suspension processing. These results suggest that suspension processing aids in the removal of unreacted material, minor surface defects, and low crystallinity coordination polymers via efficient dissolution and mass transport due to increased agitation and material-solvent contact. This improvement in bulk material purity, removing non-porous byproducts, allowed for an increase in gas uptake performance compared to the as-synthesized samples.

As seen in Figure 32(c, f and i), the thermal stability of PCN-250, HKUST-1 and UiO-66 all increased following longer suspension processing times. The overall stability of the 20 day processed PCN-250 increased by 3°C compared to the 6 hour processed sample. The TGA curve of PCN250-6hour, displays a mass loss of 6.3% below 100°C, likely the removal of MeOH from the framework. Between 100°C and 185°C, PCN250-6hour displays a mass loss event comprising 16.5% which should correspond to the removal of DMF from the framework. In comparison, PCN250-20day displays a significantly different TGA curve, showing a major mass loss of 20.5% below 100°C, but

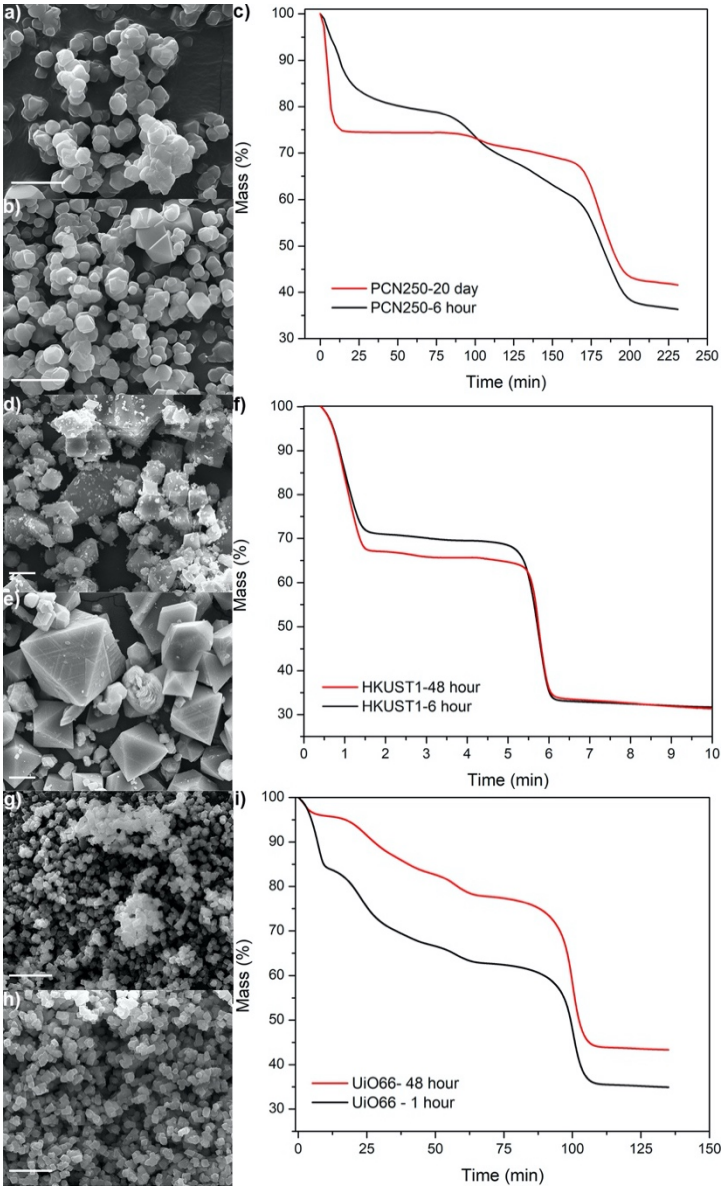

Figure 32. SEM and TGA Curves : (a)SEM Micrographs of PCN-250-6 hour; (b) SEM Micrographs of PCN250-20 day; (c) TGA Curve for PCN-250-6 hour (black) and PCN250-20 day (red); (d) SEM Micrographs of HKUST1-6 hour; (e) SEM Micrographs of HKUST1-48 hour; (f) TGA Curve for HKUST1-6 hour (black) and HKUST1-48 hour (red); (g) SEM Micrographs of UiO66-1 hour; (h) SEM Micrographs of UiO66-48 hour; (i) TGA Curve for UiO66-1 hour (black) and UiO66-48 hour (red). Ref #48

with no significant mass loss between 100°C and 185 °C (5.2%) which suggests that most of the DMF has been removed from the framework during suspension processing. More importantly, the mass loss event in the median temperature range (185°C-397/400°C) displays major differences, likely due to the effective removal of unreacted starting material, byproducts, and surface defects. The mass loss decreased significantly from 19.6% for PCN250-6 hour, to 9.7% for PCN250-20 day. Similar behavior was observed for HKUST-1 and UiO-66. We attribute the stability enhancement to improvements in pore cleaning and the removal of surface defects.

In order to analyze the practicality of suspension processing we performed an operational cost analysis comparing suspension processing to traditional solvent exchange methods. For this analysis, we defined operational costs as the cost of solvent used plus the cost of labor for the duration of the process. In all cases, suspension processing had a significantly lower operating cost compared to traditional solvent exchange methods. The traditional solvent exchange for PCN-250 was performed over a 7-day period and involves a total of 14 separate washing procedures, involving 3 different solvents (Full process listed in section 5.2). In total, the solvent used in this procedure cost approximately $4800.00 per kg of MOF. Including labor, the total cost per kg of PCN-250 using traditional solvent exchange is approximately $4901.50. For comparison, a 5-day suspension processing has a total operating cost of approximately $795.75, which represents an 84% reduction in cost. Similar improvements in operating cost were also seen with UiO-66 and HKUST-1 (Figure 33 and Table 10). This section, along with how the analysis was performed, given in detail in the Section 5.2, provide additional support

to the claims that suspension processing not only leads to higher quality MOF products, but it does so with a major reduction of the cost and time.

	Traditional Solvent Exchange Process	Suspension Processing	Reduction in Operating Cost
PCN250	$4901.50	$795.75	84%
UiO66	$5868.00	$264.50	95%
HKUST1	$6163.50	$1689.50	73%

Table 11. Total Operational Costs in US Dollars ($). Ref #48

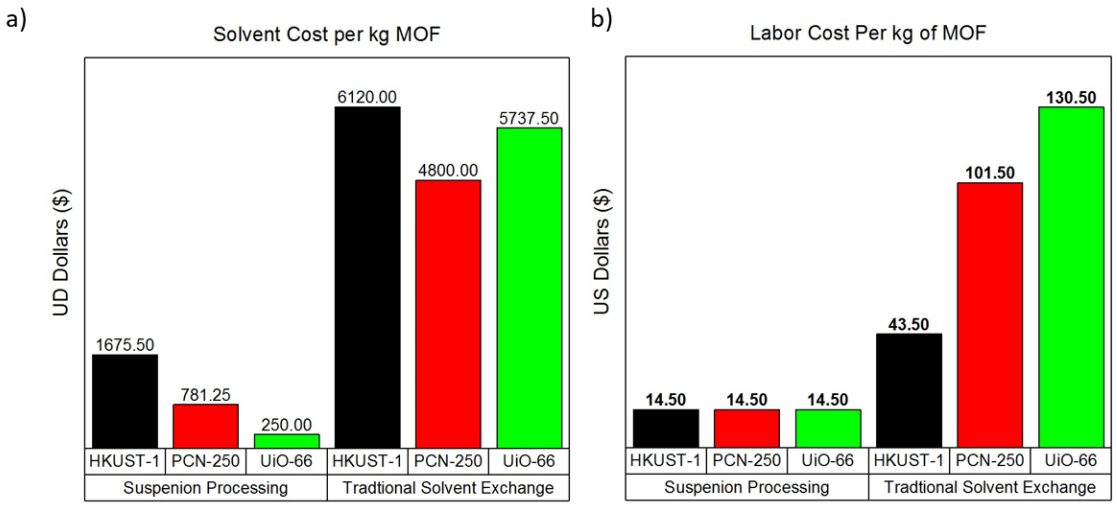

Figure 33. Operational Cost Analysis for Suspension Processing vs. Traditional Solvent Exchange: (a) Solvent cost per kg of MOF; (b) Labor cost per kg of MOF. Ref #48

5.4 Conclusion

In conclusion, suspension processing was introduced as a method for the successful post-synthetic treatment of MOFs that is a viable alternative for traditional solvent-exchange methods for both lab and commercial MOF syntheses. Through this treatment, three commercially available MOFs, with different compositions, stabilities and porosities, have shown promising improvements in gas Absorption capabilities. We ascribe the gas uptake and surface area improvements to efficient pore-cleaning and defect-removal of the MOFs after treatment. Furthermore, the treatment itself is energy-saving, economically-efficient and user-friendly. Overall, suspension processing is a potentially universal, economical, and efficient post-treatment method for industrial scale porous materials.

CHAPTER VI

SUMMARY

Over the past 20 years, the field of MOFs has grown tremendously. The field began in 1999, when Dr. Omar Yaghi reported the first ever permanently porous crystalline framework and coined the term “Metal-Organic Framework”. From that point on the field grew at a rapid pace, moving from unstable frameworks such as Zn and Cu carboxylate based frameworks, to developing crystal growth modulation techniques that allowed for Zr, Fe, and Ti based frameworks to come into the forefront of the field. Within these frameworks, many techniques such as isoreticular expansion, topology guided design, linker substitution, metal substitution, and post synthetic ligand and metal mode modifications have allowed MOFs to be precisely designed for almost any application. However, as the field rapidly expanded, many research gaps developed. For instance, early on, due to the microporous nature of a large majority of MOFs, as well as control of pore functionalities, many of the application studies of MOFs revolved around gas storage and separations as well as small molecule gas phase catalysis. One area that has not been investigated to its fullest extent is aqueous phase applications such as water purification.[9,127]

One MOF that has followed this trend is PCN-250. PCN-250 is a cheap, commercially available MOF that displays aqueous phase stabilities from pH = 2-12. Although it is stable in many acidic and basic conditions, the only published papers dealing with PCN-250’s applications all explore its ability to absorb gases such as CH_4, H_2, or perform gas phase separations such C_2H_2/C_2H_4, N_2/CO_2.[46,47,49,127–129] Therefore, my

doctoral thesis aimed to change this by investigating not only how to generate a Hierarchally Porous (HP) variant of PCN-250 in order to solve the molecular diffusion issues of a microporous framework, but also investigate PCN-250's potential applicability in water remediation. As described in Chapter II, a method for generating HP-PCN-250 was developed. The method developed, which was published in *Angewandte Chemie*, utilizes the addition of fatty acids during MOF synthesis, in order to induce and engineer hierarchal porosity within PCN-250(Fe_3O). The resulting Hierarchally Porous MOFs (HP-MOF) exhibited completely different mesoporosity in size, volume, and position. Furthermore, the HP-PCN-250(C9-1.4M) material obtained adsorbs/removes 100% of Methylene Blue, a common organic dye, from an aqueous solution, as compared to the microporous variant of PCN-250(Fe_3O), which only removes 31% in the same time frame.[79]

Chapter III builds upon the use of PCN-250 as a material for removing organic dyes from water, but utilizes PCN-250 as an Advanced Oxidation Process (AOP) catalyst, not just an adsorbent. Published in *ACS Applied Material and Interfaces*, PCN-250 was reported to be a successful and recyclable Fenton and photo-Fenton catalyst that oxidizes and degrades 100% of Methylene Blue. Overall, 4 different variants of PCN-250 were synthesized and named PCN-250(Fe_3O), PCN-250(Fe_2Ni), PCN-250(Fe_2Co), and PCN-250(Fe_2Mn). The catalytic degradation efficiency for both Fenton and photo-Fenton reactions was improved by the isomorphic substitution of Mn and Co, but inhibited by the incorporation of Ni. [130]

While performing this work, the term Per- and polyfluoroalkyl substances (PFAS) was showing up in the news in increasing rates as an emerging water contaminant that possesses severe health risks to not only animals but humans as well. When thinking about how MOFs could be used to solve the challenge of removing or degrading these species, the use of PCN-250 was not sufficient. This was because, the strength of C-F bond, which is known as the strongest in organic chemistry, with a bond strength of approximately 544 kJ/mol, is resistant to Advanced Oxidation Process (AOP) such as Fenton chemistry. Therefore, the attention shifted to Advanced Reduction Processes (ARPs). ARPs are defined as the reduction of highly oxidized wastewater contaminants by producing highly reactive reducing radicals (hydrated electrons ($e^-_{(aq)}$) or H· radicals) by combining reagents and activation methods. TiO_2 based catalysts were previous reported as successful ARP based catalysts and therefore a smooth transition to developing Ti-based MOFs for the degradation of PFAS was researched.[91] Chapter IV details the development of a Ti-based MOF named MIL-177-HT for the photo-catalytic reduction of PFOA, one of the most challenging PFAS to degrade. It is reported that through the use of a 2.5 g/L catalyst loading and 5% TEOA (sacrificial reductant) solution, 49% degradation and 21.1% fluoride mineralization of PFOA was achieved in 24 hours. To the best of our knowledge, this is the first report of the use of a MOF as a ARP based catalyst for the degradation of PFAS.

Overall, these three chapters have shown the ability to repurpose and redesign previously published MOF structures such as PCN-250 and MIL-177-HT for water based applications such as organic dye absorption and the use in both AOPs and ARPs. However,

one major gap that still remained in MOF chemistry was the high cost of processing. Therefore, as described in Chapter V, a suspension based processing method was developed in order to successfully optimize the porosity of MOFs by providing a more efficient solvent exchange, removing areas of low crystallinity from the MOF surface as well as lowering the cost of material processing. Overall, suspension processing was shown to be able to not only increase the surface of three commercially available MOFs, PCN-250, UiO-66, and HKUST-1, over their commercially available counterparts but lower the cost of processing by an average of 84%. [48]

Overall, this work can be an example of how there still exists many research gaps within the MOF field and how new applications, new discoveries, and new research directions can be obtained just from re-examining previous published MOFs.

REFERENCES

(1) Li, H.; Eddaoudi, M.; O'Keeffe, M.; Yaghi, O. M. Design and Synthesis of an Exceptionally Stable and Highly Porous Metal-Organic Framework. *Nature* **1999**, *402* (6759), 276–279. https://doi.org/10.1038/46248.

(2) Zhou, H.-C.; Long, J. R.; Yaghi, O. M. Introduction to Metal–Organic Frameworks. *Chem. Rev.* **2012**, *112* (2), 673–674. https://doi.org/10.1021/cr300014x.

(3) Li, H.; Wang, K.; Sun, Y.; Lollar, C. T.; Li, J.; Zhou, H.-C. Recent Advances in Gas Storage and Separation Using Metal–Organic Frameworks. *Materials Today* **2018**, *21* (2), 108–121. https://doi.org/10.1016/j.mattod.2017.07.006.

(4) Navalón, S.; García, H. MOFs as Photocatalysts. In *Metal-Organic Frameworks*; García, H., Navalón, S., Eds.; Wiley-VCH Verlag GmbH & Co. KGaA: Weinheim, Germany, 2018; pp 477–501. https://doi.org/10.1002/9783527809097.ch15.

(5) García, H.; Navalón, S. *Metal-Organic Frameworks: Applications in Separations and Catalysis*; John Wiley & Sons, 2018.

(6) Chen, W.; Wu, C. Synthesis, Functionalization, and Applications of Metal–Organic Frameworks in Biomedicine. *Dalton Trans.* **2018**, *47* (7), 2114–2133. https://doi.org/10.1039/C7DT04116K.

(7) Zhang, Y.; Yuan, S.; Day, G.; Wang, X.; Yang, X.; Zhou, H.-C. Luminescent Sensors Based on Metal-Organic Frameworks. *Coordination Chemistry Reviews* **2018**, *354*, 28–45. https://doi.org/10.1016/j.ccr.2017.06.007.

(8) Sevilla, M.; Mokaya, R. Energy Storage Applications of Activated Carbons: Supercapacitors and Hydrogen Storage. *Energy Environ. Sci.* **2014**, *7* (4), 1250–1280. https://doi.org/10.1039/C3EE43525C.

(9) Kirchon, A.; Feng, L.; Drake, H. F.; Joseph, E. A.; Zhou, H.-C. From Fundamentals to Applications: A Toolbox for Robust and Multifunctional MOF Materials. *Chem. Soc. Rev.* **2018**. https://doi.org/10.1039/C8CS00688A.

(10) Sholl, D. S.; Lively, R. P. Defects in Metal–Organic Frameworks: Challenge or Opportunity? *J. Phys. Chem. Lett.* **2015**, *6* (17), 3437–3444. https://doi.org/10.1021/acs.jpclett.5b01135.

(11) Cui, Y.; Li, B.; He, H.; Zhou, W.; Chen, B.; Qian, G. Metal–Organic Frameworks as Platforms for Functional Materials. *Acc. Chem. Res.* **2016**, *49* (3), 483–493. https://doi.org/10.1021/acs.accounts.5b00530.

(12) Desai, A. V.; Sharma, S.; Let, S.; Ghosh, S. K. N-Donor Linker Based Metal-Organic Frameworks (MOFs): Advancement and Prospects as Functional Materials. *Coordination Chemistry Reviews* **2019**, *395*, 146–192. https://doi.org/10.1016/j.ccr.2019.05.020.

(13) Feng, L.; Wang, K.-Y.; Lv, X.-L.; Yan, T.-H.; Zhou, H.-C. Hierarchically Porous Metal–Organic Frameworks: Synthetic Strategies and Applications. *Natl Sci Rev*. https://doi.org/10.1093/nsr/nwz170.

(14) Feng, L.; Wang, K.-Y.; Willman, J.; Zhou, H.-C. Hierarchy in Metal–Organic Frameworks. *ACS Cent. Sci.* **2020**, *6* (3), 359–367. https://doi.org/10.1021/acscentsci.0c00158.

(15) Lian, X.; Fang, Y.; Joseph, E.; Wang, Q.; Li, J.; Banerjee, S.; Lollar, C.; Wang, X.; Zhou, H.-C. Enzyme–MOF (Metal–Organic Framework) Composites. *Chem. Soc. Rev.* **2017**, *46* (11), 3386–3401. https://doi.org/10.1039/C7CS00058H.

(16) Lian, X.; Chen, Y.-P.; Liu, T.-F.; Zhou, H.-C. Coupling Two Enzymes into a Tandem Nanoreactor Utilizing a Hierarchically Structured MOF †Electronic Supplementary Information (ESI) Available. See DOI: 10.1039/C6sc01438k Click Here for Additional Data File. *Chem Sci* **2016**, *7* (12), 6969–6973. https://doi.org/10.1039/c6sc01438k.

(17) Sawano, T.; Lin, Z.; Boures, D.; An, B.; Wang, C.; Lin, W. Metal–Organic Frameworks Stabilize Mono(Phosphine)–Metal Complexes for Broad-Scope Catalytic Reactions. *J. Am. Chem. Soc.* **2016**, *138* (31), 9783–9786. https://doi.org/10.1021/jacs.6b06239.

(18) Feng, X.; Song, Y.; Li, Z.; Kaufmann, M.; Pi, Y.; Chen, J. S.; Xu, Z.; Li, Z.; Wang, C.; Lin, W. Metal–Organic Framework Stabilizes a Low-Coordinate Iridium Complex for Catalytic Methane Borylation. *J. Am. Chem. Soc.* **2019**, *141* (28), 11196–11203. https://doi.org/10.1021/jacs.9b04285.

(19) Blake, A. J.; Champness, N. R.; Easun, T. L.; Allan, D. R.; Nowell, H.; George, M. W.; Jia, J.; Sun, X.-Z. Photoreactivity Examined through Incorporation in Metal−organic Frameworks. *Nature Chemistry* **2010**, *2* (8), 688–694. https://doi.org/10.1038/nchem.681.

(20) Kim, E. J.; Siegelman, R. L.; Jiang, H. Z. H.; Forse, A. C.; Lee, J.-H.; Martell, J. D.; Milner, P. J.; Falkowski, J. M.; Neaton, J. B.; Reimer, J. A.; Weston, S. C.;

Long, J. R. Cooperative Carbon Capture and Steam Regeneration with Tetraamine-Appended Metal–Organic Frameworks. *Science* **2020**, *369* (6502), 392–396. https://doi.org/10.1126/science.abb3976.

(21) Chen, Z.; Li, P.; Anderson, R.; Wang, X.; Zhang, X.; Robison, L.; Redfern, L. R.; Moribe, S.; Islamoglu, T.; Gómez-Gualdrón, D. A.; Yildirim, T.; Stoddart, J. F.; Farha, O. K. Balancing Volumetric and Gravimetric Uptake in Highly Porous Materials for Clean Energy. *Science* **2020**, *368* (6488), 297–303. https://doi.org/10.1126/science.aaz8881.

(22) Dunning, S. G.; Nuñez, A. J.; Moore, M. D.; Steiner, A.; Lynch, V. M.; Sessler, J. L.; Holliday, B. J.; Humphrey, S. M. A Sensor for Trace H2O Detection in D2O. *Chem* **2017**, *2* (4), 579–589. https://doi.org/10.1016/j.chempr.2017.02.010.

(23) Wang, S.; Kitao, T.; Guillou, N.; Wahiduzzaman, M.; Martineau-Corcos, C.; Nouar, F.; Tissot, A.; Binet, L.; Ramsahye, N.; Devautour-Vinot, S.; Kitagawa, S.; Seki, S.; Tsutsui, Y.; Briois, V.; Steunou, N.; Maurin, G.; Uemura, T.; Serre, C. A Phase Transformable Ultrastable Titanium-Carboxylate Framework for Photoconduction. *Nature Communications* **2018**, *9* (1), 1660. https://doi.org/10.1038/s41467-018-04034-w.

(24) Burtch, N. C.; Jasuja, H.; Walton, K. S. Water Stability and Absorption in Metal–Organic Frameworks. *Chem. Rev.* **2014**, *114* (20), 10575–10612. https://doi.org/10.1021/cr5002589.

(25) Ding, M.; Cai, X.; Jiang, H.-L. Improving MOF Stability: Approaches and Applications. *Chem. Sci.* **2019**, *10* (44), 10209–10230. https://doi.org/10.1039/C9SC03916C.

(26) Li, N.; Xu, J.; Feng, R.; Hu, T.-L.; Bu, X.-H. Governing Metal–Organic Frameworks towards High Stability. *Chem. Commun.* **2016**, *52* (55), 8501–8513. https://doi.org/10.1039/C6CC02931K.

(27) Ma, S.; Zhou, H.-C. Gas Storage in Porous Metal–Organic Frameworks for Clean Energy Applications. *Chem. Commun.* **2010**, *46* (1), 44–53. https://doi.org/10.1039/B916295J.

(28) Feng, L.; Yuan, S.; Zhang, L.-L.; Tan, K.; Li, J.-L.; Kirchon, A.; Liu, L.-M.; Zhang, P.; Han, Y.; Chabal, Y. J.; Zhou, H.-C. Creating Hierarchical Pores by Controlled Linker Thermolysis in Multivariate Metal–Organic Frameworks. *J. Am. Chem. Soc.* **2018**, *140* (6), 2363–2372. https://doi.org/10.1021/jacs.7b12916.

(29) Yuan, S.; Zou, L.; Qin, J.-S.; Li, J.; Huang, L.; Feng, L.; Wang, X.; Bosch, M.; Alsalme, A.; Cagin, T.; Zhou, H.-C. Construction of Hierarchically Porous Metal–Organic Frameworks through Linker Labilization. *Nature Communications* **2017**, *8*, 15356. https://doi.org/10.1038/ncomms15356.

(30) Atzori, C.; Shearer, G. C.; Maschio, L.; Civalleri, B.; Bonino, F.; Lamberti, C.; Svelle, S.; Lillerud, K. P.; Bordiga, S. Effect of Benzoic Acid as a Modulator in the Structure of UiO-66: An Experimental and Computational Study. *J. Phys. Chem. C* **2017**, *121* (17), 9312–9324. https://doi.org/10.1021/acs.jpcc.7b00483.

(31) Yin, C.; Liu, Q.; Chen, R.; Liu, J.; Yu, J.; Song, D.; Wang, J. Defect-Induced Method for Preparing Hierarchical Porous Zr–MOF Materials for Ultrafast and Large-Scale Extraction of Uranium from Modified Artificial Seawater. *Ind. Eng. Chem. Res.* **2018**. https://doi.org/10.1021/acs.iecr.8b04034.

(32) Hu, Z.; Castano, I.; Wang, S.; Wang, Y.; Peng, Y.; Qian, Y.; Chi, C.; Wang, X.; Zhao, D. Modulator Effects on the Water-Based Synthesis of Zr/Hf Metal–Organic Frameworks: Quantitative Relationship Studies between Modulator, Synthetic Condition, and Performance. *Crystal Growth & Design* **2016**, *16* (4), 2295–2301. https://doi.org/10.1021/acs.cgd.6b00076.

(33) Cai, G.; Jiang, H.-L. A Modulator-Induced Defect-Formation Strategy to Hierarchically Porous Metal–Organic Frameworks with High Stability. *Angewandte Chemie International Edition* **2017**, *56* (2), 563–567. https://doi.org/10.1002/anie.201610914.

(34) Bradshaw, D.; El-Hankari, S.; Lupica-Spagnolo, L. Supramolecular Templating of Hierarchically Porous Metal–Organic Frameworks. *Chem. Soc. Rev.* **2014**, *43* (16), 5431–5443. https://doi.org/10.1039/C4CS00127C.

(35) Duan, C.; Huo, J.; Li, F.; Yang, M.; Xi, H. Ultrafast Room-Temperature Synthesis of Hierarchically Porous Metal–Organic Frameworks by a Versatile Cooperative Template Strategy. *Journal of Materials Science* **2018**, *53* (24), 16276–16287. https://doi.org/10.1007/s10853-018-2793-3.

(36) Duan, C.; Li, F.; Li, L.; Zhang, H.; Wang, X.; Xiao, J.; Xi, H. Hierarchically Structured Metal–Organic Frameworks Assembled by Hydroxy Double Salt–

Template Synergy with High Space–Time Yields. *CrystEngComm* **2018**, *20* (8), 1057–1064. https://doi.org/10.1039/C7CE01843F.

(37) Budin, I.; Prywes, N.; Zhang, N.; Szostak, J. W. Chain-Length Heterogeneity Allows for the Assembly of Fatty Acid Vesicles in Dilute Solutions. *Biophysical Journal* **2014**, *107* (7), 1582–1590. https://doi.org/10.1016/j.bpj.2014.07.067.

(38) Akhter, M. S.; Alawi, S. M. A Comparison of Micelle Formation of Ionic Surfactants in Formamide, in N-Methylformamide and in N,N-Dimethylformamide. *Colloids and Surfaces A: Physicochemical and Engineering Aspects* **2003**, *219* (1), 281–290. https://doi.org/10.1016/S0927-7757(03)00055-4.

(39) Huang, X.-X.; Qiu, L.-G.; Zhang, W.; Yuan, Y.-P.; Jiang, X.; Xie, A.-J.; Shen, Y.-H.; Zhu, J.-F. Hierarchically Mesostructured MIL-101 Metal–Organic Frameworks: Supramolecular Template-Directed Synthesis and Accelerated Absorption Kinetics for Dye Removal. *CrystEngComm* **2012**, *14* (5), 1613–1617. https://doi.org/10.1039/C1CE06138K.

(40) Li, K.; Lin, S.; Li, Y.; Zhuang, Q.; Gu, J. Aqueous-Phase Synthesis of Mesoporous Zr-Based MOFs Templated by Amphoteric Surfactants. *Angewandte Chemie International Edition* **2018**, *57* (13), 3439–3443. https://doi.org/10.1002/anie.201800619.

(41) Li, S.; Huo, F. Metal-Organic Framework Composites: From Fundamentals to Applications. *Nanoscale* **2015**, *7* (17), 7482–7501. https://doi.org/10.1039/c5nr00518c.

(42) Zhang, Z.; Zaworotko, M. J. Template-Directed Synthesis of Metal–Organic Materials. *Chem. Soc. Rev.* **2014**, *43* (16), 5444–5455. https://doi.org/10.1039/C4CS00075G.

(43) Zieliński, R.; Ikeda, S.; Nomura, H.; Kato, S. Effect of Temperature on Micelle Formation in Aqueous Solutions of Alkyltrimethylammonium Bromides. *Journal of Colloid and Interface Science* **1989**, *129* (1), 175–184. https://doi.org/10.1016/0021-9797(89)90428-1.

(44) Jusufi, A.; Sanders, S.; Klein, M. L.; Panagiotopoulos, A. Z. Implicit-Solvent Models for Micellization: Nonionic Surfactants and Temperature-Dependent Properties. *J. Phys. Chem. B* **2011**, *115* (5), 990–1001. https://doi.org/10.1021/jp108107f.

(45) Khoshnood, A.; Lukanov, B.; Firoozabadi, A. Temperature Effect on Micelle Formation: Molecular Thermodynamic Model Revisited. *Langmuir* **2016**, *32* (9), 2175–2183. https://doi.org/10.1021/acs.langmuir.6b00039.

(46) Yuan, S.; Sun, X.; Pang, J.; Lollar, C.; Qin, J.-S.; Perry, Z.; Joseph, E.; Wang, X.; Fang, Y.; Bosch, M.; Sun, D.; Liu, D.; Zhou, H.-C. PCN-250 under Pressure: Sequential Phase Transformation and the Implications for MOF Densification. *Joule* **2017**, *1* (4), 806–815. https://doi.org/10.1016/j.joule.2017.09.001.

(47) Feng, D.; Wang, K.; Wei, Z.; Chen, Y.-P.; Simon, C. M.; Arvapally, R. K.; Martin, R. L.; Bosch, M.; Liu, T.-F.; Fordham, S.; Yuan, D.; Omary, M. A.; Haranczyk, M.; Smit, B.; Zhou, H.-C. Kinetically Tuned Dimensional Augmentation as a Versatile Synthetic Route towards Robust Metal–Organic

Frameworks. *Nature Communications* **2014**, *5*, 5723. https://doi.org/10.1038/ncomms6723.

(48) Kirchon, A.; Day, G. S.; Fang, Y.; Banerjee, S.; Ozdemir, O. K.; Zhou, H.-C. Suspension Processing of Microporous Metal-Organic Frameworks: A Scalable Route to High-Quality Adsorbents. *iScience* **2018**, *5*, 30–37. https://doi.org/10.1016/j.isci.2018.06.009.

(49) Chen, Y.; Qiao, Z.; Wu, H.; Lv, D.; Shi, R.; Xia, Q.; Zhou, J.; Li, Z. An Ethane-Trapping MOF PCN-250 for Highly Selective Absorption of Ethane over Ethylene. *Chemical Engineering Science* **2018**, *175*, 110–117. https://doi.org/10.1016/j.ces.2017.09.032.

(50) Thommes, M. Physical Absorption Characterization of Nanoporous Materials. *Chemie Ingenieur Technik* **2010**, *82* (7), 1059–1073. https://doi.org/10.1002/cite.201000064.

(51) Groen, J. C.; Peffer, L. A. A.; Pérez-Ramírez, J. Pore Size Determination in Modified Micro- and Mesoporous Materials. Pitfalls and Limitations in Gas Absorption Data Analysis. *Microporous and Mesoporous Materials* **2003**, *60* (1–3), 1–17. https://doi.org/10.1016/S1387-1811(03)00339-1.

(52) Kaneko, K. Determination of Pore Size and Pore Size Distribution: 1. Adsorbents and Catalysts. *Journal of Membrane Science* **1994**, *96* (1), 59–89. https://doi.org/10.1016/0376-7388(94)00126-X.

(53) Storck, S.; Bretinger, H.; Maier, W. F. Characterization of Micro- and Mesoporous Solids by Physisorption Methods and Pore-Size Analysis. *Applied*

Catalysis A: General **1998**, *174* (1), 137–146. https://doi.org/10.1016/S0926-860X(98)00164-1.

(54) N,N-Dimethylformamide (DMF) Dynamic Viscosity - SpringerMaterials https://materials.springer.com/thermophysical/docs/vis_c72#experimental-data-table_wrapper (accessed May 19, 2019).

(55) Mattoon, R. W.; Mathews, M. B. Micelles in Non-Aqueous Media. *The Journal of Chemical Physics* **1949**, *17* (5), 496–497. https://doi.org/10.1063/1.1747295.

(56) Oturan, M. A.; Aaron, J.-J. Advanced Oxidation Processes in Water/Wastewater Treatment: Principles and Applications. A Review. *Critical Reviews in Environmental Science and Technology* **2014**, *44* (23), 2577–2641. https://doi.org/10.1080/10643389.2013.829765.

(57) Fenton, H. J. H. LXXIII.—Oxidation of Tartaric Acid in Presence of Iron. *J. Chem. Soc., Trans.* **1894**, *65* (0), 899–910. https://doi.org/10.1039/CT8946500899.

(58) Bataineh, H.; Pestovsky, O.; Bakac, A. PH-Induced Mechanistic Changeover from Hydroxyl Radicals to Iron(IV) in the Fenton Reaction. *Chem. Sci.* **2012**, *3* (5), 1594–1599. https://doi.org/10.1039/C2SC20099F.

(59) Dunford, H. B. Oxidations of Iron(II)/(III) by Hydrogen Peroxide: From Aquo to Enzyme. *Coordination Chemistry Reviews* **2002**, *233–234*, 311–318. https://doi.org/10.1016/S0010-8545(02)00024-3.

(60) Enami, S.; Sakamoto, Y.; Colussi, A. J. Fenton Chemistry at Aqueous Interfaces. *PNAS* **2014**, *111* (2), 623–628. https://doi.org/10.1073/pnas.1314885111.

(61) Dhakshinamoorthy, A.; Navalon, S.; Alvaro, M.; Garcia, H. Metal Nanoparticles as Heterogeneous Fenton Catalysts. *ChemSusChem* **2012**, *5* (1), 46–64. https://doi.org/10.1002/cssc.201100517.

(62) Garrido-Ramírez, E. G.; Theng, B. K. G.; Mora, M. L. Clays and Oxide Minerals as Catalysts and Nanocatalysts in Fenton-like Reactions — A Review. *Applied Clay Science* **2010**, *47* (3–4), 182–192. https://doi.org/10.1016/j.clay.2009.11.044.

(63) Munoz, M.; de Pedro, Z. M.; Casas, J. A.; Rodriguez, J. J. Preparation of Magnetite-Based Catalysts and Their Application in Heterogeneous Fenton Oxidation – A Review. *Applied Catalysis B: Environmental* **2015**, *176–177*, 249–265. https://doi.org/10.1016/j.apcatb.2015.04.003.

(64) Neyens, E.; Baeyens, J. A Review of Classic Fenton's Peroxidation as an Advanced Oxidation Technique. *Journal of Hazardous Materials* **2003**, *98* (1), 33–50. https://doi.org/10.1016/S0304-3894(02)00282-0.

(65) Cheng, M.; Lai, C.; Liu, Y.; Zeng, G.; Huang, D.; Zhang, C.; Qin, L.; Hu, L.; Zhou, C.; Xiong, W. Metal-Organic Frameworks for Highly Efficient Heterogeneous Fenton-like Catalysis. *Coordination Chemistry Reviews* **2018**, *368*, 80–92. https://doi.org/10.1016/j.ccr.2018.04.012.

(66) Qin, L.; Li, Z.; Hu, Q.; Xu, Z.; Guo, X.; Zhang, G. One-Pot Assembly of Metal/Organic-Acid Sites on Amine-Functionalized Ligands of MOFs for Photocatalytic Hydrogen Peroxide Splitting. *Chem. Commun.* **2016**, *52* (44), 7110–7113. https://doi.org/10.1039/C6CC02453J.

(67) Ahmad, M.; Chen, S.; Ye, F.; Quan, X.; Afzal, S.; Yu, H.; Zhao, X. Efficient Photo-Fenton Activity in Mesoporous MIL-100(Fe) Decorated with ZnO Nanosphere for Pollutants Degradation. *Applied Catalysis B: Environmental* **2019**, *245*, 428–438. https://doi.org/10.1016/j.apcatb.2018.12.057.

(68) Zhang, C.; Ai, L.; Jiang, J. Solvothermal Synthesis of MIL–53(Fe) Hybrid Magnetic Composites for Photoelectrochemical Water Oxidation and Organic Pollutant Photodegradation under Visible Light. *J. Mater. Chem. A* **2015**, *3* (6), 3074–3081. https://doi.org/10.1039/C4TA04622F.

(69) Li, X.; Pi, Y.; Wu, L.; Xia, Q.; Wu, J.; Li, Z.; Xiao, J. Facilitation of the Visible Light-Induced Fenton-like Excitation of H2O2 via Heterojunction of g-C3N4/NH2-Iron Terephthalate Metal-Organic Framework for MB Degradation. *Applied Catalysis B: Environmental* **2017**, *202*, 653–663. https://doi.org/10.1016/j.apcatb.2016.09.073.

(70) Saliba, D.; Ammar, M.; Rammal, M.; Al-Ghoul, M.; Hmadeh, M. Crystal Growth of ZIF-8, ZIF-67, and Their Mixed-Metal Derivatives. *J. Am. Chem. Soc.* **2018**, *140* (5), 1812–1823. https://doi.org/10.1021/jacs.7b11589.

(71) Liu, T.-F.; Zou, L.; Feng, D.; Chen, Y.-P.; Fordham, S.; Wang, X.; Liu, Y.; Zhou, H.-C. Stepwise Synthesis of Robust Metal–Organic Frameworks via Postsynthetic Metathesis and Oxidation of Metal Nodes in a Single-Crystal to Single-Crystal Transformation. *J. Am. Chem. Soc.* **2014**, *136* (22), 7813–7816. https://doi.org/10.1021/ja5023283.

(72) Abednatanzi, S.; Derakhshandeh, P. G.; Depauw, H.; Coudert, F.-X.; Vrielinck, H.; Voort, P. V. D.; Leus, K. Mixed-Metal Metal–Organic Frameworks. *Chem. Soc. Rev.* **2019**, *48* (9), 2535–2565. https://doi.org/10.1039/C8CS00337H.

(73) Sun, D.; Sun, F.; Deng, X.; Li, Z. Mixed-Metal Strategy on Metal–Organic Frameworks (MOFs) for Functionalities Expansion: Co Substitution Induces Aerobic Oxidation of Cyclohexene over Inactive Ni-MOF-74. *Inorg. Chem.* **2015**, *54* (17), 8639–8643. https://doi.org/10.1021/acs.inorgchem.5b01278.

(74) Kim, S. H.; Lee, Y. J.; Kim, D. H.; Lee, Y. J. Bimetallic Metal–Organic Frameworks as Efficient Cathode Catalysts for Li–O2 Batteries. *ACS Appl. Mater. Interfaces* **2018**, *10* (1), 660–667. https://doi.org/10.1021/acsami.7b15499.

(75) Sun, Q.; Liu, M.; Li, K.; Han, Y.; Zuo, Y.; Chai, F.; Song, C.; Zhang, G.; Guo, X. Synthesis of Fe/M (M = Mn, Co, Ni) Bimetallic Metal Organic Frameworks and Their Catalytic Activity for Phenol Degradation under Mild Conditions. *Inorg. Chem. Front.* **2017**, *4* (1), 144–153. https://doi.org/10.1039/C6QI00441E.

(76) Gao, C.; Chen, S.; Quan, X.; Yu, H.; Zhang, Y. Enhanced Fenton-like Catalysis by Iron-Based Metal Organic Frameworks for Degradation of Organic Pollutants. *Journal of Catalysis* **2017**, *356*, 125–132. https://doi.org/10.1016/j.jcat.2017.09.015.

(77) Tang, J.; Wang, J. Metal Organic Framework with Coordinatively Unsaturated Sites as Efficient Fenton-like Catalyst for Enhanced Degradation of Sulfamethazine. *Environ. Sci. Technol.* **2018**, *52* (9), 5367–5377. https://doi.org/10.1021/acs.est.8b00092.

(78) Costa, R. C. C.; Lelis, M. F. F.; Oliveira, L. C. A.; Fabris, J. D.; Ardisson, J. D.; Rios, R. R. V. A.; Silva, C. N.; Lago, R. M. Novel Active Heterogeneous Fenton System Based on Fe3−xMxO4 (Fe, Co, Mn, Ni): The Role of M2+ Species on the Reactivity towards H2O2 Reactions. *Journal of Hazardous Materials* **2006**, *129* (1), 171–178. https://doi.org/10.1016/j.jhazmat.2005.08.028.

(79) Kirchon, A.; Li, J.; Xia, F.; Day, G. S.; Becker, B.; Chen, W.; Sue, H.-J.; Fang, Y.; Zhou, H.-C. Modulation versus Templating: Fine-Tuning of Hierarchally Porous PCN-250 Using Fatty Acids To Engineer Guest Absorption. *Angewandte Chemie International Edition 0* (0). https://doi.org/10.1002/anie.201905006.

(80) Castells-Gil, J.; Padial, N. M.; Martí-Gastaldo, C. Structural Reorganization in a Hydrogen-Bonded Organic Framework. *New Journal of Chemistry* **2018**, *42* (19), 16138–16143. https://doi.org/10.1039/C8NJ02738B.

(81) Thommes, M.; Kaneko, K.; Neimark, A. V.; Olivier, J. P.; Rodriguez-Reinoso, F.; Rouquerol, J.; Sing, K. S. W. Physisorption of Gases, with Special Reference to the Evaluation of Surface Area and Pore Size Distribution (IUPAC Technical Report). *Pure and Applied Chemistry* **2015**, *87* (9–10). https://doi.org/10.1515/pac-2014-1117.

(82) *NIST X-Ray Photoelectron Spectroscopy Database*; National Institute of Standards and Technology, Gaithersburg, 2012.

(83) Allen, G. C.; Harris, S. J.; Jutson, J. A.; Dyke, J. M. A Study of a Number of Mixed Transition Metal Oxide Spinels Using X-Ray Photoelectron Spectroscopy.

Applied Surface Science **1989**, *37* (1), 111–134. https://doi.org/10.1016/0169-4332(89)90977-X.

(84) Brabers, V. A. M.; van Setten, F. M.; Knapen, P. S. A. X-Ray Photoelectron Spectroscopy Study of the Cation Valencies in Nickel Manganite. *Journal of Solid State Chemistry* **1983**, *49* (1), 93–98. https://doi.org/10.1016/0022-4596(83)90220-7.

(85) Tan, B. J.; Klabunde, K. J.; Sherwood, P. M. A. XPS Studies of Solvated Metal Atom Dispersed (SMAD) Catalysts. Evidence for Layered Cobalt-Manganese Particles on Alumina and Silica. *J. Am. Chem. Soc.* **1991**, *113* (3), 855–861. https://doi.org/10.1021/ja00003a019.

(86) McIntyre, N. S.; Cook, M. G. X-Ray Photoelectron Studies on Some Oxides and Hydroxides of Cobalt, Nickel, and Copper. *Anal. Chem.* **1975**, *47* (13), 2208–2213. https://doi.org/10.1021/ac60363a034.

(87) Zhong, Y.; Liang, X.; He, Z.; Tan, W.; Zhu, J.; Yuan, P.; Zhu, R.; He, H. The Constraints of Transition Metal Substitutions (Ti, Cr, Mn, Co and Ni) in Magnetite on Its Catalytic Activity in Heterogeneous Fenton and UV/Fenton Reaction: From the Perspective of Hydroxyl Radical Generation. *Applied Catalysis B: Environmental* **2014**, *150–151*, 612–618. https://doi.org/10.1016/j.apcatb.2014.01.007.

(88) Sun, Q.; Liu, M.; Li, K.; Han, Y.; Zuo, Y.; Wang, J.; Song, C.; Zhang, G.; Guo, X. Controlled Synthesis of Mixed-Valent Fe-Containing Metal Organic Frameworks

for the Degradation of Phenol under Mild Conditions. *Dalton Trans.* **2016**, *45* (19), 7952–7959. https://doi.org/10.1039/C5DT05002B.

(89) Domingo, J. L.; Nadal, M. Human Exposure to Per- and Polyfluoroalkyl Substances (PFAS) through Drinking Water: A Review of the Recent Scientific Literature. *Environmental Research* **2019**, *177*, 108648. https://doi.org/10.1016/j.envres.2019.108648.

(90) Horst, J.; McDonough, J.; Ross, I.; Dickson, M.; Miles, J.; Hurst, J.; Storch, P. Water Treatment Technologies for PFAS: The Next Generation. *Groundwater Monitoring & Remediation* **2018**, *38* (2), 13–23. https://doi.org/10.1111/gwmr.12281.

(91) Cui, J.; Gao, P.; Deng, Y. Destruction of Per- and Polyfluoroalkyl Substances (PFAS) with Advanced Reduction Processes (ARPs): A Critical Review. *Environ. Sci. Technol.* **2020**, *54* (7), 3752–3766. https://doi.org/10.1021/acs.est.9b05565.

(92) Möller, A.; Ahrens, L.; Surm, R.; Westerveld, J.; van der Wielen, F.; Ebinghaus, R.; de Voogt, P. Distribution and Sources of Polyfluoroalkyl Substances (PFAS) in the River Rhine Watershed. *Environmental Pollution* **2010**, *158* (10), 3243–3250. https://doi.org/10.1016/j.envpol.2010.07.019.

(93) US EPA, O. Reducing PFAS in Drinking Water with Treatment Technologies https://www.epa.gov/sciencematters/reducing-pfas-drinking-water-treatment-technologies (accessed Sep 1, 2020).

(94) US EPA, O. Basic Information on PFAS https://www.epa.gov/pfas/basic-information-pfas (accessed Sep 1, 2020).

(95) Kwiatkowski, C. F.; Andrews, D. Q.; Birnbaum, L. S.; Bruton, T. A.; DeWitt, J. C.; Knappe, D. R. U.; Maffini, M. V.; Miller, M. F.; Pelch, K. E.; Reade, A.; Soehl, A.; Trier, X.; Venier, M.; Wagner, C. C.; Wang, Z.; Blum, A. Scientific Basis for Managing PFAS as a Chemical Class. *Environ. Sci. Technol. Lett.* **2020**, *7* (8), 532–543. https://doi.org/10.1021/acs.estlett.0c00255.

(96) ACUTE TOXICITY TO AQUATIC INVERTABRATES (DAPHNIA MAGNA) https://www.ag.state.mn.us/Office/Cases/3M/docs/PTX/PTX1143.pdf (accessed Aug 19, 2020).

(97) PFAS Acute Oral Toxicity - Rats https://www.ag.state.mn.us/Office/Cases/3M/docs/PTX/PTX1132.pdf (accessed Aug 19, 2020).

(98) Biodegradation Studies of Fluorocarbons - II https://www.ag.state.mn.us/Office/Cases/3M/docs/PTX/PTX1153.pdf (accessed Aug 19, 2020).

(99) Biodegradatio. Studies of Fluorocarbons -III https://www.ag.state.mn.us/Office/Cases/3M/docs/PTX/PTX1179.pdf (accessed Aug 19, 2020).

(100) Barpaga, D.; Zheng, J.; Han, K. S.; Soltis, J. A.; Shutthanandan, V.; Basuray, S.; McGrail, B. P.; Chatterjee, S.; Motkuri, R. K. Probing the Sorption of Perfluorooctanesulfonate Using Mesoporous Metal–Organic Frameworks from Aqueous Solutions. *Inorg. Chem.* **2019**. https://doi.org/10.1021/acs.inorgchem.9b00380.

(101) Gagliano, E.; Sgroi, M.; Falciglia, P. P.; Vagliasindi, F. G. A.; Roccaro, P. Removal of Poly- and Perfluoroalkyl Substances (PFAS) from Water by Absorption: Role of PFAS Chain Length, Effect of Organic Matter and Challenges in Adsorbent Regeneration. *Water Research* **2020**, *171*, 115381. https://doi.org/10.1016/j.watres.2019.115381.

(102) Ji, W.; Xiao, L.; Ling, Y.; Ching, C.; Matsumoto, M.; Bisbey, R. P.; Helbling, D. E.; Dichtel, W. R. Removal of GenX and Perfluorinated Alkyl Substances from Water by Amine-Functionalized Covalent Organic Frameworks. *J. Am. Chem. Soc.* **2018**, *140* (40), 12677–12681. https://doi.org/10.1021/jacs.8b06958.

(103) Punyapalakul, P.; Suksomboon, K.; Prarat, P.; Khaodhiar, S. Effects of Surface Functional Groups and Porous Structures on Absorption and Recovery of Perfluorinated Compounds by Inorganic Porous Silicas. *Separation Science and Technology* **2013**, *48* (5), 775–788. https://doi.org/10.1080/01496395.2012.710888.

(104) Ochoa-Herrera, V.; Sierra-Alvarez, R. Removal of Perfluorinated Surfactants by Sorption onto Granular Activated Carbon, Zeolite and Sludge. *Chemosphere* **2008**, *72* (10), 1588–1593. https://doi.org/10.1016/j.chemosphere.2008.04.029.

(105) Senevirathna, S. T. M. L. D.; Tanaka, S.; Fujii, S.; Kunacheva, C.; Harada, H.; Ariyadasa, B. H. A. K. T.; Shivakoti, B. R. Absorption of Perfluorooctane Sulfonate (n-PFOS) onto Non Ion-Exchange Polymers and Granular Activated Carbon: Batch and Column Test. *Desalination* **2010**, *260* (1), 29–33. https://doi.org/10.1016/j.desal.2010.05.005.

(106) Qu, Y.; Zhang, C.; Li, F.; Bo, X.; Liu, G.; Zhou, Q. Equilibrium and Kinetics Study on the Absorption of Perfluorooctanoic Acid from Aqueous Solution onto Powdered Activated Carbon. *Journal of Hazardous Materials* **2009**, *169* (1), 146–152. https://doi.org/10.1016/j.jhazmat.2009.03.063.

(107) Conte, L.; Falletti, L.; Zaggia, A.; Milan, M. Polyfluorinated Organic Micropollutants Removal from Water by Ion Exchange and Absorption. *1* **2015**, *43*, 2257–2262. https://doi.org/10.3303/CET1543377.

(108) Carter, K. E.; Farrell, J. Removal of Perfluorooctane and Perfluorobutane Sulfonate from Water via Carbon Absorption and Ion Exchange. *Separation Science and Technology* **2010**, *45* (6), 762–767. https://doi.org/10.1080/01496391003608421.

(109) Deng, S.; Yu, Q.; Huang, J.; Yu, G. Removal of Perfluorooctane Sulfonate from Wastewater by Anion Exchange Resins: Effects of Resin Properties and Solution Chemistry. *Water Research* **2010**, *44* (18), 5188–5195. https://doi.org/10.1016/j.watres.2010.06.038.

(110) Zaggia, A.; Conte, L.; Falletti, L.; Fant, M.; Chiorboli, A. Use of Strong Anion Exchange Resins for the Removal of Perfluoroalkylated Substances from Contaminated Drinking Water in Batch and Continuous Pilot Plants. *Water Research* **2016**, *91*, 137–146. https://doi.org/10.1016/j.watres.2015.12.039.

(111) Deng, S.; Nie, Y.; Du, Z.; Huang, Q.; Meng, P.; Wang, B.; Huang, J.; Yu, G. Enhanced Absorption of Perfluorooctane Sulfonate and Perfluorooctanoate by

Bamboo-Derived Granular Activated Carbon. *Journal of Hazardous Materials* **2015**, *282*, 150–157. https://doi.org/10.1016/j.jhazmat.2014.03.045.

(112) Schröder, H. F.; Meesters, R. J. W. Stability of Fluorinated Surfactants in Advanced Oxidation Processes--A Follow up of Degradation Products Using Flow Injection-Mass Spectrometry, Liquid Chromatography-Mass Spectrometry and Liquid Chromatography-Multiple Stage Mass Spectrometry. *J Chromatogr A* **2005**, *1082* (1), 110–119. https://doi.org/10.1016/j.chroma.2005.02.070.

(113) Sharma, V. K.; Feng, M. Water Depollution Using Metal-Organic Frameworks-Catalyzed Advanced Oxidation Processes: A Review. *Journal of Hazardous Materials* **2017**. https://doi.org/10.1016/j.jhazmat.2017.09.043.

(114) Fu, Y.; Sun, D.; Chen, Y.; Huang, R.; Ding, Z.; Fu, X.; Li, Z. An Amine-Functionalized Titanium Metal–Organic Framework Photocatalyst with Visible-Light-Induced Activity for CO2 Reduction. *Angewandte Chemie International Edition* **2012**, *51* (14), 3364–3367. https://doi.org/10.1002/anie.201108357.

(115) Vellanki, B. P.; Batchelor, B. Perchlorate Reduction by the Sulfite/Ultraviolet Light Advanced Reduction Process. *Journal of Hazardous Materials* **2013**, *262*, 348–356. https://doi.org/10.1016/j.jhazmat.2013.08.061.

(116) Vellanki, B. P.; Batchelor, B.; Abdel-Wahab, A. Advanced Reduction Processes: A New Class of Treatment Processes. *Environmental Engineering Science* **2013**, *30* (5), 264–271. https://doi.org/10.1089/ees.2012.0273.

(117) Xiao, Q.; Yu, S.; Li, L.; Wang, T.; Liao, X.; Ye, Y. An Overview of Advanced Reduction Processes for Bromate Removal from Drinking Water: Reducing

Agents, Activation Methods, Applications and Mechanisms. *Journal of Hazardous Materials* **2017**, *324*, 230–240. https://doi.org/10.1016/j.jhazmat.2016.10.053.

(118) Diebold, U. The Surface Science of Titanium Dioxide. *Surface Science Reports* **2003**, *48* (5), 53–229. https://doi.org/10.1016/S0167-5729(02)00100-0.

(119) Gomez-Ruiz, B.; Ribao, P.; Diban, N.; Rivero, M. J.; Ortiz, I.; Urtiaga, A. Photocatalytic Degradation and Mineralization of Perfluorooctanoic Acid (PFOA) Using a Composite TiO2 −rGO Catalyst. *Journal of Hazardous Materials* **2018**, *344*, 950–957. https://doi.org/10.1016/j.jhazmat.2017.11.048.

(120) Xu, B.; Ahmed, M. B.; Zhou, J. L.; Altaee, A.; Wu, M.; Xu, G. Photocatalytic Removal of Perfluoroalkyl Substances from Water and Wastewater: Mechanism, Kinetics and Controlling Factors. *Chemosphere* **2017**, *189*, 717–729. https://doi.org/10.1016/j.chemosphere.2017.09.110.

(121) Chen, M.-J.; Lo, S.-L.; Lee, Y.-C.; Huang, C.-C. Photocatalytic Decomposition of Perfluorooctanoic Acid by Transition-Metal Modified Titanium Dioxide. *Journal of Hazardous Materials* **2015**, *288*, 168–175. https://doi.org/10.1016/j.jhazmat.2015.02.004.

(122) Li, M.; Yu, Z.; Liu, Q.; Sun, L.; Huang, W. Photocatalytic Decomposition of Perfluorooctanoic Acid by Noble Metallic Nanoparticles Modified TiO2. *Chemical Engineering Journal* **2016**, *286*, 232–238. https://doi.org/10.1016/j.cej.2015.10.037.

(123) Chambers, M. B.; Wang, X.; Ellezam, L.; Ersen, O.; Fontecave, M.; Sanchez, C.; Rozes, L.; Mellot-Draznieks, C. Maximizing the Photocatalytic Activity of Metal–Organic Frameworks with Aminated-Functionalized Linkers: Substoichiometric Effects in MIL-125-NH2. *J. Am. Chem. Soc.* **2017**, *139* (24), 8222–8228. https://doi.org/10.1021/jacs.7b02186.

(124) L. Nguyen, H. The Chemistry of Titanium-Based Metal–Organic Frameworks. *New Journal of Chemistry* **2017**, *41* (23), 14030–14043. https://doi.org/10.1039/C7NJ03153J.

(125) Sampaio, R. N.; Grills, D. C.; Polyansky, D. E.; Szalda, D. J.; Fujita, E. Unexpected Roles of Triethanolamine in the Photochemical Reduction of CO2 to Formate by Ruthenium Complexes. *J. Am. Chem. Soc.* **2020**, *142* (5), 2413–2428. https://doi.org/10.1021/jacs.9b11897.

(126) Pellegrin, Y.; Odobel, F. Sacrificial Electron Donor Reagents for Solar Fuel Production. *Comptes Rendus Chimie* **2017**, *20* (3), 283–295. https://doi.org/10.1016/j.crci.2015.11.026.

(127) Silva, P.; Vilela, S. M. F.; Tomé, J. P. C.; Almeida Paz, F. A. Multifunctional Metal-Organic Frameworks: From Academia to Industrial Applications. *Chem Soc Rev* **2015**, *44* (19), 6774–6803. https://doi.org/10.1039/c5cs00307e.

(128) Dong, H.; Zhang, X.; Lu, Y.; Yang, Y.; Zhang, Y.-P.; Tang, H.-L.; Zhang, F.-M.; Yang, Z.-D.; Sun, X.; Feng, Y. Regulation of Metal Ions in Smart Metal-Cluster Nodes of Metal-Organic Frameworks with Open Metal Sites for Improved

Photocatalytic CO2 Reduction Reaction. *Applied Catalysis B: Environmental* **2020**, *276*, 119173. https://doi.org/10.1016/j.apcatb.2020.119173.

(129) Gopalsamy, K.; Babarao, R. Heterometallic Metal Organic Frameworks for Air Separation: A Computational Study. *Ind. Eng. Chem. Res.* **2020**, *59* (35), 15718–15731. https://doi.org/10.1021/acs.iecr.0c02449.

(130) Kirchon, A.; Zhang, P.; Li, J.; Joseph, E. A.; Chen, W.; Zhou, H.-C. Effect of Isomorphic Metal Substitution on the Fenton and Photo-Fenton Degradation of Methylene Blue Using Fe-Based Metal–Organic Frameworks. *ACS Appl. Mater. Interfaces* **2020**, *12* (8), 9292–9299. https://doi.org/10.1021/acsami.9b21408.

APPENDIX A.

PUBLISHED PAPERS CONTAINED

This dissertation included published papers shown below:

1. **Kirchon, A**.; Feng, L.; Drake, H. F.; Joseph, E. A.; Zhou, H.-C. From Fundamentals to Applications: A Toolbox for Robust and Multifunctional MOF Materials. *Chem. Soc. Rev*., **2018**, 47, 8611-8638.
2. **Kirchon, A.;** Li, J.; Xia, F.; Day, G. S.; Becker, B.; Chen, W.; Sue, H.-J.; Fang, Y.; Zhou, H.-C. Modulation versus Templating: Fine-Tuning of Hierarchally Porous PCN-250 Using Fatty Acids To Engineer Guest Absorption., *Angew. Chem. Int. Ed.* **2019,** 58 (36), 12425-12430**.**.
3. **Kirchon, A**.; Zhang, P.; Li, J.; Joseph, E. A.; Chen, W.; Zhou, H.-C. Effect of Isomorphic Metal Substitution on the Fenton and Photo-Fenton Degradation of Methylene Blue Using Fe-Based Metal–Organic Frameworks. *ACS Appl. Mater. Interfaces*, **2020**, 12 (8), 9292–9299.
4. **Kirchon, A.;** Day, G. S.; Fang, Y.; Banerjee, S.; Ozdemir, O. K.; Zhou, H.-C. Suspension Processing of Microporous Metal-Organic Frameworks: A Scalable Route to High-Quality Adsorbents. iScience **2018**, 5, 30–37.

APPENDIX B

MS/MS DATA

Mass Spec / Mass Spec data from LC-MS of 2.5 g/L CAT, 5.0 % TEOA, 1 ppm PFOA - Degradation (light on) reaction

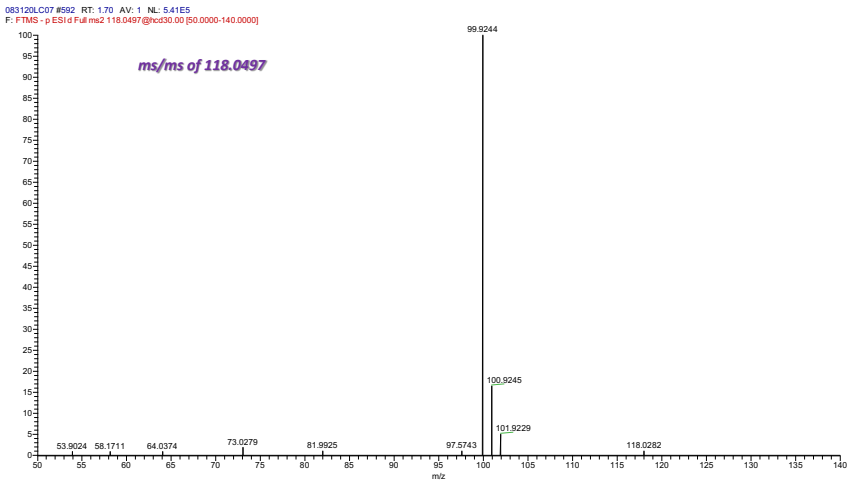

Figure 34. MS/MS data for 118 m/z

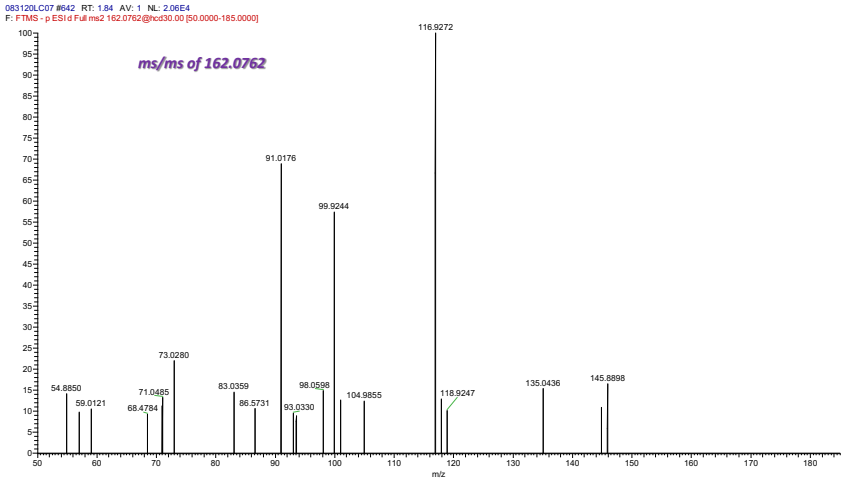

Figure 35. MS/MS data for 162 m/z

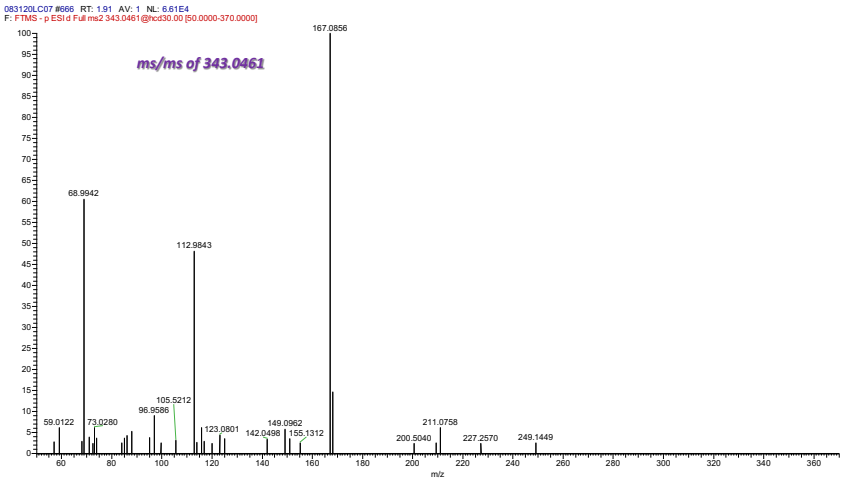

Figure 36. MS/MS data for 343 m/z

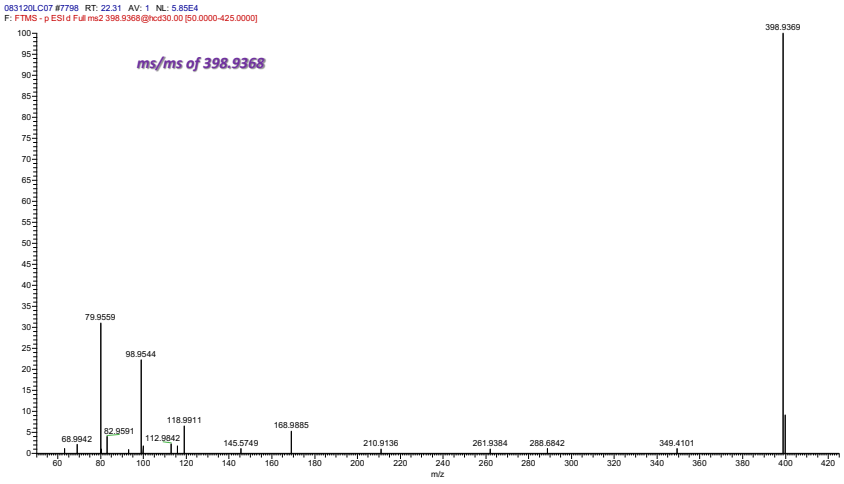

Figure 37. MS/MS data for 398 m/z

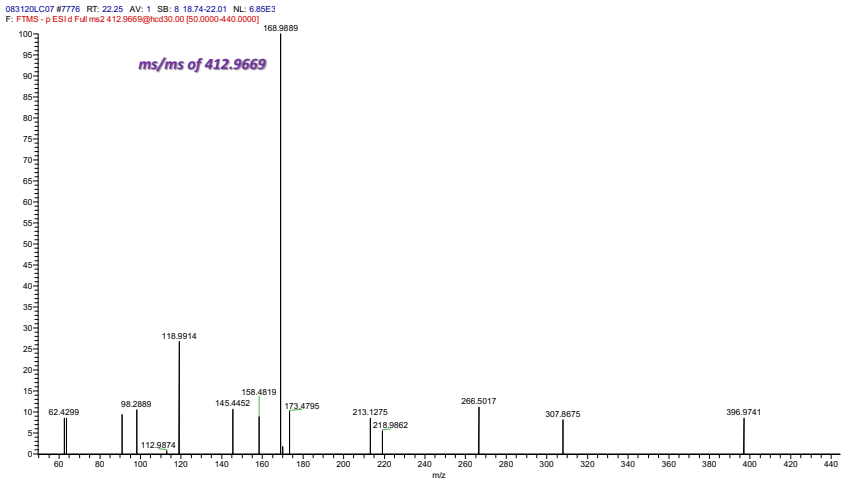

Figure 38. MS/MS data for 413 m/z